

RESEARCH REPORT

A STUDY OF THE INFLUENCE OF FUEL ATOMIZATION
VAPORIZATION, AND MIXING PROCESSES ON POLLUTANT
EMISSIONS FROM MOTOR-VEHICLE POWERPLANTS

to

ENVIRONMENTAL PROTECTION AGENCY
OFFICE OF AIR PROGRAMS


Contract No. CPA 70-20

January 31, 1972



Battelle

Columbus Laboratories



BATTELLE'S COLUMBUS LABORATORIES comprises the original research center of an international organization devoted to research and development.

Battelle is frequently described as a "bridge" between science and industry — a role it has performed in more than 90 countries. It conducts research encompassing virtually all facets of science and its application. It also undertakes programs in fundamental research and education.

Battelle-Columbus — with its staff of 2500 — serves industry and government through contract research. It pursues:

- research embracing the physical and life sciences, engineering, and selected social sciences
- design and development of materials, products, processes, and systems
- information analysis, socioeconomic and technical economic studies, and management planning research.

PHASE II REPORT

on

A STUDY OF THE INFLUENCE OF FUEL ATOMIZATION
VAPORIZATION, AND MIXING PROCESSES ON POLLUTANT
EMISSIONS FROM MOTOR-VEHICLE POWERPLANTS

to

ENVIRONMENTAL PROTECTION AGENCY
OFFICE OF AIR PROGRAMS

Contract No. CPA 70-20

January 31, 1972

by

D. A. Trayser, J. A. Gieseke, R. D. Fischer, and
F. A. Creswick

BATTELLE
Columbus Laboratories
505 King Avenue
Columbus, Ohio 43201
Franklin County

ABSTRACT

This report summarizes the Phase II study of automotive-engine induction systems conducted by Battelle-Columbus for the Environmental Protection Agency under Contract Number CPA-70-20. Results of the Phase I study (Under Contract Number CPA 22-69-9) are covered in a report dated April 30, 1969.

The objectives of this experimental Phase II program were to obtain experimental data on droplet impaction characteristics, fuel-film flow on manifold walls, and fuel vaporization for a better understanding of induction-system phenomena; and to demonstrate the potential of improved fuel atomization, fuel vaporization, and intake manifold design for improving air-fuel mixing and distribution.

Results of this study showed that ultrafine atomization, minimum manifold-passage turning angle, long passage bend radii, and low air velocity can reduce droplet impaction in an induction system. However, appreciable droplet impaction still occurs, even with droplet sizes as low as 14 microns, because of deposition by flow-induced air turbulence. Consequently, fuel vaporization by intake air preheating and by manifold surface heating is recommended in addition to improved atomization to reduce further the fuel film on the wall.

An improved induction-system concept recommended by the project staff includes: an air-atomizing fuel nozzle operating on the ultrasonic Hartmann-whistle principle, a mixing section similar in construction to a can-type combustor, an unconventional throttle valve such as a plug valve between the mixture generator and the intake manifold or a butterfly valve upstream of the mixture generator, and a single-plane manifold with a separate branch for each cylinder having equally spaced, equal-area, radial entrances.

Recommendations for additional research include: experimental studies of fuel-droplet transport and vaporization, with emphasis on vaporization, and design and development of the advanced induction-system concepts resulting from this Phase II study.

TABLE OF CONTENTS

	<u>Page</u>
INTRODUCTION	1
OBJECTIVES	2
SUMMARY OF STUDY	2
CONCLUSIONS	4
RECOMMENDATIONS	6
EXPERIMENTAL WORK	7
The Laboratory Flow System	7
Manifold Test Section Geometries	22
Discussion of Fluids	30
Mixture Quality Measurement	35
Experimental Program	48
Experimental Results	56
DESIGN CONCEPTS	83
Induction System Concept	83
Fuel Vaporization	98
ACKNOWLEDGEMENTS	104
LIST OF REFERENCES	105
APPENDIX A, IMPACTOR STAGE DESIGN FOR VAPOR DROPLET SAMPLERS . . .	A-1
APPENDIX B, CALIBRATION CURVES	B-1

LIST OF FIGURES

FIGURE 1. Schematic of Laboratory Flow System for Induction System Fundamental Studies	9
FIGURE 2. Oscilloscope Traces of Pulsating Flow	11
FIGURE 3. Time Variation of Pulsating Flow	12
FIGURE 4. Air Flow Capacity of Laboratory Flow System	14
FIGURE 5. Layout Drawing of Mixture Generator	16
FIGURE 6. Detail of Mixture Generator Fuel Skimmer System	18

LIST OF FIGURES (Continued)

	<u>Page</u>
FIGURE 7. Modification to Mixture Generator to Reduce Impaction. . .	21
FIGURE 8. Detail of Discharge Burner	23
FIGURE 9A. 30-Degree-Bend Manifold Test Section	26
FIGURE 9B. 90-Degree, 0-Inch-Radius-Bend Manifold Test Section. . .	27
FIGURE 9C. 90-Degree, 4-Inch-Radius-Bend Manifold Test Section. . .	28
FIGURE 10. Sketch of Aluminum Instrumented Test Section Showing Thermocouple Locations	29
FIGURE 11. Comparison of Liquid Viscosities	32
FIGURE 12. Standard Distillation Curves for a Representative Composite Gasoline and for Stoddard Solvent	34
FIGURE 13. Vapor/Droplet Sampling Probe -- Design 1	37
FIGURE 14. Vapor/Droplet Sampling Probe -- Design 2	38
FIGURE 15. Vapor/Droplet Sampling Probe -- Design 3	38
FIGURE 16. Simple Tube Sampling Probe	40
FIGURE 17. Fuel-Film Wall Skimmer Design	41
FIGURE 18. Equilibrium Vapor Content in Air Over Stoddard Solvent at Atmospheric Pressure	44
FIGURE 19. Flow Diagram of Sampling System	46
FIGURE 20. Cross-Section of Manifold Test Section Showing Probe Positions as Viewed from Outlet	50
FIGURE 21. Collection Apparatus for Drop Sizing	53
FIGURE 22. Size Distributions for Drops Entering Test Sections . .	55
FIGURE 23. Wall Fuel-Film Flow Rate as a Function of Air Flow Rate and Test-Section Geometry	69
FIGURE 24. Fraction of Liquid Fuel Impacted as a Function of Air Flow Rate and Test-Section Geometry	70
FIGURE 25. Entrained-Fuel-Droplet Stratification at Straight Test-Section Exit	72

LIST OF FIGURES (Continued)

	<u>Page</u>
FIGURE 26. Entrained-Fuel-Droplet Stratification at 30-Degree-Bend Test-Section Exit	72
FIGURE 27. Entrained-Fuel-Droplet Stratification at 90-Degree, 4-Inch-Radius-Bend Test-Section Exit	73
FIGURE 28. Entrained-Fuel-Droplet Stratification at 90-Degree, 0-Inch-Radius-Bend Test-Section Exit	73
FIGURE 29. Wall Fuel-Film Flow Patterns in 30-Degree Test Section .	76
FIGURE 30. Wall Fuel-Film Flow Patterns in 90-Degree, 4-Inch Radius Test Section	77
FIGURE 31. Wall Fuel-Film Flow Patterns in 90-Degree, 0-Inch Radius Test Section	78
FIGURE 32. Sketch Layout of Prototype Improved Induction System-- Section View	84
FIGURE 33. Sketch Layout of Prototype Improved Induction System-- Plan View	85
FIGURE 34. Sketch Layout of Intake-Passage Configuration for Paired-Port Engine -- Section View	86
FIGURE 35. Sketch Layout of Intake-Passage Configuration for Paired-Port Engine -- Plan View.	87
FIGURE 36. Sketch of Proposed Air-Atomizing Hartmann-Whistle- Type Fuel Nozzle	90
FIGURE 37. Sketch of Proposed Induction System With Plug Throttle .	93
FIGURE 38. Sketch Layout of Proposed Induction System with Alternative Inlet-Air Throttle -- Section View	95
FIGURE 39. Sketch Layout of Proposed Induction System with Alternative Inlet-Air Throttle -- Plan View	96
FIGURE 40. Fin and Tube Geometry for Fuel Vaporization Chamber . .	101
FIGURE 41. Sketch Layout of Vaporization Chamber	103
FIGURE 42. Fuel Vaporization Apparatus	104

LIST OF FIGURES (Continued)

	<u>Page</u>
FIGURE A-1. Droplet Size Distribution Used for Calibration of the Vapor/Droplet Sampler	A-3
FIGURE A-2. Vapor/Droplet Sampler Calibration Arrangement	A-4
FIGURE A-3. Collection Efficiency of the Vapor/Droplet Sampler as a Function of Droplet Size	A-6
FIGURE B-1. Computed Flow vs Pressure Differential Data for Square-Edged Orifice Flowmeter with 1D and 1/2 D Taps . .	B-2
FIGURE B-2. Calibration Curve for Fuel System Flow Meter	B-3
FIGURE B-3. Drop Size Distribution at 28,000 RPM and 1 cm ³ /sec . .	B-4
FIGURE B-4. Drop Size Distribution at 40,000 RPM and 1 cm ³ /sec . .	B-5
FIGURE B-5. Drop Size Distribution at 46,000 RPM and 1 cm ³ /sec . .	B-6
FIGURE B-6. Drop Size Distribution at 53,000 RPM and 1 cm ³ /sec . .	B-7
FIGURE B-7. Drop Size Distribution at 59,000 RPM and 1 cm ³ /sec . .	B-8
FIGURE B-8. Drop Size Distribution at 64,000 RPM and 1 cm ³ /sec . .	B-9
FIGURE B-9. Drop Size Distribution at 32,000 RPM and 0.5 cm ³ /sec .	B-10
FIGURE B-10. Drop Size Distribution at 43,000 RPM and 0.5 cm ³ /sec .	B-11
FIGURE B-11. Drop Size Distribution at 50,000 RPM and 0.5 cm ³ /sec .	B-12
FIGURE B-12. Drop Size Distribution at 56,000 RPM and 0.5 cm ³ /sec .	B-13
FIGURE B-13. Drop Size Distribution at 61,000 RPM and 0.5 cm ³ /sec .	B-14
FIGURE B-14. Drop Size Distribution at 65,000 RPM and 0.5 cm ³ /sec .	B-15
FIGURE B-15. Standard Calibration of Primary Sampling Rotameters . .	B-16
FIGURE B-16. Temperature and Pressure Corrections for Sampling Rotameters	B-17
FIGURE B-17. Hydrocarbon Analyzer Calibration	B-18

LIST OF TABLES

	<u>Page</u>
TABLE 1. Geometry of Test Sections	25
TABLE 2. Matrix of Test Conditions	51
TABLE 3. Experimental Data for Test-Section Entrance	58
TABLE 4. Reduced Data for Test-Section Entrance	58
TABLE 5. Experimental Data for Straight Test Section	59
TABLE 6. Reduced Data for Straight Test Section	59
TABLE 7. Experimental Data for 30-Degree-Bend Test Section	60
TABLE 8. Reduced Data for 30-Degree-Bend Test Section	60
TABLE 9. Experimental Data for 90-Degree, 4-Inch-Radius-Bend Test Section	61
TABLE 10. Reduced Data for 90-Degree, 4-Inch-Radius-Bend Test Section	61
TABLE 11. Experimental Data for 90-Degree, 0-Inch-Radius-Bend Test Section	62
TABLE 12. Reduced Data for 90-Degree, 0-Inch-Radius-Bend Test Section	62
TABLE 13. Experimental Data for Replication Test With 90-Degree, 4-Inch-Radius-Bend Test Section	63
TABLE 14. Reduced Data for Replication Test With 90-Degree, 4-Inch-Radius-Bend Test Section	63
TABLE 15. Experimental Data for Rough-Wall and Heated Test Sections	64
TABLE 16. Reduced Data for Rough-Wall and Heated Test Sections	64
TABLE 17. Fuel Mass-Balance Summary	65
TABLE 18. Wall-Temperature Data for Heated Test Section	81
TABLE 19. Comparison of Alternative Atomization Systems	90

PHASE II REPORT

on

A STUDY OF THE INFLUENCE OF FUEL ATOMIZATION, VAPORIZATION, AND MIXING PROCESSES ON POLLUTANT EMISSIONS FROM MOTOR-VEHICLE POWERPLANTS

by

D. A. Trayser, J. A. Gieseke, R. D. Fischer,
and F. A. Creswick

INTRODUCTION

This study was initiated in 1968 with an 8-month Phase I analytical program to explore the incentives for achieving engine operation with leaner mixtures as a means of reducing exhaust emissions, and to develop information on potential means of extending the lean operating limit through improved induction-system design concepts and improved analytical design approaches. A report on the Phase I program was issued on April 30, 1969.^{(1)*}

Among the significant conclusions of the Phase I program were: improving air-fuel distribution to extend the lean operating limit can lead to worthwhile reductions in exhaust emissions, and the most promising approach to achieving improved distribution is through use of fuel atomizing devices that will produce droplet sizes approaching 10 or 20 microns under all operating conditions and by design of the induction system for minimum impaction of fuel droplets.

It was recommended at the conclusion of the study to extend the investigation into a Phase II experimental program to demonstrate the technical feasibility of improved induction-system design for reducing exhaust emissions. It was also recommended that, as a part of this extended investigation, experimental studies of fundamental induction phenomena be carried out.

In the course of conducting the Phase I study, it had become clear that very little was known about droplet dynamics, wall fuel-film characteristics, and vaporization as they apply to the induction system of an automotive

* References are listed at the end of the report.

engine. Very little data are available on these phenomena, and even less has been published on methods of measuring and/or evaluating these parameters.

Mathematical approaches to predicting droplet impaction and wall fuel-film patterns are limited, for practical reasons, to idealized one-dimensional steady air flow. Predicting fuel vaporization from fundamental data is frustrated by the complexity of gasoline composition. Consequently, experimental studies were needed to augment the simplified analytical studies that had been conducted in Phase I, and to guide the selection of improved induction system components.

OBJECTIVES

The objectives of this Phase II study were to obtain experimental data on droplet impaction characteristics, fuel-film flow on manifold walls, and fuel vaporization for a better understanding of induction-system phenomena; and to evaluate the potential of improved fuel atomization, fuel vaporization, and intake manifold design for improving air-fuel mixing and distribution.

SUMMARY OF STUDY

The Phase II program was primarily experimental. The study included three major tasks: development of instrumentation for measuring mixture properties, experimental studies of induction-system phenomena, and conception of a prototype improved induction system. A fourth major task, construction and demonstration of the prototype improved induction system, was originally part of the planned program but had to be eliminated when the first two tasks required more time and effort than was anticipated.

Development of Instrumentation

Instrumentation and procedures were investigated to measure the amount of fuel in droplet and vapor form in the air-fuel mixture stream and the amount of fuel on the manifold-passage walls. A single-stage impactor

probe was developed to separate the liquid and vapor while sampling from the mixture. The sampled liquid and vapor streams were analyzed separately for fuel concentration using a Flame Ionization Detector Hydrocarbon Analyzer. An elaborate apparatus was set up to obtain accurate flow measurements of the sampled gas quantities and to maintain all fuel in vapor form for the analyzer. A previous method tried for fuel concentration measurements, using gas-chromatography equipment, was unsuccessful.

After considerable data were accumulated using the impactor sample probe it was found that, under certain conditions, the probe was intermittently failing to fully separate the fuel vapor and droplets. At this point a non-separating sample probe was introduced and only the total entrained fuel was sampled and measured.

A fuel skimmer system was developed to trap and measure the fuel on the manifold-passage walls. With this system, fuel having deposited on the walls of the manifold elbow or passage was pulled by vacuum through porous-metal inserts in the walls at the passage outlet and subsequently condensed and weighed.

Experimental Studies

Studies were conducted to measure the amount of fuel impacting on the walls of various manifold geometries under different operating conditions. To accomplish this, a laboratory flow system was developed to provide a simulation of the fuel and air mixing and flow in an automotive induction system. Manifold test sections of different bend radii, bend angle, and surface roughness were used in the experiments. A spinning-disk-atomizer mixture generator was used to generate fuel droplets of about 14 microns mean diameter for the laboratory flow system.

Liquid-film transport on the manifold walls was observed visually under the different geometry and operating conditions. The amount of fuel flowing on the manifold walls was measured by the fuel skimmer system developed in the first task of the program. Fuel entrained in the mixture stream was measured using the sampler probe and measurement system also developed in the first task.

Fuel vaporization from entrained droplets and from the manifold walls was also studied to a limited extent in the laboratory flow system, both by heating the air entering the apparatus and by means of a special heated test section.

Improved Induction System Design Concept

Sketch layouts were prepared of a recommended improved fuel-atomization system, a low-impaction intake manifold, and a fuel vaporization chamber. The fuel atomizer and intake manifold were sized to fit under the hood of a standard size automobile. The fuel vaporization chamber was conceived as a laboratory experimental tool.

CONCLUSIONS

The results of this Phase II experimental study have led to the following conclusions with respect to induction-system phenomena and directions to be taken in future development efforts:

- (1) Droplet impaction in an induction system can be minimized by ultrafine atomization, minimum manifold-passage turning angle, long bend radii, and low air velocity. However, it does not appear possible to avoid appreciable droplet impaction, even with mean droplet sizes as low as 14 microns, because of deposition by flow-induced air turbulence. Twenty to fifty percent droplet impaction, depending upon air velocity, was observed in a 1-foot long straight test section with 14-micron droplets.
- (2) Accordingly, while improved fuel atomization and the design of manifold passages for low droplet impaction can probably improve mixture distribution, these design features alone are not sufficient to avoid an appreciable fuel-film accumulation on the passage walls, and the attendant fuel "hangup" and possibility of maldistribution. Therefore, it is concluded that fuel vaporization should also be employed

to some extent in the design of advanced carbureted induction systems.

- (3) Fortunately, ultrafine fuel atomization also promotes rapid fuel-droplet evaporation. It appears that 14-micron fuel droplets, as used principally in this study, may approach complete vaporization in residence times typical of low-speed engine operation with current induction-system design. Also, it appears that droplet vaporization may be appreciable even at in-manifold residence times consistent with moderately high-speed engine operation. Accordingly, the use of preheated intake air, preferably above the dew point of the mixture, is highly desirable. (The increase in air density resulting from the cooling effect of fuel vaporization more than offsets the displacement of air by fuel vapor and should result in an increase in engine volumetric efficiency.)
- (4) Tests conducted with a test section heated to 190 F resulted in effectively alleviating most of the wall fuel-film that would have accumulated under conditions when droplet impaction would otherwise have been substantial. This is probably due to the combined effects of vaporization directly off the test-section wall and increased droplet-vaporization resulting from increased air temperature. Accordingly, it is concluded that moderate, uniform manifold heat is adequate to virtually eliminate the unavoidable wall fuel-film in an improved-atomization, low-impaction system.
- (5) The most promising approach to the design of a carburetion-type induction system appears to be through the use of the following features:
- A fuel atomizer capable of producing droplet sizes in the range of 20 microns and smaller.
 - The use of preheated intake air (100 F or higher).
 - Intake manifold design for minimum turning angle, long bend radii, and moderate air velocity.
 - Good mixing and long residence time in the mixture generator, ahead of the manifold.

- Moderate, uniform manifold heat (in the range of 190 F).
- (6) The design approach preferred by the project staff incorporates the following design features:
- An air-atomizing fuel nozzle operating on the ultrasonic Hartmann-whistle principle.
 - A mixing section similar in construction to a can-type combustor.
 - An unconventional throttle valve: either a plug valve between the mixture generator and intake manifold or a butterfly valve upstream of the mixture generator.
 - A single-plane intake manifold with a separate branch for each cylinder having equally spaced, equal-area, radial entrances.
- (7) Experimental techniques for sampling fuel/air mixture properties need further development. Our understanding of droplet impaction phenomena is far from complete; however, further knowledge in this area is not of crucial importance at present, since it is evident that droplet impaction cannot be avoided completely under any circumstances. Further experimental information on fuel-droplet vaporization could be of considerable help at present in advanced induction-system design.

RECOMMENDATIONS

(1) Experimental studies of fuel-droplet transport and vaporization should be continued in support of advanced induction-system development. Fuel-droplet vaporization should receive primary emphasis at this time.

(2) Design and development of advanced induction-system concepts based on present knowledge should be carried out expeditiously. Detail design, fabrication, and experimental evaluation of the preferred system concept presented in this report is recommended.

EXPERIMENTAL WORK

The objective of the experimental program was to determine, by actual measurements, the effects of droplet size, manifold geometry, and operating conditions on droplet impaction, wall-film characteristics and fuel vaporization characteristics. The approach taken to accomplish this was to construct an air- and fuel-flow system to simulate the mixing and flow of air-fuel mixtures through manifold passages.

A system was developed to accomplish these objectives. However, actually obtaining meaningful measurements of mixture quality turned out to be far more difficult than anticipated. Many problems were encountered, both in developing the air- and fuel-flow system and in developing measurement techniques. As a result, not all of the objectives of the program were fully met. However, it is believed that the experimental results that were obtained represent new and useful insights into induction system phenomenon.

The topics covered in this section of the report include: the laboratory flow system manifold test-section geometries, fluids used in the experiments, mixture quality measurement, the experimental studies performed, and the results of these studies.

The Laboratory Flow System

Performance Criteria

The aim of the laboratory flow system was to simulate air and fuel flow characteristics as they occur in real induction systems, but under conditions that could be controlled, measured, and varied. Specifically, it was desired to simulate the flow through a single branch of the manifold on a 300 CID engine from idle to maximum speed for different engine load conditions, over an air/fuel ratio range from about 12:1 to 20:1, and using fuel droplets from about 20 μ up to at least 100 μ in diameter. Additionally, it was desired to control the temperature of the air entering the system over a range from 80 F to 150 F.

Descriptions of Components

Figure 1 is a schematic of the laboratory flow system showing the major components and subsystems. The major components are: the air flow system, the fuel system, the mixture generator, the air preheater, and the discharge burner. These will be described in the following paragraphs. Shown also in Figure 1 are the test section and the sample-probe section. These are described in other sections of the report.

Air Flow System. The air flow system consists of a flow-inlet section, a flow-control section, and a high-vacuum pump.

Air flow through the laboratory system is filtered and metered at the flow-inlet section. Four dry-type automotive air filters were clamped together to provide effective filtration with low pressure loss. At the maximum system air flow of 93 scfm, this pressure loss is 5.3 in. H_2O .

Average system air-flow rate is measured with an ASME square-edged orifice meter in a 1-1/2-inch pipe with 1 D and 1/2 D taps. An air-flow range of 3 to 100 scfm can be measured with this meter with an accuracy of ± 0.75 percent using one of three orifices having orifice diameters of 0.400, 0.860, and 1.239 inch. With the largest orifice, the differential pressure at maximum system air flow is 15.3 in. H_2O .

Computed flow vs pressure differential data for the orifices used in the experimental program are presented in Appendix B, Figure B-1. These data were calculated using equations from Fluid Meters⁽²⁾ for standard ASME square-edged orifice meters.

Vacuum in the test section is controlled by a gate valve located downstream of the air-flow orifice meter. Higher vacuum can be obtained by closing this valve. With the valve wide open, minimum vacuum in the test section is fixed by the flow losses from the air-filter inlet to the test-section inlet. At the maximum system air flow, this minimum vacuum in the test section due to flow losses is 2.7 in. Hg.

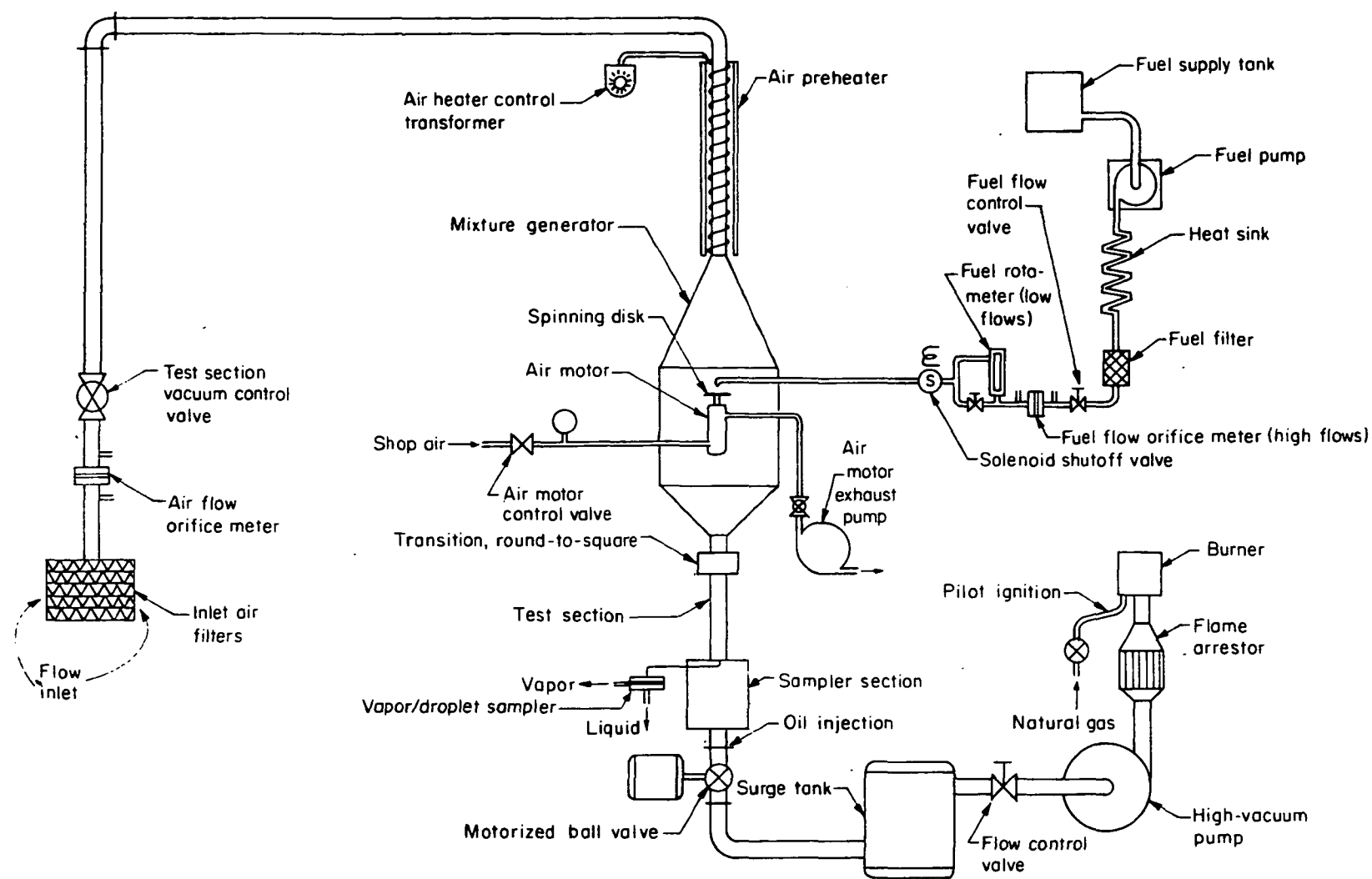


FIGURE 1. SCHEMATIC OF LABORATORY FLOW SYSTEM FOR INDUCTION SYSTEM FUNDAMENTAL STUDIES

A ball valve driven with an electric motor is used to produce pulsating flow in the test section. A standard 2-in. ball valve with "Teflon" seats was modified for use at driven speeds up to 1400 rpm. A central shaft was added to support the ball, which is normally supported only by the "Teflon" seats. The seats were lightly loaded against the ball with wave springs. A small amount of oil is injected into the air flow system immediately upstream of the ball valve to lubricate the ball.

The performance of the ball valve was evaluated in the laboratory flow system with the flow and vacuum control valves set for maximum flow. The ball valve was operated at several different speeds and the flow velocity was measured at the test section inlet with a Thermal Systems hot-wire anemometer. Average flow rates were measured with the flow system orifice.

Figure 2 shows oscilloscope traces of the flow velocity-time data from the hot-wire anemometer. Average flow rates for the six ball-valve speeds are as follows: 62.5 scfm at 400 rpm, 58 scfm at 760 rpm, 66.5 scfm at 800 rpm, 69.5 scfm at 1000 rpm, 68 scfm at 1200 rpm, and 64.5 scfm at 1400 rpm. The average flow increased with increasing speed up to 1000 rpm. Beyond that speed the average flow decreased slightly. An operating speed of 1000 rpm was selected for the test program as yielding the maximum average air flow with an acceptable velocity-time curve shape.

Figure 3 shows that the time variation of the pulsating flow produced by the ball valve is expected to simulate something between that existing in a manifold runner and that existing in a manifold branch. At 1000 rpm the ball valve will produce a pulsating frequency equivalent to that in a manifold branch at 4000 rpm engine speed or in a manifold runner at 2000 rpm engine speed.

A 30-gallon surge tank is used to dampen the flow surges caused by the vacuum pump. At the maximum system flow, the amplitude of the pressure pulses in the surge tank was calculated to be about 1/2-in. H_2O .

Air flow in the laboratory apparatus is controlled with a flow-control valve mounted between the vacuum pump and the surge tank as shown on Figure 1. Maximum system air flow is obtained with this valve wide open and is a function of the capacity of the vacuum pump and the system pressure losses. Flow can be reduced by partially closing the valve and thereby reducing the density of air

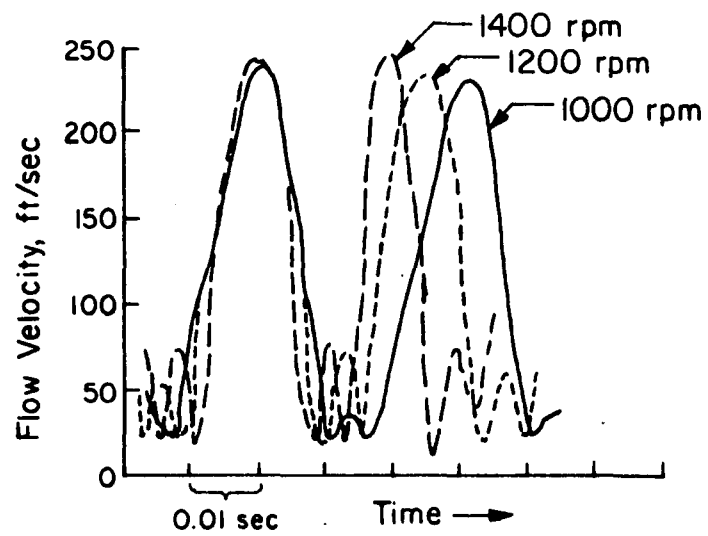
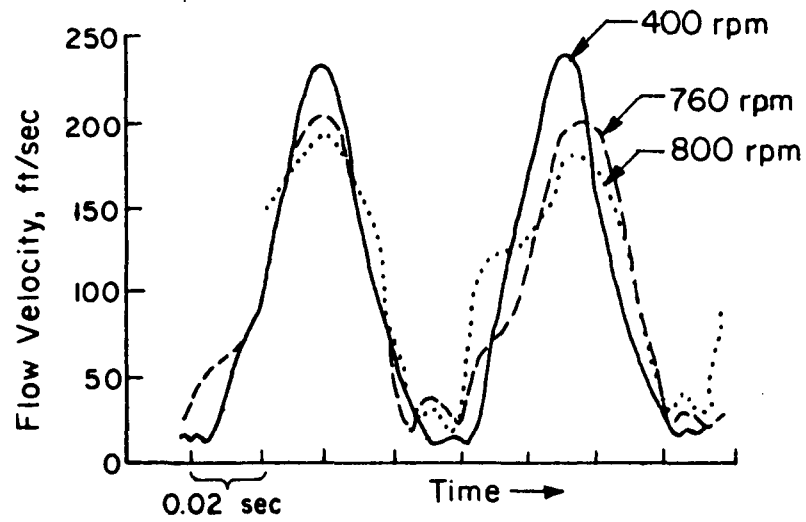


FIGURE 2. OSCILLOSCOPE TRACES OF PULSATING FLOW

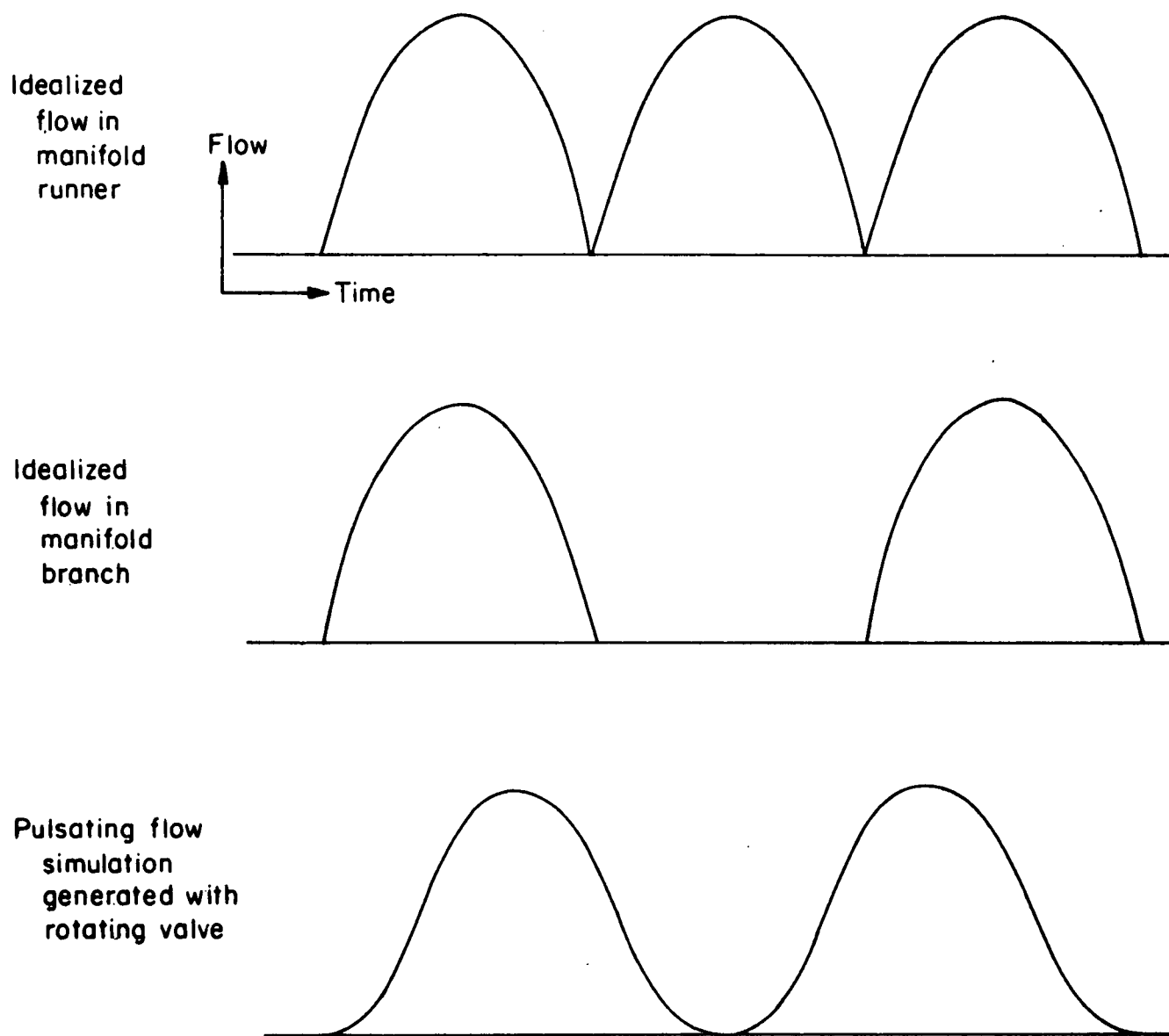


FIGURE 3. TIME VARIATION OF PULSATING FLOW

at the inlet to the pump. System air flow is directly proportional to air density at the vacuum pump inlet because the pump is a constant-volumetric-displacement machine.

Air is pumped through the laboratory system by a rotary-vane, high-vacuum pump which was available in the lab. The pump is equipped with a closed-cycle, cooling-oil system for high vacuum operation. For use in the laboratory flow system, the oil that is injected into the pump inlet is not collected and returned to the pump but is burned with the fuel vapor. Proper vane lubrication can be achieved with a very low oil flow.

The pump volume flow is relatively constant at 115 cfm referenced to the inlet vacuum condition. A vacuum of 20 in. Hg or lower can be produced at the test section. The maximum system air flow with minimum system restriction is 93 scfm or 7.1 lb/min.

Figure 4 shows the relationship between air flow and manifold vacuum for the laboratory flow system operating at both steady and pulsating flow conditions. To develop these curves, the flow control valve was fully opened and the vacuum control valve was adjusted at various settings from nearly closed to fully opened. The vacuum was measured at the manifold test section.

The representative carburetor flow curve included on Figure 4 depicts the flow through one barrel of a two-barrel carburetor fitted on a 283 CID V-8 engine. The air flow capacity of the laboratory flow system approximately matches this representative carburetor flow curve with pulsating flow, and greatly exceeds it at steady flow.

Other types of air pumps were considered in the design of the laboratory flow system but none were considered as suitable as the present arrangement with a steady-flow vacuum pump and motorized ball valve. One alternative arrangement considered was a motored automobile engine equipped with a modified manifold. This setup was judged to be a relatively expensive installation even if set up with an inexpensive, used six-cylinder engine because of the setup time and the long-term use of a motoring dynamometer facility. The engine could be motored with a 10 to 15 hp electric motor but the speed range would then be limited. Manifolds would have to be fabricated to connect the intake ports of the active cylinders to the test section and the exhaust ports to the fuel-vapor burner.

Another alternative arrangement of air pump considered was a large, reciprocating vacuum pump. Rotational speed of most reciprocating vacuum pumps is limited to about 1000 rpm, which would provide simulation of the flow in a manifold branch at 2000 rpm engine speed, but would provide simulation of the pulse frequency in a manifold runner at only 1000 rpm engine speed. In addition, single cylinder compressors with adequate capacity were judged to be too expensive.

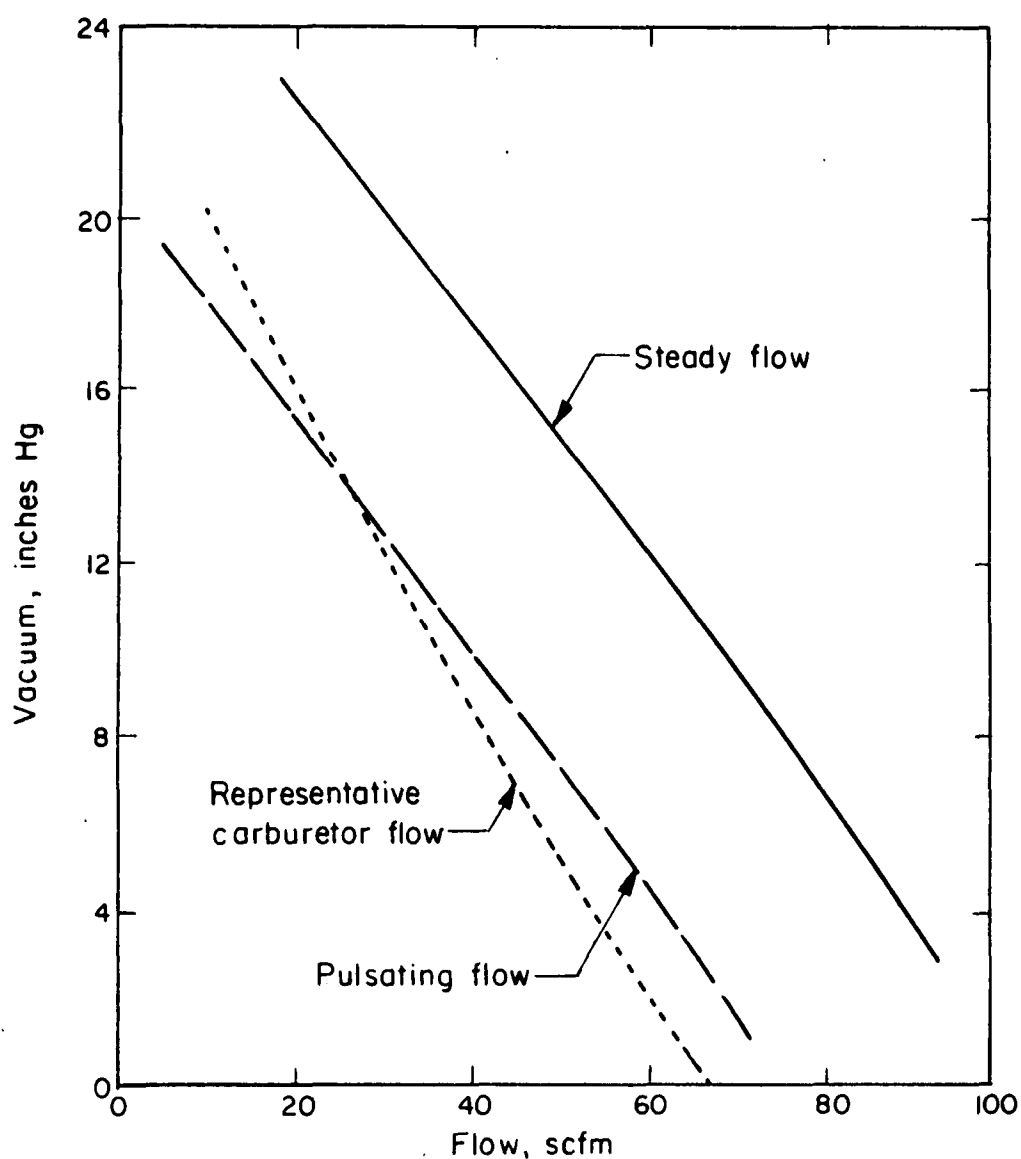


FIGURE 4. AIR FLOW CAPACITY OF LABORATORY FLOW SYSTEM

An arrangement with two inexpensive two-cylinder compressors coupled together with a timing belt was also considered. Compressor intakes could be connected together to provide simulation of the wave forms of the pulsating flow in either a manifold branch or runner. Operation at 1500 rpm was felt to be feasible by increasing the size of the intake valves. Further consideration of this two-compressor arrangement was dropped when the large rotary-vane vacuum pump became available.

Fuel System. Fuel is supplied to the atomizer in the laboratory system with a centrifugal transfer pump which has a stable flow range of 0 to 240 gal/hr. Pressure rise at zero flow is 13 ft of fluid being pumped. Seal leakage between motor and impeller is eliminated with a magnetic coupling.

Fuel is pumped from a 55-gallon container, installed outside the building, into a heat sink to bring the fuel to room temperature. Following the heat sink, which consists of a coil of 1/4-in. copper tubing, the fuel is filtered in an automotive fuel filter. Fuel flow rate is controlled with a precision flow control valve following the filter, and is measured with a rotameter. A fuel rate of about 4.6 gal/hr is required to provide a 15:1 air-fuel ratio at the test section at maximum system air flow. Following the meter, the fuel flows through a solenoid shut-off valve and into the atomizer. This valve is used to prevent the fuel from draining back to the supply tank when the transfer pump is shut off.

A calibration curve on the rotameter used for fuel flow measurement is presented in Appendix B, Figure B-2. This calibration curve was obtained using Stoddard Solvent.

Mixture Generator. Figure 5 is a layout drawing of the mixture generator showing locations and orientations of its components. The housing consists of a cylindrical center section with conical expansion and contraction sections upstream and downstream. The cylindrical portion contains a spinning-disk atomizer with supporting members and a fuel feed system. A collector is provided at the outlet to remove fuel from the flow system which has impacted on the wall of the mixture generator. The overall length of the system is 24 inches. All joints are leak-tight with neoprene gaskets or O-ring glands.

The center cylindrical section is 9 inches in diameter and formed from "Lucite". Fuel which does deposit on the walls is removed at the exit from the downstream conical section by a "skimmer". This is simply an annular space into which the fuel is collected externally in a small chamber where it can be measured either by weight or volume. Pressure equilization between this chamber and the mixture chamber allows the fuel to flow freely.

Figure 6 is a detail sketch of the fuel skimmer system. While setting up equilibrium conditions for a run, Valve 1 is closed and Valve 2 is open so that fuel collecting in the skimmer is continuously purged out. When making a run at steady state conditions, Valve 2 is closed and Valve 1 is open. The vacuum draws fuel into the graduated cylinder from the skimmer. The time is recorded to reach a predetermined volume. The rate at which fuel is drawn from the skimmer chamber by the vacuum is adjusted carefully so that only liquid fuel and not vapor is pulled from the mixture chamber. This is accomplished by maintaining the skimmer fuel flow just below the point where bubbles begin to appear.

The major component in the mixture generator is the spinning-disk atomizer. The aluminum disk itself was machined in the shape of a low-height inverted cone with a thickness of 15 mils at the outside edge and an integral shaft on the underside. The disk is driven by an air turbine at speeds up to 85,000 rpm.

The head or top portion of a commercially available air turbine* was replaced with a specially designed section which traps air leakage from the turbine and prevents its escape into the mixture generator. A vacuum pump is used to maintain a negative turbine-exhaust pressure to increase the maximum-speed capability of the turbine and to make it possible to adjust the pressure in the turbine head so that it equals the pressure in the mixture generator. Pressure taps in the turbine head and the wall of the mixture generator are connected to a manometer so that the pressure difference can be adjusted to zero.

The motive air for the turbine is controlled up to 90 psig and enters at the bottom of the turbine through one of the supporting tubes. A second symmetrical supporting tube at the bottom serves as a line to the manometer for the head-pressure equalization scheme. The motive air exits through supporting tubes at the upper end of the turbine.

* ARO Corporation Model No. 7980.

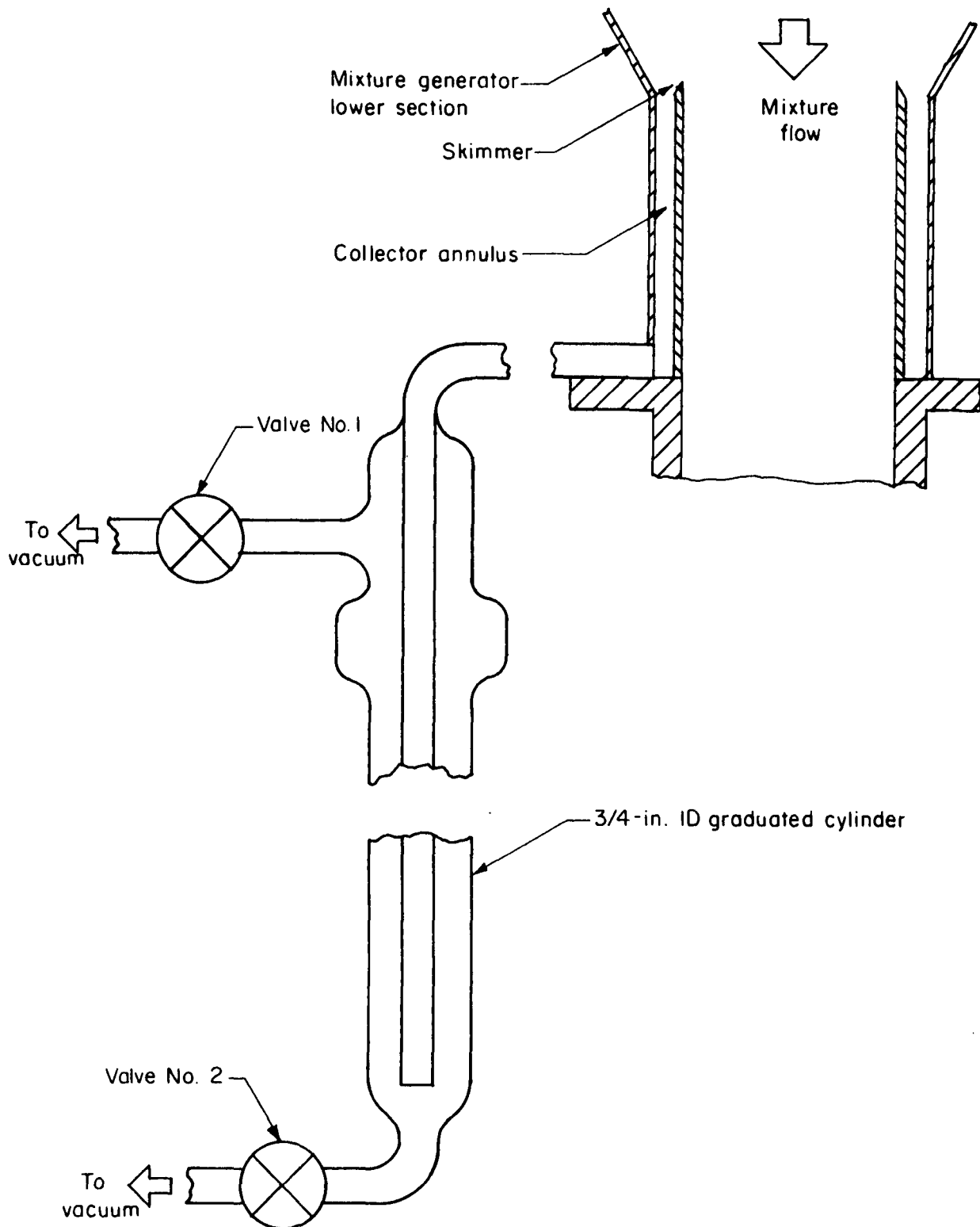


FIGURE 6. DETAIL OF MIXTURE GENERATOR FUEL SKIMMER SYSTEM

The rotational speed of the turbine is monitored by a Strobotac connected to an electronic counter.

The fuel enters through a tube above the spinning-disk and passes down onto the center of the disk through a hypodermic needle. It is important that this needle be located at the center of the disk; otherwise uneven and slugging atomization results.

The range of fuel-feed rates possible with this system is up to 50 lb/hr. An upper limit of 25 lb/hr is required to provide an air-fuel ratio of 20:1 for the air-flow rates planned for the experimental program.

The spinning-disk atomizer proved to be unacceptably noisy when operated at the high speeds which were necessary to obtain small droplet sizes. After spending some time attempting to pinpoint the cause of the high noise level and attempting to isolate the atomizer from the mixture-generator housing components, we concluded that the only solution was to enclose the entire system. To this end a "soundproof" box was built around the mixture generator including the conical metal transition sections before and after the atomizer housing. This box consisted of an outer shell of 3/4-inch plywood, a layer of 0.065-inch lead sheet, and 2 inches of foam plastic. The box was made in two halves hinged together so that access to the mixture generator for service and adjustments would be facilitated. A window on one side permits observation of the spray patterns and monitoring of the disk speed when in operation.

Other problems with the spinning-disk atomizer included an air-motor bearing failure and air leakage at the top bearing. The failed bearing proved to be defective and was replaced. The air-leakage problem was solved by attaching a vacuum pump to the air motor exhaust and to a "trapping" chamber built onto the air motor at the top bearing. The vacuum in this trapping chamber was maintained equal to the vacuum in the atomizer chamber by means of a control valve, so that no leakage of air or air-fuel mixture would occur between the two spaces.

An attempt was made to operate the air motor and disk upside down so that tubes and supports in the mixture flow path could be eliminated. A uniform spray pattern could not be achieved under these conditions.

A large percentage of the fuel atomized by the spinning disk deposited on the mixture generator walls before it could enter the test section. This was particularly true at low flow rates. The diameter of the mixture generator housing was originally selected after observing the atomization pattern in quiescent air. However, the droplet trajectories turned out to be quite different when the atomizer was operated in the mixture generator. The primary causes of the high rate of impaction appeared to be the relatively low axial air-flow velocity in the chamber, a radial air flow created by the spinning disk, and a swirl pattern also created by the spinning disk.

A means was finally devised to eliminate or minimize the above-mentioned phenomena. Modifications were made to the mixture generator and the results appeared favorable.

Figure 7 is a sketch of the mixture generator center section showing the modifications. A 6-1/4-inch diameter baffle was installed in the center of the chamber in two sections, one above the disk and the other below the disk. A 1-inch spacing was provided between the two sections for the spinning disk and fuel spray. Each section was split in an axial plane so it could be installed without disturbing the air motor and tubing. Both sections were closed and sealed at both ends. Six equally spaced vanes were longitudinally mounted in the 1-3/8-inch annular flow passage between the baffle and chamber wall.

The narrow space between the baffle sections provided relatively quiescent air for the fuel spray to pass through which reduced their trajectory length. The smaller flow area provided by the annulus passage increases the air and mixture velocity considerably, a factor which would also reduce the amount of vaporization occurring in the mixture generator. The longitudinal vanes prevented a swirl pattern from developing, although they undoubtedly become impaction surfaces in themselves. Loss of fuel droplets to the mixture generator walls was considerably reduced by the baffle and guide vanes, although the size of the droplets entering the manifold test sections appeared to be unchanged.

Air Preheater. Air temperature at the test section is controlled by heating the air to a constant value in an electrical resistance heater. The heater is a 4-foot length of 1-1/2-in. diameter pipe which is wrapped with two

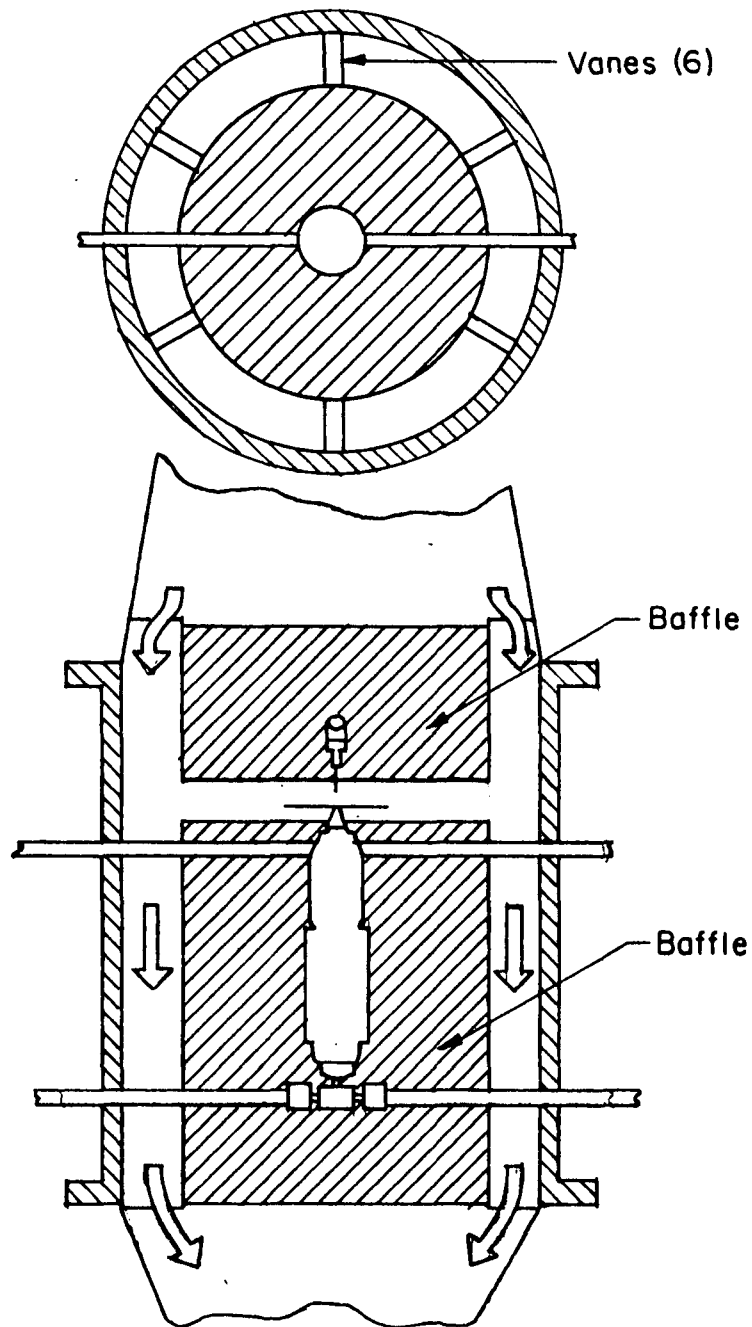


FIGURE 7. MODIFICATION TO MIXTURE GENERATOR
TO REDUCE IMPACTION

768-watt heating tapes and insulated with 1-1/2-inch thick high-temperature insulation. Maximum heater-tape temperature is 900 F. Power input to the heater is controlled with a Variac autotransformer, which varies the voltage input.

Temperature of the room air can be increased 59 F at 53 scfm and 41 F at 90 scfm. Heater effectiveness, expressed as heat transferred to the air divided by input power, is 73 percent at 53 scfm and 86 percent at 90 scfm.

Discharge Burner. Fuel and oil vapors are disposed of in a burner connected to the vacuum pump outlet. The burner is set up with a continuous natural-gas pilot flame and has a weighted poppet valve at the inlet to prevent flash-back.

A flame arrestor is installed between the burner and the vacuum pump as an additional precaution against explosions. The flame arrestor has an aluminum matrix which quenches the flame by cooling.

Figure 8 is a sketch of the burner showing the anti-flashback poppet valve.

Manifold Test Section Geometries

Requirements

One objective of the experimental work was to obtain verification of the analytical predictions of droplet impaction, fuel-film, and vaporization characteristics made during the Phase I study. Consequently, the manifold geometries selected for this study were based on the geometries described in the Phase I Report of April 30, 1969.⁽¹⁾

It was also required that the passage shape be similar to actual intake manifold passages, and that the cross-sectional area be selected in conjunction with the air flow system capacity to yield a maximum flow velocity equivalent to that which occurs in real manifolds.

Inside surfaces of real manifolds are rough from the casting process. Consideration was given to attempting to duplicate this roughness in the experimental manifold test sections. It was believed that surface condition has very little influence on the droplet impaction phenomenon. Therefore, it was decided

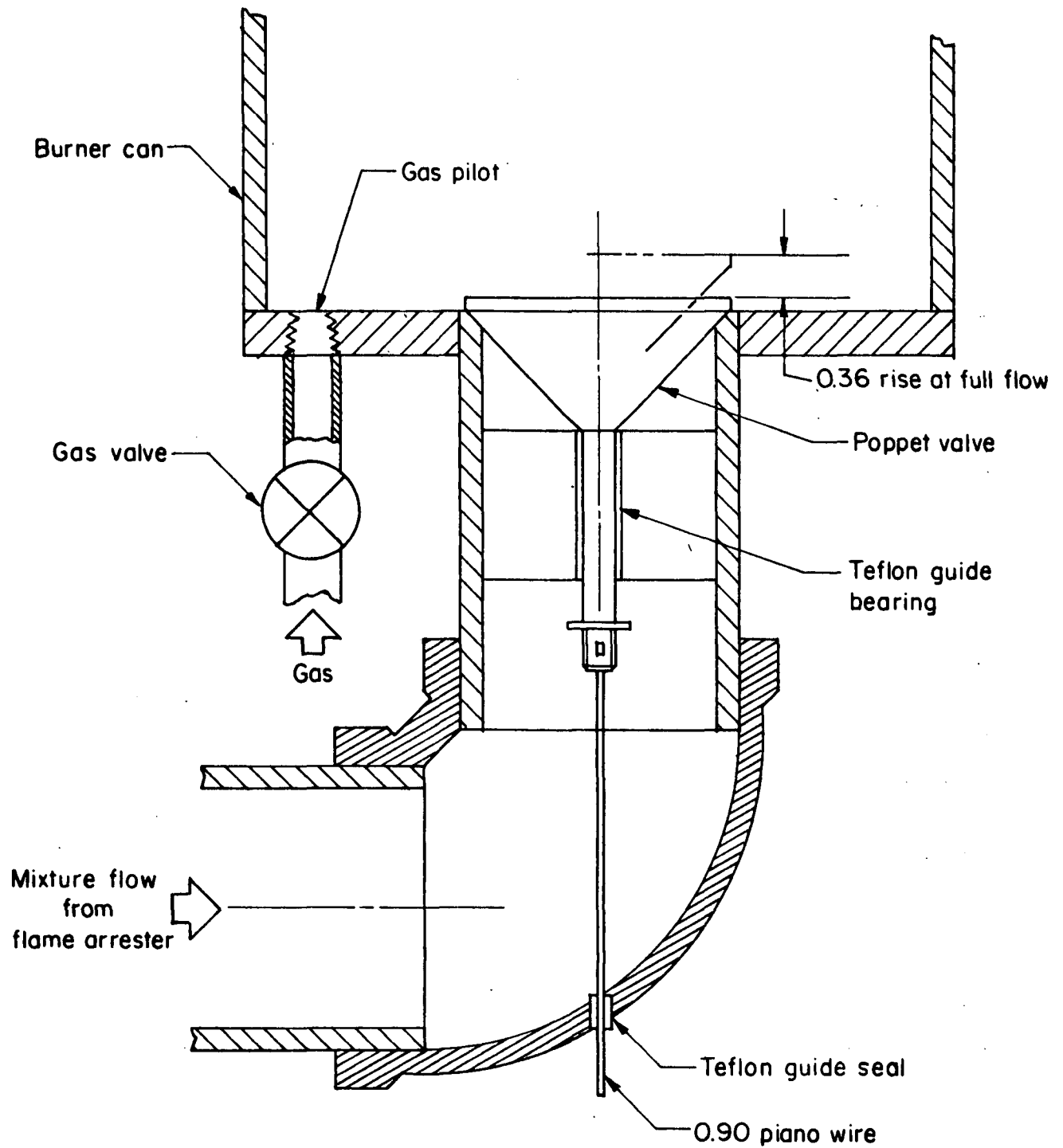


FIGURE 8. DETAIL OF DISCHARGE BURNER

to select the material for the majority of the test sections for other considerations such as ease of construction and transparency for observing the wall fuel-film flow patterns. However, surface roughness could play a significant role in fuel-film transport and in reentrainment, thus, one test section was provided with rough surfaces.

Description of Manifold Test Sections

Test sections for the impaction studies were fabricated from 1/4-inch thick, clear acrylic-plastic sheets glued together to form a square duct. Side walls were machined with the circular-bend outline and then the top and bottom walls were heated and bent to conform to the side wall radii. With this construction, elbows with constant cross sectional area with the desired bend radii were easily fabricated. These test sections with square cross section provide a reasonable simulation of rectangular intake-manifold passages used on many engines. The transparent walls facilitated visual observations of flow phenomena.

Table 1 gives pertinent geometry of the available test sections. The 1-1/4-inch width was judged to be about minimum size compatible with practical vapor/droplet sampling probes. The length of each test section was fixed at 1.0 ft to approximate the length of a single manifold passage in a V-8 engine intake manifold. All test sections were made the same length so that droplet impaction measurements would reflect only the influence of bend angle, radius and wall surface texture.

As noted in Table 1, the walls of one of the test sections were roughened to simulate a sand casting. This was accomplished by brushing the acrylic plastic with a steel brush soaked in acetone solvent. The rough-surface section duplicated a test section with smooth surfaces so that a direct comparison could be made of the effects of surface condition.

Drawings of the clear plastic manifold test sections used in the experimental program are shown in Figures 9A to 9C.

The aluminum instrumented test section listed in Table 1 is also a duplicate of one of the clear-plastic test sections. This section, when mounted in the flow system, is wrapped with electrical heating tape so that all surfaces

can be heated to observe the effects of wall fuel-film vaporization. Ten thermocouples are mounted at strategic locations on the test-section surfaces to measure the wall temperatures. Figure 10 shows the locations of these thermocouples.

TABLE 1. GEOMETRY OF TEST SECTIONS

Cross Section Shape	Duct Width, in.	Outer Bend Radii, in.	Bend Angle, deg.	Surface Texture	Comments
Square	1-1/4	Infinite	0	Smooth	Straight duct for reference
Square	1-1/4	0	90	Smooth	
Square	1-1/4	4	90	Smooth	
Square	1-1/4	4-7/8	30	Smooth	
Square	1-1/4	4	90	Rough	
Square	1-1/4	4	90	Smooth	Aluminum instrumented test section for manifold heating tests

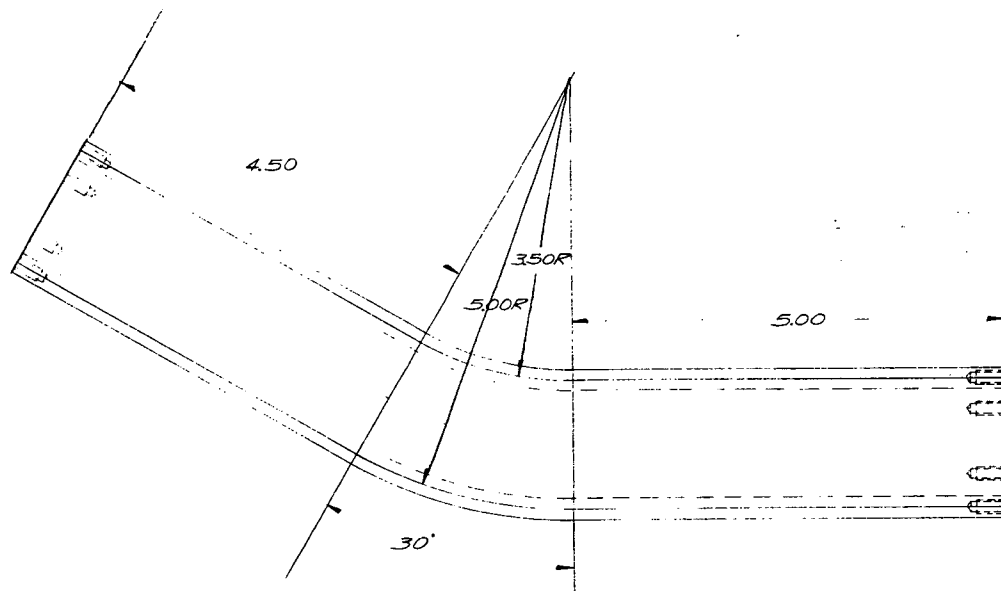
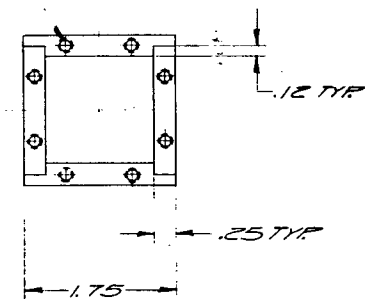


FIGURE 9A. 30-DEGREE, 4-7/8-INCH RADIUS MANIFOLD TEST SECTION

#5-40 NC-2B X .31 DEEP
8 HOLES LOCATED FROM
PART 0011 @ EACH END



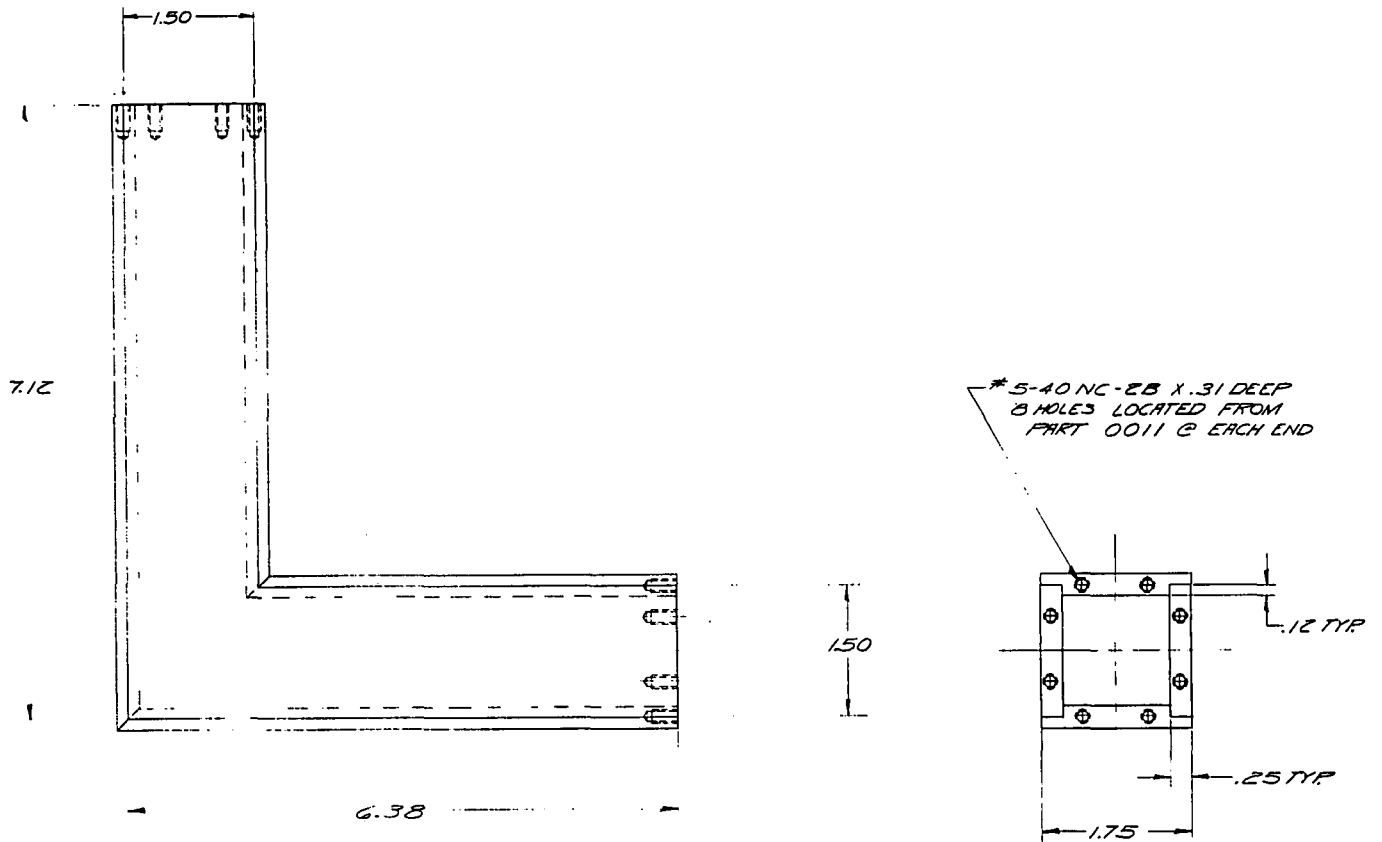


FIGURE 9B. 90-DEGREE, 0-INCH RADIUS MANIFOLD TEST SECTION

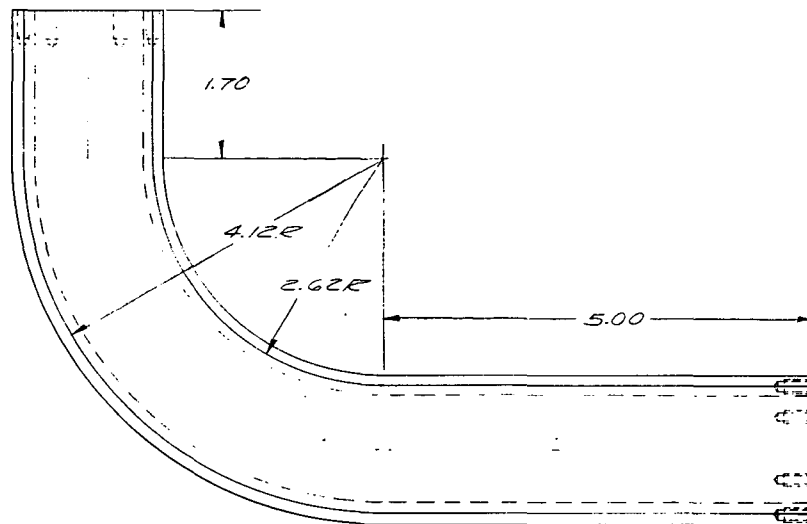
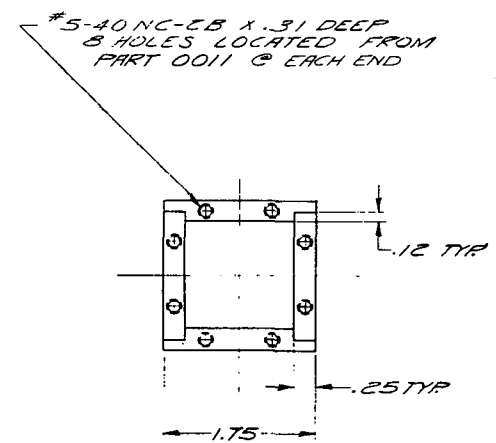


FIGURE 9C. 90-DEGREE, 4-INCH RADIUS MANIFOLD TEST SECTION



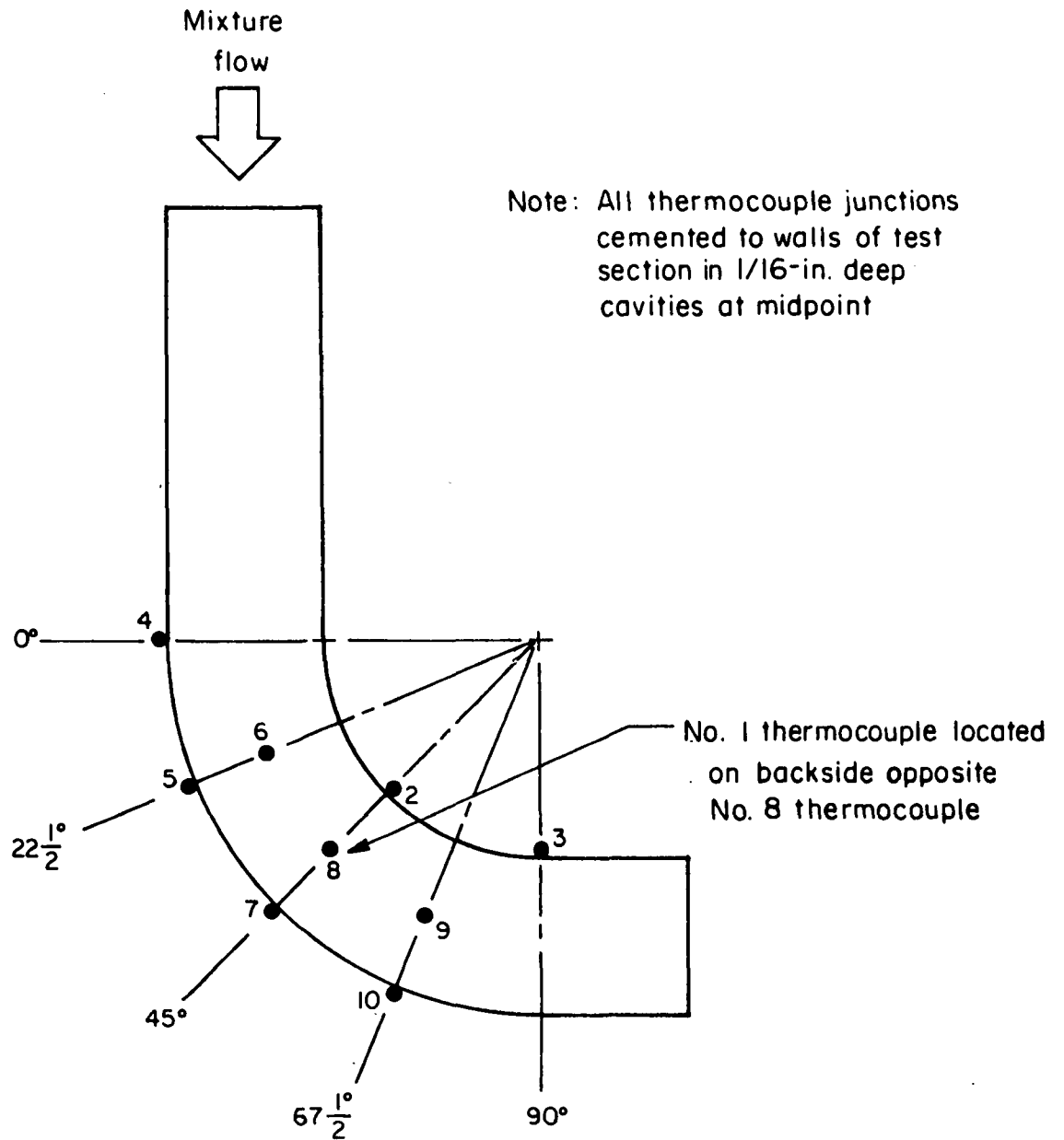


FIGURE 10. SKETCH OF ALUMINUM INSTRUMENTED TEST SECTION
SHOWING THERMOCOUPLE LOCATIONS

Discussion of Fluids

The impaction of gasoline on the walls of a manifold can be predicted by the use of dimensionless equations which have been shown to provide proper correlations. Except for density, the physical properties of the fluid do not apply in the correlations. Consequently, if densities are known and are reasonably close numerically, an alternate fluid can be successfully used for droplet impaction studies. For instance, the density of Stoddard Solvent is 48.8 lb/ft³ compared to 44.9 lb/ft³ for gasoline, thus, any correction for density would be small and probably not significant with respect to practical considerations.

A dimensional analysis indicates that three dimensionless groups control droplet impaction.⁽³⁾ These are

- Impaction parameter

$$K = (2\pi n)^{1/2} \left[\frac{\rho_d u_g}{18\mu_g D_m} \right]^{1/2} D_d$$

- Parameter characterizing non-Stokes law behavior

$$\phi = \frac{9\rho_g^2 u_g^2 D_m}{\rho_d \mu_g}$$

- Geometry of bend

$$R_b/D_m$$

Where:

n = number or fraction of 360-degree turns in bend

ρ_d = density of the droplet

u_g = velocity of the gas

μ_g = dynamic viscosity of the gas

D_m = manifold passage diameter

D_d = droplet diameter

ρ_g = density of the gas

R_b = bend radius.

The case for an ideal gas has been analyzed by Ranz⁽³⁾ and the results have been presented as a dimensionless correlation of impaction efficiency in two-dimensional ducts as a function of the impaction parameter, K , for various values of the combined parameter, $\Phi / (2\pi n)^2 (R_b/D_m)^2$.

Correlations for droplet impaction efficiencies using the dimensionless groups described above serve to predict deposition on the walls. Since this is the objective of the droplet impaction studies, the correlating techniques should prove to be satisfactory. There are, however, other phenomena occurring which cannot be modeled in such a direct manner.

The more difficult problems are concerned with reentrainment of drops from the tube walls, the flow in a liquid film along the walls, and vaporization of the fuel. These, of course, could be studied directly with a gasoline-air system. However, the important physical properties of gasoline can be identified and matched with a substitute fluid, or alternatively, differences in fluid properties can be accounted for by proper analysis.

Absolute vaporization rates should be studied directly with gasoline because the multi-component nature of gasoline makes this process difficult to analyze. The multi-component composition gives rise to vaporization rates which vary as a function of amount vaporized since the vapor pressure changes with the amount vaporized. However, knowledge of vapor pressures for various fluids will allow compensations to be made in vaporization rates if fluids other than gasoline are used.

In the additional areas of concern, film transport and reentrainment will be the same for an alternate liquid if the liquid viscosity and surface tension are similar to those for gasoline. Figure 11 shows a comparison between the viscosities of gasoline and n-heptane, one of the hydrocarbon compounds in gasoline. It is evident that in the temperature range of interest (60 - 80 F), the two fluids have viscosities that are nearly identical. Viscosity data for Stoddard Solvent were not available; however, its widespread use as a test fluid in carburetor development work would suggest that it has suitable properties. A comparison between the surface tensions for Stoddard Solvent, n-heptane, and gasoline is not easily made, again because of a lack of good data. However, most hydrocarbons of the types predominating in gasoline and Stoddard Solvent have very similar surface-tension properties.

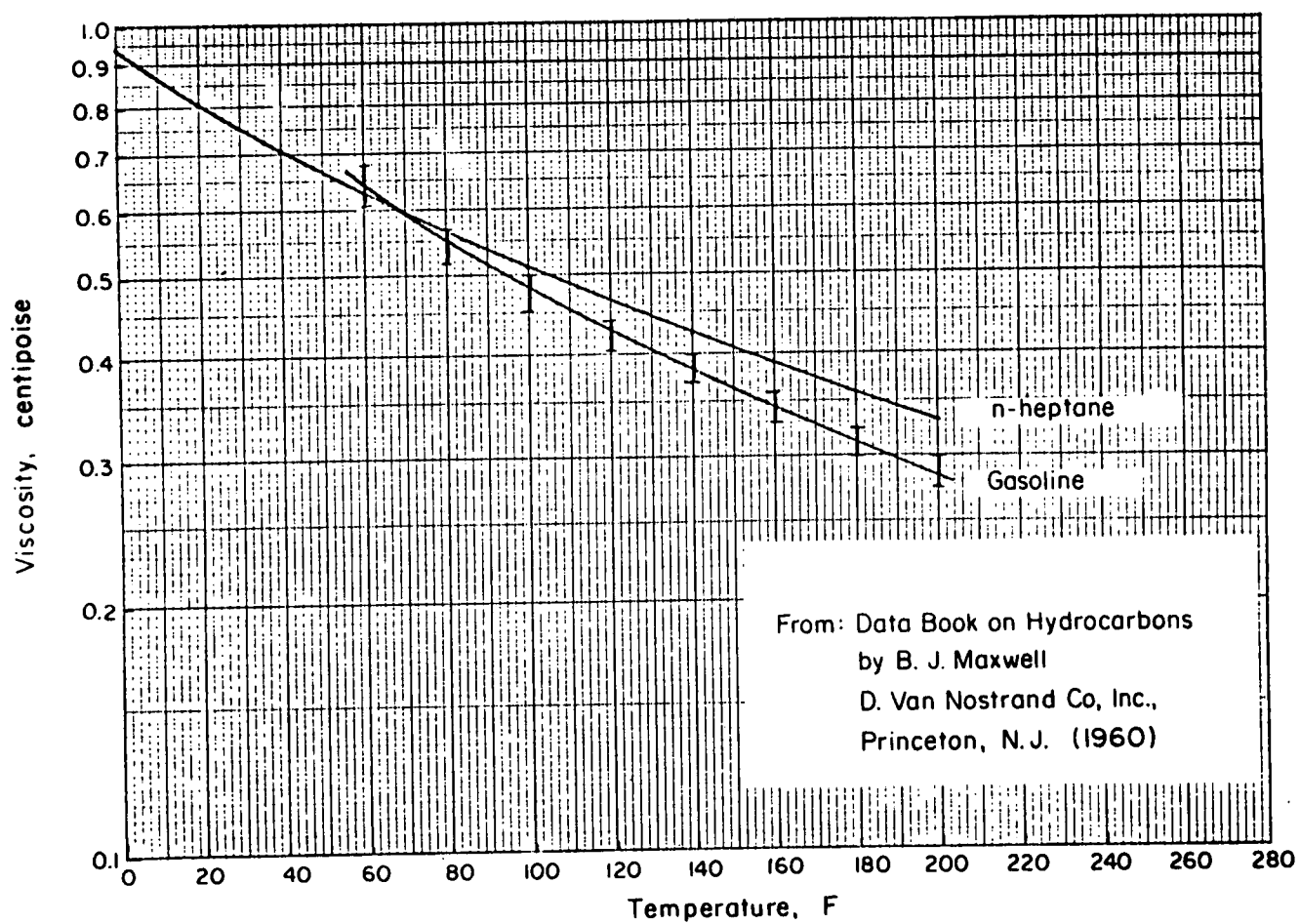


FIGURE II. COMPARISON OF LIQUID VISCOSITIES

The aromatic components are somewhat higher in viscosity than the paraffins but are less abundant in both gasoline and Stoddard Solvent. The following tabulation shows surface tension data for selected hydrocarbons and includes the value for water as a reference.⁽⁴⁾

<u>Hydrocarbon</u>	<u>Surface Tension dynes/cm at 72F</u>
n-hexane	18.2
n-heptane	20.0
n-octane	21.4
2 methylhexane (iso-heptane)	19.1
2 methylheptane (iso-octane)	20.5
2,2,4 trimethylpentane (iso-octane)	18.6
toluene	28.1
o-xylene	29.5
m-xylene	28.2
p-xylene	27.8
1,3,5 trimethylbenzene	28.5
1,2,4 trimethylbenzene	29.3
water	72.6

It is expected that the values for n-heptane and Stoddard Solvent should be very close to that for gasoline.

A comparison between gasoline and Stoddard Solvent can be made on the basis of distillation curves. Stoddard Solvent, like gasoline, is a grade of petroleum distillate, but generally of lower volatility than gasoline. The distillation curves for a typical gasoline (according to ASTM specification D484-52) and Stoddard Solvent (according to ASTM specification D-86) are compared in Figure 12. Stoddard Solvent can be considered as a high-boiling fraction of gasoline and as such should have properties similar to those of gasoline with the exception of vapor pressure.

The approximate composition of the Stoddard Solvent used in this study was 51.4 percent (by volume) paraffins, 39.8 percent naphthenes, 8.8 percent aromatics, and 0 percent olefins. By comparison, a "typical" pump gasoline

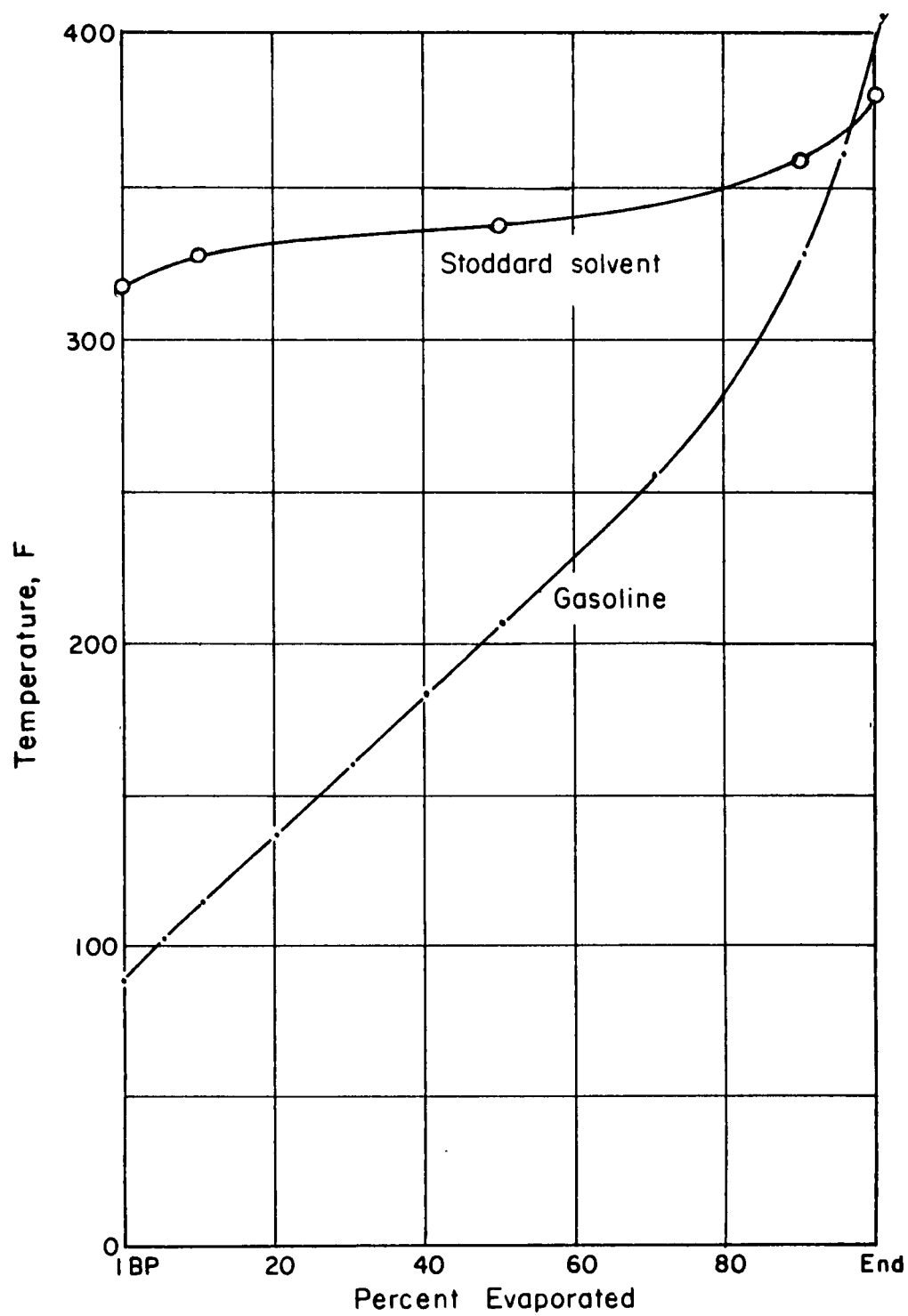


FIGURE 12. STANDARD DISTILLATION CURVES FOR A REPRESENTATIVE COMPOSITE GASOLINE AND FOR STODDARD SOLVENT

would contain about 59 percent paraffins, 0 percent napthenes, 31 percent aromatics, and 10 percent olefins.

From the comparisons between viscosity, density, composition, and surface tension, we believe that both n-heptane and Stoddard Solvent are suitable substitutes for gasoline in studies of droplet impaction, liquid film transport, and droplet reentrainment. We believe also that useful information can be gained by measuring vaporization rates for these fluids during the droplet impaction studies.

Mixture Quality Measurement

The requirements for the mixture quality measurements were primarily to assess the extent of impaction of fuel droplets on the walls of the test sections and to provide information on the distribution of fuel droplets in the cross section of the test sections. A secondary requirement was to allow measurement of the distribution of fuel between the vapor and liquid phases.

Several sampling techniques were considered as possible alternatives and two techniques were used. The sampling technique used for the reported measurements was a simple probe, which collected both drops and vapor at various positions in the test section cross-sectional area, coupled with liquid skimmers on the walls and liquid temperature measurements. Analyses of the collected samples were attempted by use of a thermal conductivity cell in a gas chromatograph, condensation with subsequent weighing, a F.I.D. hydrocarbon analyzer, and a combination of weighing and the hydrocarbon analyzer. The hydrocarbon analyzer alone was used for the reported measurements.

Vapor/Droplet Samplers

Several vapor/droplet sampler designs were used in attempts to separate liquid droplets from the mixture stream quickly in order to measure fuel content as vapor and as liquid. The premise behind these designs was that little vaporization of the liquid droplets could occur in a single-stage impactor because the residence time would be short before the liquid was separated from the air. Further, if the liquid droplets could be impacted on a surface from which they could be removed and measured, the remaining mixture

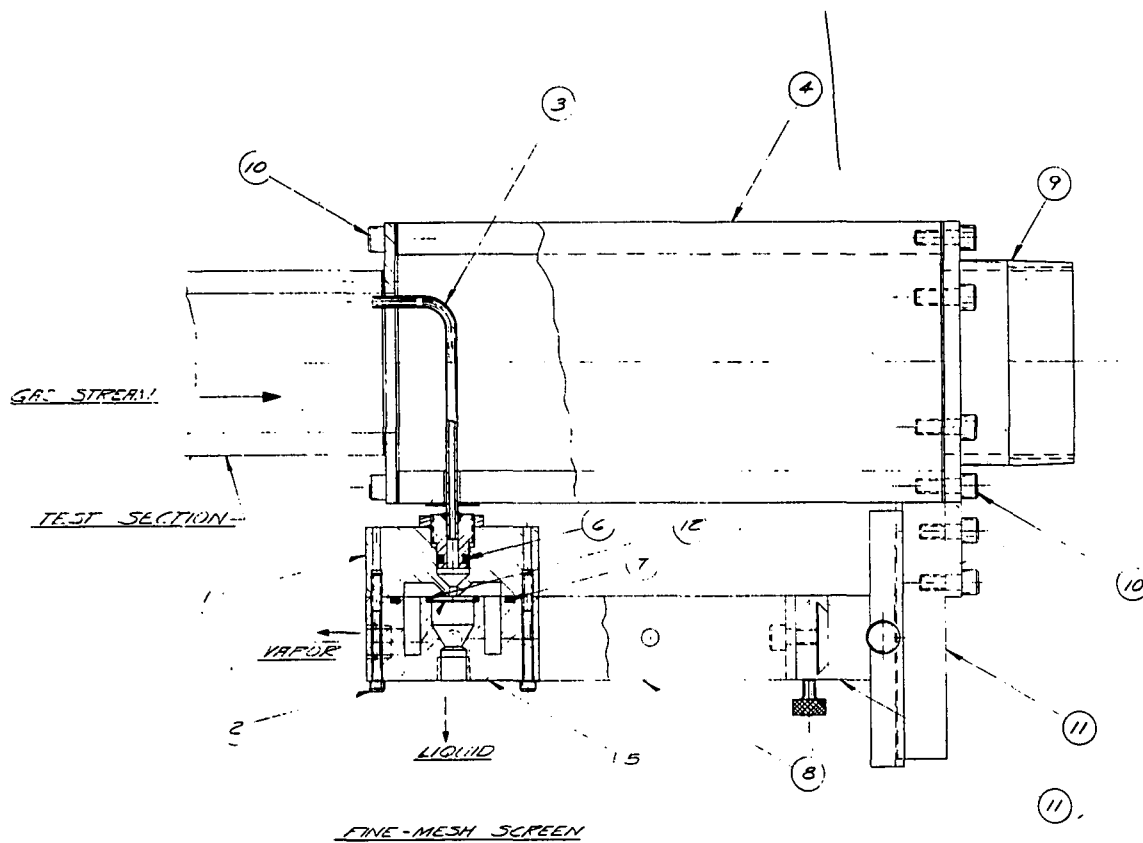
would contain only vaporized fuel. To accomplish this separation, several different impactors having a fine screen or wire mesh as an impaction surface were designed. These impactors are designated as Designs 1, 2, and 3 and are illustrated in Figures 13, 14, and 15.

A discussion of the procedures and principles used to design the impactor samplers for this study is given in Appendix A.

The design shown in Figure 13 was tested with and without air flow through the wire mesh impaction surface. This design was abandoned because there was found to be excessive loss of droplets to the walls of the probe which, because of the apparatus geometry, were up to 6 inches in length with one or two bends. Furthermore, experimental checks and analytical estimations indicated that if the fuel had not saturated the air stream at the point of sampling there could be significant changes in the liquid-vapor distribution of the fuel within the length of the sampling probes which in some cases were almost one-half as long as the test section.

The second impactor design, shown in Figure 14, was abandoned because of excessive loss of liquid to the wall on the vapor side within the impactor. The cause of this loss was assumed to be that the impaction surface (screen) was too small in diameter in comparison to the impactor jet diameter.

The third impactor design, shown in Figure 15, contained a larger impaction surface which was intended to remedy the assumed cause of unsatisfactory operation of the design shown in Figure 14. However, it was found that the same problem still occurred with this design. The source of the problem was traced to intermittent release of liquid deposited on the inner wall of the probe tip which flowed along the wall and collected on the inside of the impactor housing next to the jet itself. Release of drops from this location caused liquid to be flung against the wall on the vapor side of the impactor. The importance of this loss of liquid to the vapor side could not be quantitatively assessed but it was decided that the measurements of vapor concentration in the mixture could be seriously in error. It should be noted that in short duration testing and checkout of this design the loss of liquid to the vapor side did not show up. The concentrations of liquid in the mixture passing through the test section compounded the problem by causing liquid rates into the impactor which exceeded the capability of the impactor to adequately separate the liquid from the vapor. The flow rate through the liquid side



1	SAMPLING PROBE HOUSING - TOP
2	#5-40 HEX. HD CAP SC. X $1\frac{1}{2}$ " LG.
3	SAMPLING PROBE TUBE
4	CALIBRATION BOX
5	SAMPLING PROBE HOUSING - BOTTOM
6	PARKER #E-010 O-RING $\frac{1}{4}$ " I.D. X $\frac{3}{8}$ " O.D.
7	PARKER #E-026 O-RING $1\frac{1}{4}$ " I.D. X $\frac{3}{8}$ " O.D.
8	SAMPLING PROBE BECKET
9	CALIBRATION BOX END FLANGE
10	#10-24 HEX. HD CAP SC. X $1\frac{1}{2}$ " LG.
11	STOELTING DOVETAIL SLIDE #SA-800
12	SAMPLING PROBE RETAINING RING

FIGURE 13. VAPOR/DROPLET SAMPLING PROBE - DESIGN I

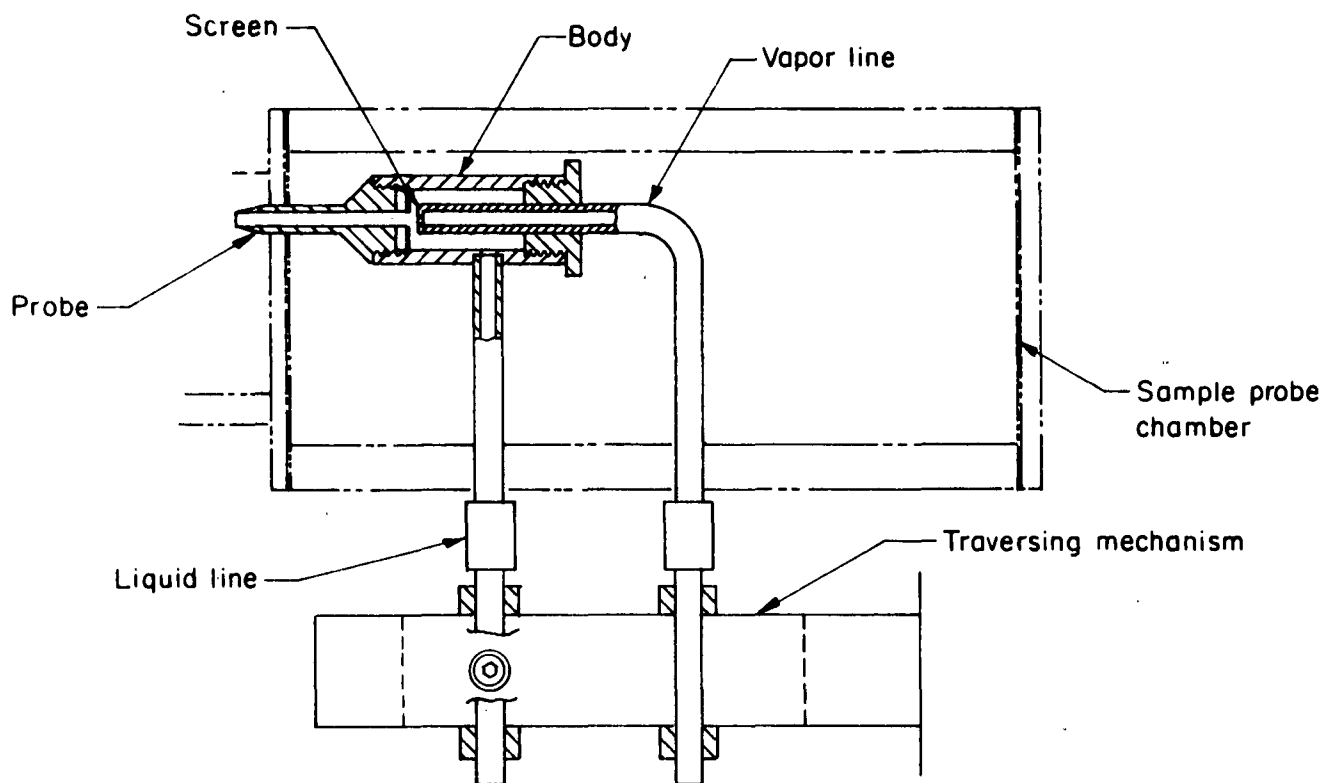


FIGURE 14. VAPOR/DROPLET SAMPLING PROBE - DESIGN 2

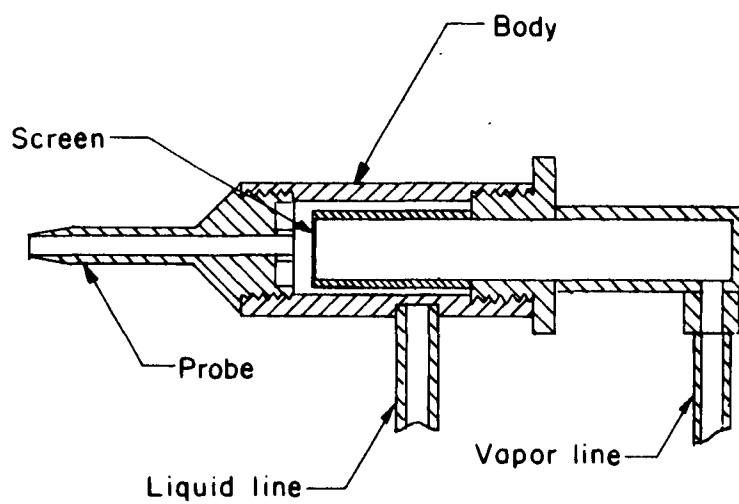


FIGURE 15. VAPOR/DROPLET SAMPLING PROBE - DESIGN 3

had little effect on liquid loss to the walls of the impactor housing even for rates through the liquid side which were as high as three times the rate on the vapor side.

As was mentioned, the major problems with the vapor/droplet samplers were liquid collecting along the outside of the jet plus high liquid loadings in operation which in combination led to loss of liquid onto the vapor side. An attempt was made to circumvent these problems by modifying sampler Design 2. A wire mesh screen was installed to replace the solid surface around the jet. The liquid collecting on this screen was drawn off through a plenum behind the screen and added to the liquid-side sample. This procedure worked fairly well but was abandoned because of continued liquid leakages and losses into the vapor side with this design resulting from the high liquid loadings. It would be instructive to attempt the same procedure with sampler Design 3, since for this design the impaction surface is larger and more adequate for high liquid loadings than that of Design 2, and removal of the liquid collecting around the jet holds considerable promise of giving satisfactory operation. However, due to time constraints and continuing problems, all of the vapor/droplet sampler designs were abandoned and an alternative technique using wall fuel-film skimmers and a total droplet/vapor sampler was adopted.

The final sampling probe which was used in this study was a simple tube, shown in Figure 16, which collected both the vapor and liquid simultaneously. The probe tips were sized to give isokinetic sampling. When samples collected in this manner were coupled with liquid temperature measurements and liquid skimmer rates, calculation of the desired information on liquid distribution in the test section could be made.

Wall Fuel-Film Skimmers

The major effort of the droplet-impaction studies was to determine the fraction of liquid as droplets that deposited on the walls of the test sections from the mixture entering the test sections. The amount of liquid deposited and remaining on the walls of the test sections was determined by direct measurement by weight over measured time periods of the liquid removed from the wall by fuel-film skimmers.

The concept of a wall-skimmer design is based on the premise that liquid flowing along the walls of the test sections can be removed by suction through an opening in the wall. The wall section at the opening should be designed to not obstruct the main mixture flow, and air and fuel vapor flow through the opening should be minimized. To accomplish these objectives, short skimmer sections were installed at the entrance and at the exit of the test section. The walls of these skimmer sections were constructed of porous metal with an annular space behind them. Suction on the annular space caused air and liquid to be drawn through the porous metal. The operation of the skimmers was controlled so that the air flow was no greater than that required to completely remove the wall film. In all cases the air flow through the skimmer sections was in the range of 0.6 to 1.0 scfm.

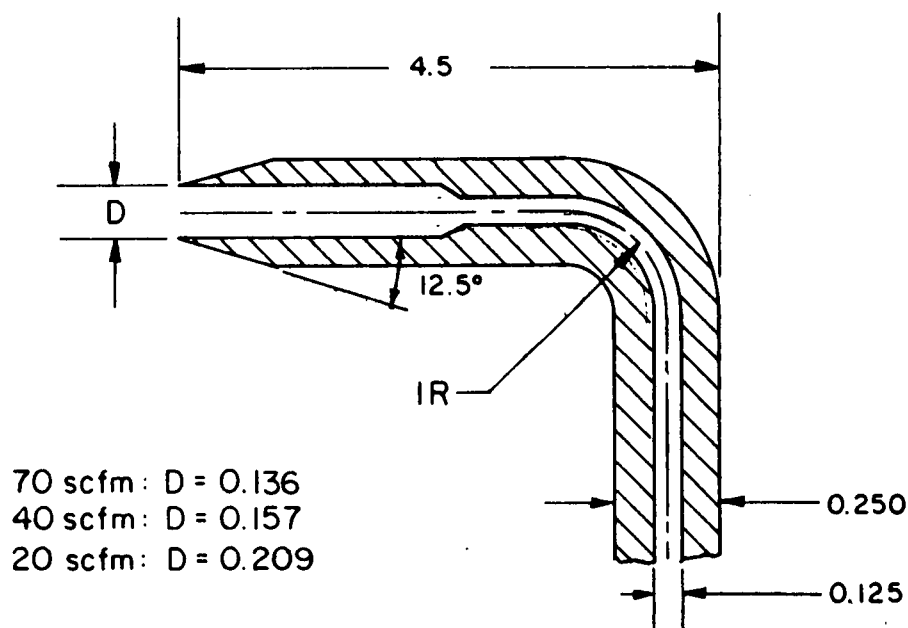


FIGURE 16. SIMPLE TUBE SAMPLING PROBE

Figure 17 is a detailed drawing of the skimmer sections. Flow from the annular space behind the porous metal plates was from each of the four sides of the square cross section. This allowed for liquid removal in any orientation of the skimmer section. The liquid and air removed from the skimmers

passed through an all-glass impinger submerged in an ice-water bath. The impinger also contained a glass fiber demister at the outlet so that droplets entrained by the gas bubbling through the collected liquid would be retained within the impinger.

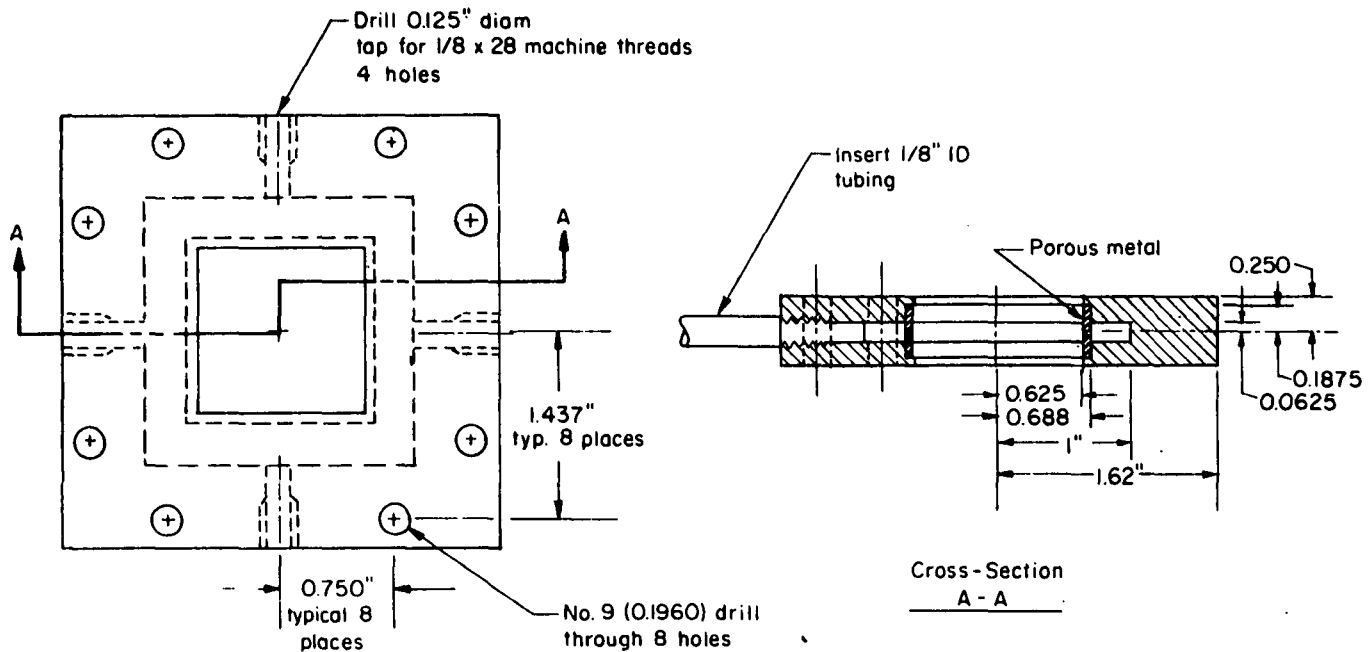


FIGURE 17. FUEL-FILM WALL-SKIMMER DESIGN

The wall-skimmer positioned at the entrance to the test section assured that no previously deposited liquid film entered the test section. The second wall skimmer, positioned at the exit from the test section, collected liquid deposited and remaining on the test section wall at this position. This second skimmer then gave a direct measurement of the total amount of liquid deposited and remaining on the wall of the test section. It can be shown that a mass balance on fuel injected into the test section is possible with measurements made on the injected fuel amount, the wall-skimmers, and the total vapor-plus-droplet sample. This total mass balance however does not provide a measure of the amount of fuel entering or exiting the test section as a vapor. To approximate the amount of vapor in the mixture, additional measurements in the form of fuel temperature are required.

Fuel Vaporization Measurements

The extent of fuel vaporization within the test section was measured in a somewhat indirect method by determining the fuel temperature at the inlet section and at the exit from the test section, and by calibration of the equilibrium vaporization amounts for the fuel as a function of temperature. The assumption inherent in using fuel temperatures as an indication of the extent of vaporization is that the vaporized fuel is in equilibrium with the liquid fuel. Experiments with the vapor/droplet sampler for short time periods, before liquid leakage onto the vapor side of the sampler became troublesome, indicated that this assumption was correct. Special experiments were also conducted by introducing fuel into the system at different temperatures.

In these special experiments the ambient air temperature was 79 F, the air flow rate was 70 scfm, and fuel was introduced onto the spinning disk atomizer at 49 and 74 F. The resulting fuel temperatures at the inlet to the test chamber were nearly equal at 58.5 and 59 F, respectively. Nearly adiabatic conditions can be assumed for the passages between the spinning disk and the test section, consequently, the nearly equal final fuel temperatures indicate that equilibrium was reached at the inlet to the test chamber.

In the experimental apparatus the liquid temperatures were measured with thermocouples located in the wall fuel film at both the inlet and outlet from the test section. The thermocouple beads were positioned off the wall surface, but within the liquid film. For a few tests a thermocouple was attached alongside the sampling probe and measured the temperature of the air-droplet flow. The results of these special experiments using different inlet fuel temperatures and the short-time results with the vapor/droplet samplers indicated that the vaporized fuel is in equilibrium with the liquid fuel at the inlet to the test section. Knowledge of the amount of fuel vapor in equilibrium with the liquid at different temperatures allowed fuel temperature to be used as an indicator of fuel vapor content in the air.

Calibrations were performed to determine the equilibrium content of fuel vapor in air over liquid fuel. Because Stoddard Solvent, which was the fuel used in the experiments, has some distribution of molecular weights in its compositional makeup it is important that the amount of liquid used in

the experimental equilibrium determinations should be such that the fraction evaporated during calibration is comparable to the fraction expected to evaporate in the test section. This effect was taken into account in two ways. First, an estimate of the amount of fuel vaporized in the test section as compared with the total amount of fuel injected was used as a guideline in choosing the amount of fuel to be used in the equilibrium determinations. Secondly, various amounts of fuels were used to note any effect that quantity might have.

The equilibrium determinations were performed by partially filling a nylon bag with air and injecting the fuel into the bag in such a quantity that there would be sufficient fuel remaining after equilibrium had been reached. The bag was then allowed to remain at the temperature of interest for several hours after which the amount of fuel in the air-fuel vapor mixture in the bag was measured. The results of these equilibrium determinations are shown in Figure 18.

These special procedures were used rather than the standard equilibrium-air-distillation (EAD) procedure because the primary objective of the calibration was to determine the fraction of fuel evaporated under conditions duplicating the actual test conditions as nearly as possible.

The ASTM distillation curve for Stoddard Solvent, shown on Figure 12, can be used to estimate the dew point temperatures for a range of air-fuel ratios. The dew point temperature is the temperature of the 100 percent evaporated point of the EAD. This was done for air-Stoddard Solvent mixtures using the Bridgeman⁽⁵⁾ alignment charts. The resulting dew point temperatures were: 125 F for a 16:1 air-fuel ratio, 104 F for a 30:1 air-fuel ratio, and 75 F for a 70:1 air-fuel ratio. On most of the test runs, except for the vaporization tests, the mixture temperature was less than 80 F and generally less than 75 F. Consequently, it is possible in almost all cases to have vaporized fuel in equilibrium with the liquid fuel.

Vapor Analysis System

The amount of fuel contained in a gas sample was determined by a Beckman Hydrocarbon Analyzer employing a flame ionization detector. Several other techniques were attempted throughout the course of this study and included a gas chromatograph with a thermal conductivity detector and a condensation

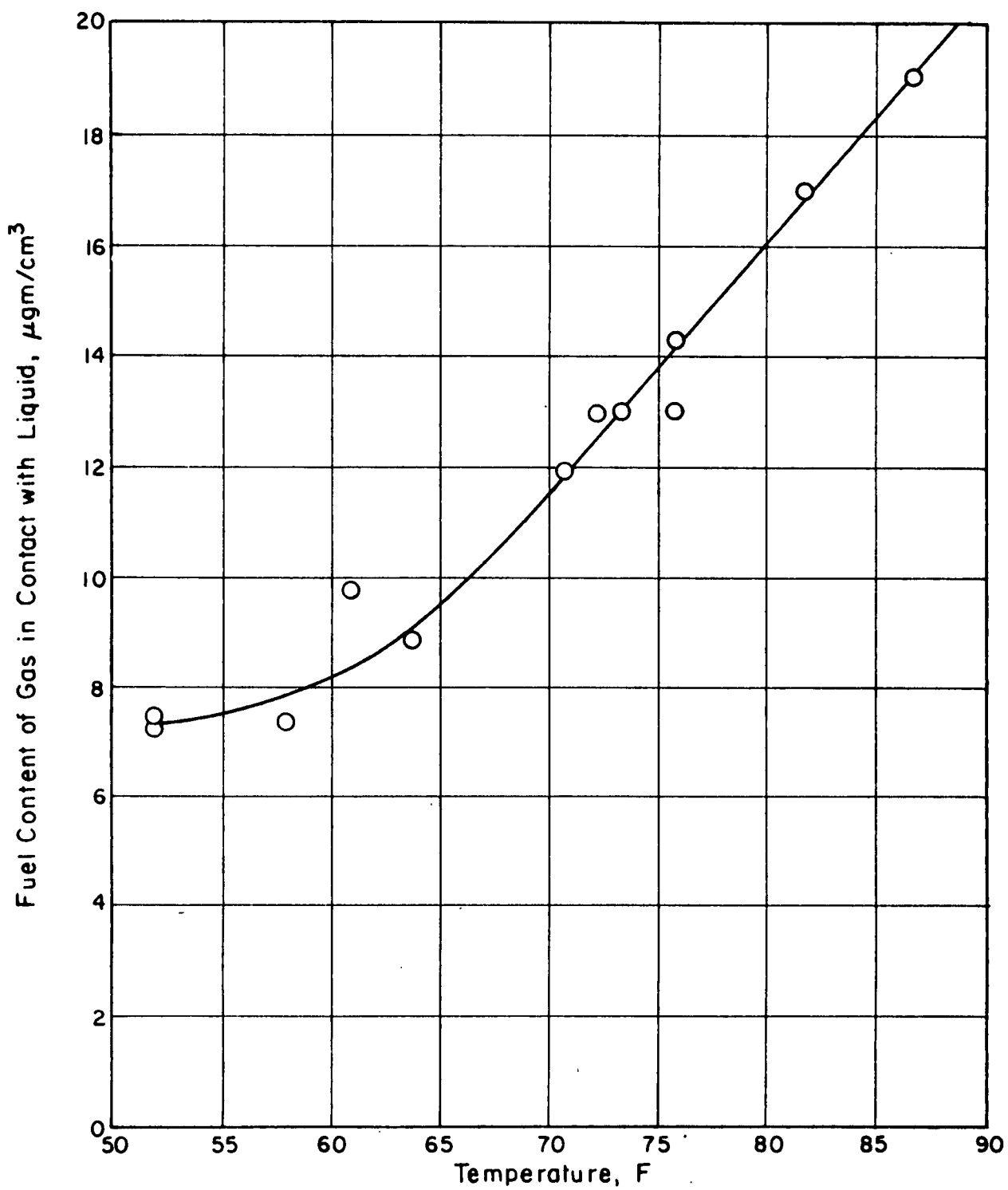


FIGURE 18. EQUILIBRIUM VAPOR CONTENT IN AIR OVER STODDARD SOLVENT AT ATMOSPHERIC PRESSURE

technique which collected vapor from the gas sample for subsequent weighing. These latter two techniques were not found to be suitable for various reasons.

The gas chromatograph technique was intended to be a continuous measurement of hydrocarbon content in the gas sample. In this case a steady stream of the gas sample was passed through the thermal conductivity detector in a gas chromatographic unit. It was found, however, that it was not possible to control the pressure and temperature of the sampled gas stream with sufficient precision so that the indicated hydrocarbon content could be accurately measured. In addition, the heated tungsten wire of the thermal conductivity detector oxidized badly in the gas stream and deteriorated rapidly with use. For these reasons this technique was abandoned.

The second alternate technique employed a cold trap to condense fuel vapor from the gas sample on a continuous basis for subsequent measurement. There were two main problems with this technique. First, water vapor in the ambient air also condensed in the cold traps making mass measurements of the fuel difficult. It would have been necessary to design and build a dryer for all the incoming air to the test section to conveniently avoid this problem and it was decided that such an approach was impractical. A second problem with the condensation scheme was the time required to obtain a measurable sample. A mass analysis by weighing the collected liquid was felt to be the most direct technique; however, the sampling times to give a weighable sample were excessive.

The technique employed in the study using the hydrocarbon analyzer was direct and convenient. A gas sample was drawn from the test section through the sampling probe into a nylon holding bag from which the sample was then passed into the hydrocarbon analyzer. This sampling bag technique was necessary because the hydrocarbon analyzer can only be operated at ambient pressures, whereas, sampling had to be done at the test section vacuums. Adjustment to ambient pressures was possible after a sample had been collected in the bag.

Gas Sampling System

The gas sampling system was designed to collect both vapor and droplets in the mixture stream at the exit from the test section. The sampling system is shown in Figure 19 and consisted of a sampling probe positioned at

the exit from the test section with the capability of traversing or being moved in the test section cross-sectional area. The sampling flow rate was fixed at 20 liters/min (0.071 scfm) through the sampling nozzles which were sized to sample at the average air velocity through the test section, even though the flow was pulsing and sampling could not be isokinetic. Vacuum pumps were used to

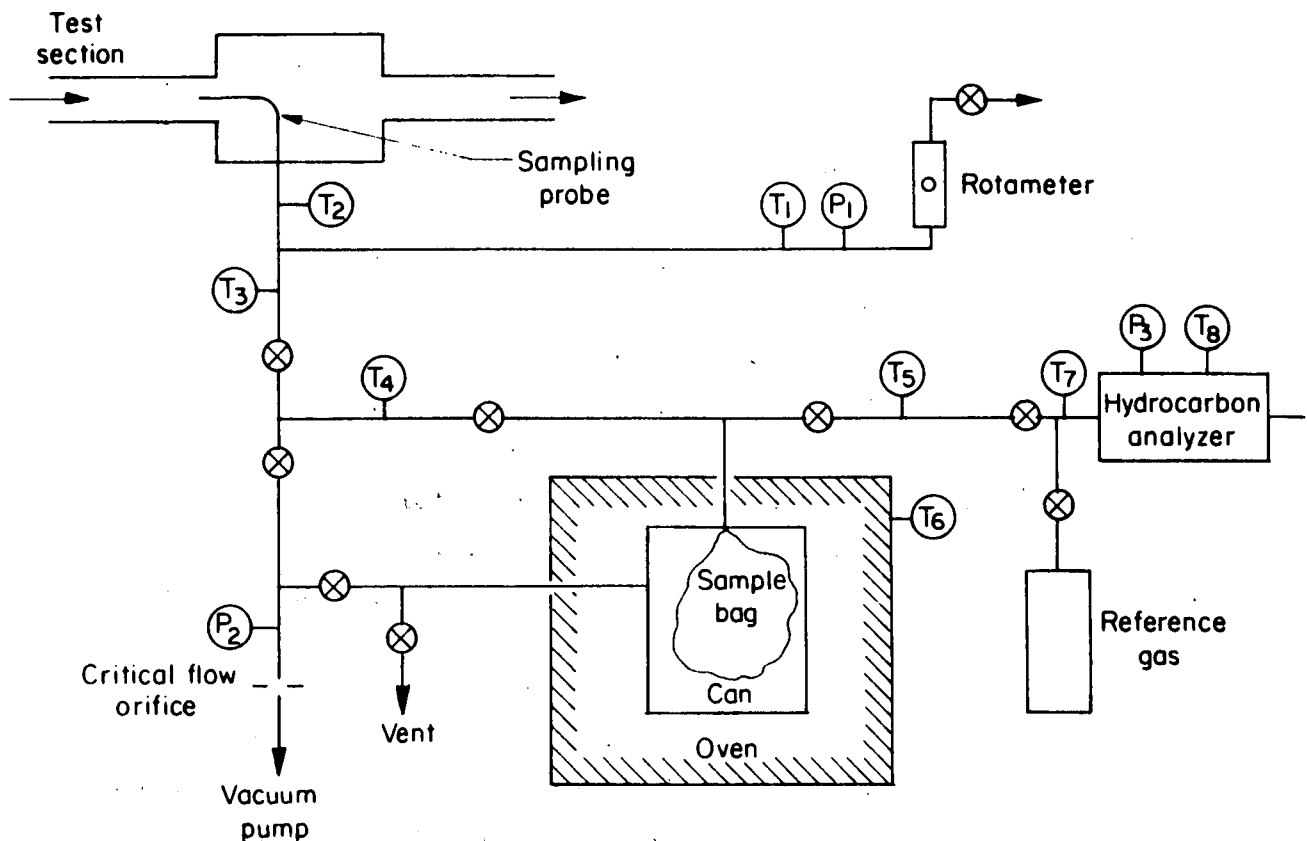


FIGURE 19. FLOW DIAGRAM OF SAMPLING SYSTEM

draw the sampling flow through a primary sampling line where the flow rate was monitored with a rotameter and with temperature and pressure measurements for flow correction. The sample for analysis was taken from this primary line into the sample bag at a rate of $700 \text{ cm}^3/\text{min}$ (0.025 scfm) as controlled by a calibrated critical flow orifice.

The nylon sample bag was contained within a metal canister inside an oven maintained at 150 F. Sample was drawn into the bag by pulling a vacuum on the metal canister in which it was contained. Samples were collected for analysis over time periods of approximately 5 minutes and at all other times the flow through this take-off line was bypassed around the sample bags so that this take-off flow rate was maintained at $700 \text{ cm}^3/\text{min}$. All sample lines leading from the sample probe through the rotameter, the sample bag, and the critical flow orifice, and from the sample bag to the hydrocarbon analyzer were maintained at about 200 F. The analysis of the sample bag was performed by drawing a sample from the bag through the hydrocarbon analyzer.

The rotameter on the primary sample line was calibrated to provide a correction factor as a function of temperature and pressure of the gas entering the rotameter. These correction factors in conjunction with the calibration curve for the rotameter at standard temperature and pressure permitted calculation of the flow through the rotameter based on standard conditions. The flow into the sampling nozzle was then obtained by correcting the standard flow for the conditions which were present in the test section. The standard calibration of the rotameter and the experimentally determined correction factors are presented in Appendix B, Figures B-15 and B-16.

The analysis of the hydrocarbon content of the gas sample collected in the nylon bag was obtained with the hydrocarbon analyzer as calibrated with Stoddard Solvent. The calibration of the hydrocarbon analyzer is presented in Appendix B, Figure B-17. This calibration was performed by injecting predetermined amounts of Stoddard Solvent into a nylon bag which was then filled with air to a known volume. The volume of the calibration bag was 3960 cm^3 (0.14 ft^3) and was filled to this volume by measuring the gas pressure in the bag and filling it until the gas pressure was the same in all cases. The injected fuel was allowed to vaporize while the sample bag was contained in the oven maintained at 150 F. After the injected fuel was completely vaporized, a sample was drawn from the bag through the hydrocarbon analyzer and the reading noted.

It was found that the gas pressure at the hydrocarbon analyzer had some effect on the indicated readings. For this reason the pressure of the gas in the hydrocarbon analyzer was monitored with a water manometer. Calibration

on a daily basis was performed with the pressure being adjusted for each daily calibration such that the desired reading for a known hydrocarbon source was obtained. This pressure was then maintained for all measurements taken on that day. It was also found that the temperature of the hydrocarbon analyzer had a small effect on the indicated readings but more important, if the temperature of the hydrocarbon analyzer was sufficiently low, such as room temperature, adsorption of the fuel vapors could occur within the analyzer. To avoid this complication the hydrocarbon analyzer was maintained at a temperature of about 135 F through the tests. This temperature was found sufficient to maintain the hydrocarbon in the gas stream without appreciable adsorption or condensation within the instrument. This was experimentally determined by maintaining the hydrocarbon analyzer at various temperatures until a level was found which did not lead to hold-up by adsorption within the hydrocarbon analyzer as determined by subsequent desorption indicated by the detector in the hydrocarbon analyzer.

Owing to the possibility that adsorption of hydrocarbons from the sample gas stream onto the inner surfaces of the sampling lines could occur to varying degrees depending on temperature of the sampling line, experiments were performed to determine the importance of this factor. The experiments consisted of operating the sampling system with the sampling lines at room temperature and again at 150 F, and for each temperature drawing an air-vapor sample of the same concentration into the hydrocarbon analyzer. It was found that for air saturated with Stoddard Solvent at room temperature there was no appreciable loss by adsorption of the hydrocarbon on the internal surfaces of the sampling lines even if the lines were maintained at room temperature. However, to avoid such problems the sampling lines were maintained at elevated temperatures.

Experimental Program

The experimental program was designed to provide information on droplet impaction in simulated intake manifold sections as a function of drop size, air flow rate, manifold geometry, mixture temperature, mixture pressure, and surface roughness. Further, the characteristics of liquid-film flow along the walls of the test sections were to be determined in terms of liquid-flow patterns and the amount of liquid carried along the wall. Fuel

vaporization was also investigated as a function of inlet-air temperature and temperature of the test section walls.

Laboratory System Limitations

The laboratory system was limited in several respects. First, the flow rate which could be achieved through the test sections was dependent on whether steady or pulsed flow existed and the pressure level desired in the test section. The capabilities of the air flow in this regard are illustrated in Figure 4. Another serious limitation of the experimental apparatus was concerned with the vaporization of the liquid fuel as it flowed to the atomizer. Vacuums of greater than 15 inches of mercury resulted in serious formation of bubbles within the fuel lines. This was controlled somewhat by the fuel being chilled in an ice-water bath prior to its passage through the control valve where bubbling most often occurred. This cooling in conjunction with system operation at vacuums less than 12 inches of mercury ensured operation without vaporization.

Experimental Conditions

The experimental conditions were held constant to the extent possible with the exception of the variables being studied. All experiments were run with the inlet air at ambient temperature, the liquid fuel at about 50 F, an air flow pulse rate of 1000 cycles per second, and a fuel injection rate of 0.344 lb/min. Temperatures of the sampling and sample transfer lines were maintained at about 200 F and of the oven at 150 F. The sampling and sample transfer lines were heated with electrical heating tape and temperatures at points along the lines were measured with thermocouples. The hydrocarbon analyzer was kept at 135 F.

The variables consisted of air-flow rate, fuel-droplet size, and test-section geometry. Mixture samples were taken from at least three locations in each test section cross-sectional area. Figure 20 shows the sample probe locations for the different test runs. A sample taken from one probe position constitutes a test run. A matrix of the variable test conditions is given in Table 2. From the matrix it is seen that almost 80 test runs were recorded. Over 200 test runs were made prior to these recorded test runs during

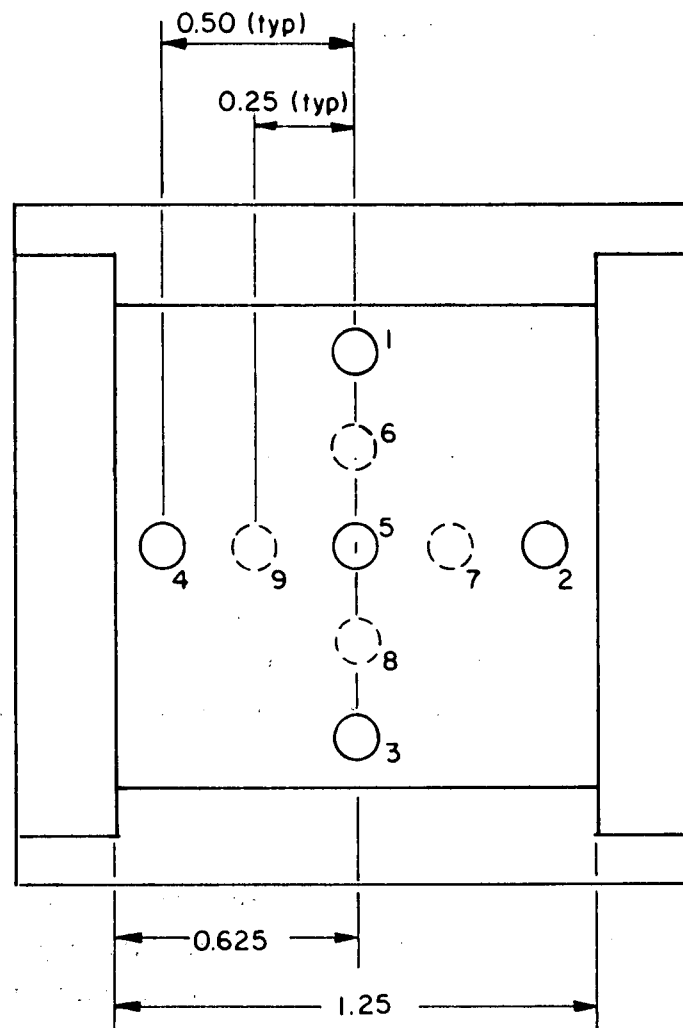


FIGURE 20. CROSS-SECTION OF MANIFOLD TEST SECTION SHOWING PROBE POSITIONS, VIEWED FROM OUTLET

TABLE 2. MATRIX OF TEST CONDITIONS

Test Section Geometry	System Air Flow			
	20 scfm	40 scfm	70 scfm	
			(1)	(2)
Entrance to Test Sections	2,5,4*	2,5,4	2,5,4	2,5,4
Straight	2,5,4	2,5,4	2,5,4	2,5,4
30°	1,5,3	1,5,3	1,5,3	1,5,3
90° 4" R	1,5,3	1,5,3	1,5,3	1,5,3
90° 0" R	1,5,3	1,5,3	1,5,3	1,5,3
90° 4" R ^(a)		1,2,3 4,5,6 7, 9		
90° 4" R ^(b)		1,5,3		
90° 4" R ^(c)		1,5,3		
90° 4" R ^(d)		1,5,3		
Disk speeds: 20 scfm: 55,000 rpm 70 scfm (1): 55,000 rpm				
40 scfm: 55,000 rpm 70 scfm (2): 26,000 rpm				
Vacuums in test section: 20 scfm: 11" Hg				
(All tests at pulsed flow) 40 scfm: 8.5" Hg				
70 scfm: 2" Hg				

* Probe positions -- See Figure 20

- (a) Replication with more detailed traverse
- (b) Rough-wall test section
- (c) Aluminum test section -- heated inlet air
- (d) Aluminum test section -- heated walls

checkout and preliminary studies. Most of these were concerned with solving problems occurring with the vapor/droplet samplers, mixture generator, hydrocarbon analysis technique and sampling flow system. In addition, a number of runs were lost because of leaks in the sampling bags.

The experimental conditions were chosen to simulate, to the extent practical, the flow, pressure, and velocity in an intake manifold. The pressure level in the test sections at the lowest flow rate is somewhat higher than would be encountered in an actual induction system at a comparable air flow rate because of the vaporization-bubbling problem previously mentioned. The experimental apparatus was operated at 11 in. Hg vacuum for 20 scfm air flow while the vacuum expected in an induction system for this flow would be about 16 in.Hg.

Another deviation from an exact simulation for an induction system is in the air/fuel ratio entering the test section. The fuel atomized in the mixture generator at the set rate of 0.344 lb/min corresponds to air/fuel ratios of 18:1 at 70 scfm air flow down to 5:1 at 20 scfm. However, because of the considerable loss to the wall in the mixture generator, the air/fuel ratios entering the test sections were of the order of 30 to 70. This is probably not a significant factor in a study of deposition rates but would be significant in studies of reentrainment after deposition.

Drop Sizes Entering the Test Section

Another test condition of importance is the size distribution of the drops entering the test sections. This was measured with an impaction-slide scheme. A drawing of the device specially constructed for this purpose is shown as Figure 21. This drop sizing device is designed to fit into the laboratory flow system just upstream of the test sections. Since the impaction surface disrupted the air and fuel-droplet flow, the sizing apparatus was installed only for the purposes of collecting drops and at all other times was removed.

The principle of operation is that the air flow in the system cross-sectional area is sufficient to give deposition into a slot on the traversing slide and allow the droplets to impact onto the coated glass slide. Calculations based on impaction into recessed bodies⁽⁶⁾ maintained in a free air stream (velocities taken as averages for test conditions) indicate that the

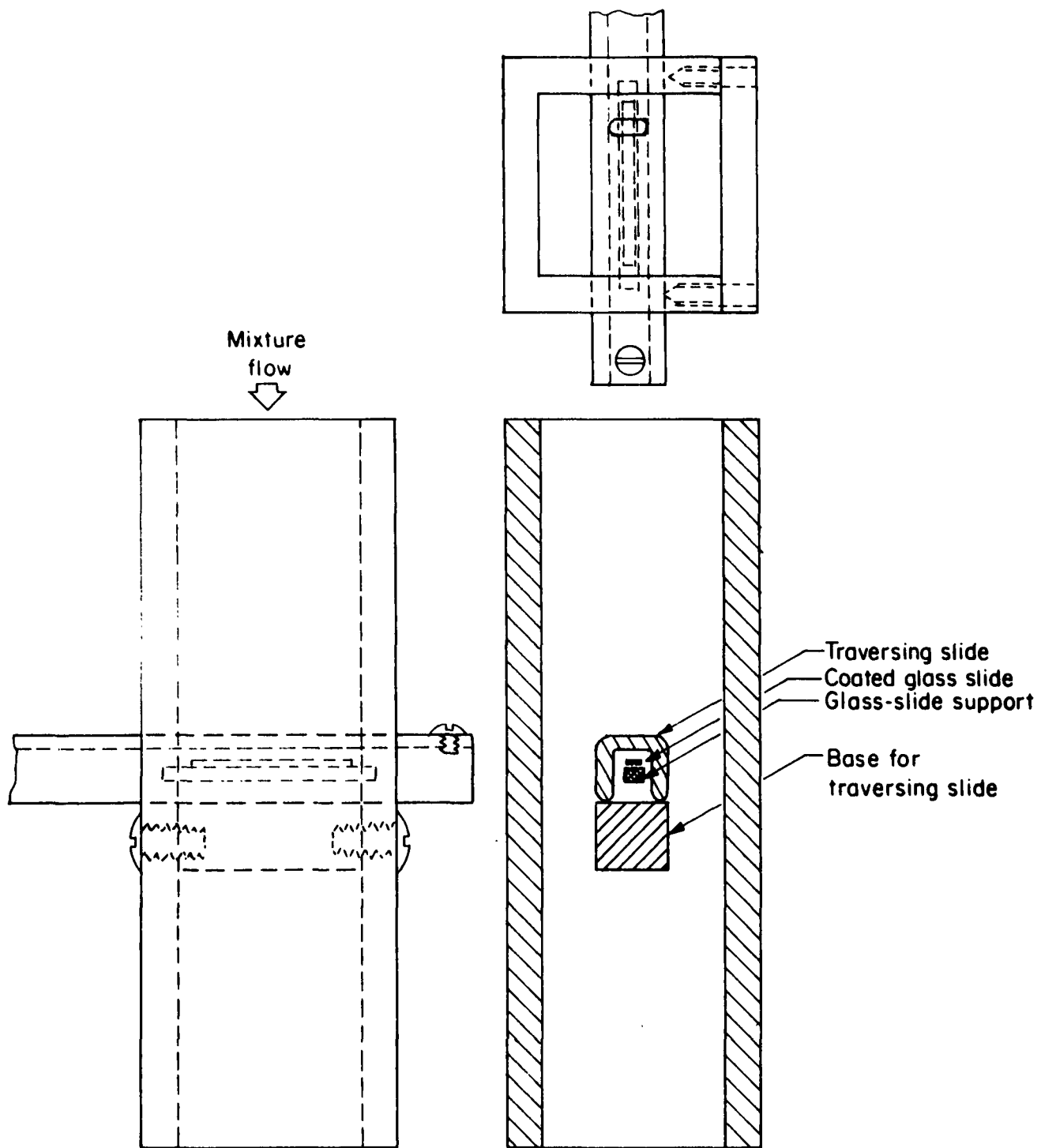


FIGURE 21. COLLECTION APPARATUS FOR DROP SIZING

impaction device should be adequate to collect droplets about 5 microns and larger. In practice the system was more effective than predicted. The glass slide impaction surfaces were coated with magnesium oxide particles into which the droplet impacted, leaving a crater.

The fuel-air flow was first allowed to stabilize while the traversing slide was kept in a position such that the opening was outside the apparatus. Sampling was then accomplished by passing the traversing slide with the sampling opening across the flowing gas stream. As the opening or slot passed across, drops were impacted by their inertia through the opening onto the coated slide.

The slide coating was a loose agglomerated mass of magnesium oxide smoke particles. This coating was penetrated by each drop as it impacted on the slide, leaving a crater in the coating as an indication of drop size. Extensive calibration of this technique has indicated that the true drop sizes are 0.81 times the crater size⁽⁵⁾. Size distributions were determined with an optical microscope.

The size distributions of the drops entering the test sections at different gas flow rates are shown in Figure 22. All size distributions given are averages across the test-section cross-sectional area as provided by the slide movement. The disk speed for air flow rates of 20, 40 and 70 (1) scfm was 55,000 rpm. For the case noted 70 (2) the speed was 26,000 rpm. As is seen there is little difference among the size distributions. On a mass or volume basis there would be some differences because the case 70 (2) indicated a number of very large ($\sim 250\mu$) drops which would significantly shift a mass mean to larger sizes.

General Test Procedures

The procedures employed in performing the tests were quite direct and, except for setting up the primary sampling rate, involved only adjustment to prescribed values. The primary sampling rate was fixed by an iterative process involving calculated temperature and pressure corrections with subsequent flow adjustments until the sampling rate was 20 liters/min (0.706 scfm).

The general procedure was to first allow all controlled temperatures to be brought to the desired levels. The temperatures of interest in this regard are the sampling lines (200 F), the oven (150 F), and the hydrocarbon

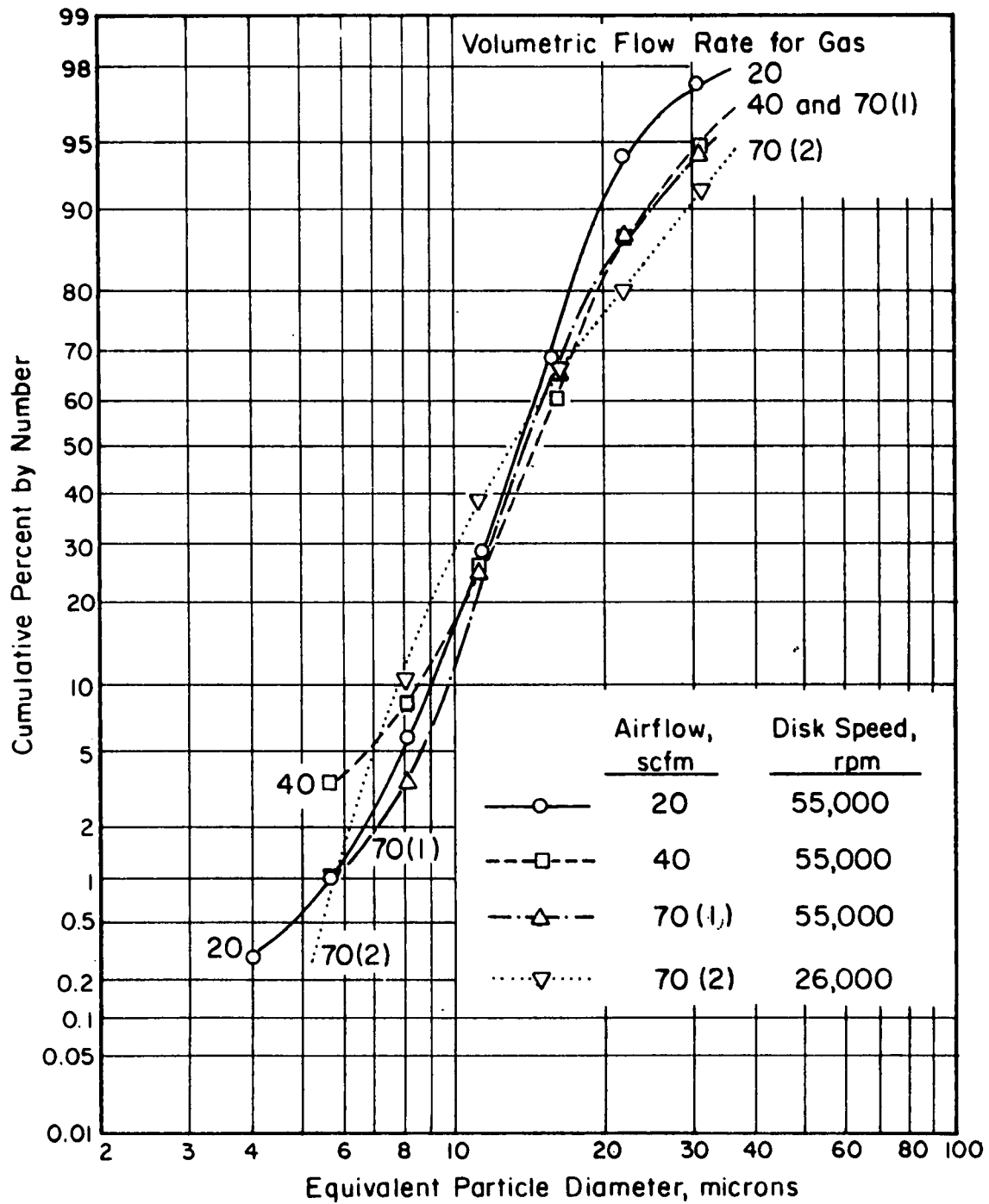


FIGURE 22. SIZE DISTRIBUTIONS FOR DROPS ENTERING TEST SECTIONS

analyzer (135 F). After the proper temperatures had been achieved, the main air flow, pulser motor, and skimmer flows were started. Pulse rate was adjusted to 1000 cps and then air flow rate and pressure in the test section were set at the prescribed values. At this point the primary and take-off sample flows were started and adjusted.

After proper adjustment of all conditions and flows had been achieved, the spinning disk rotation rate was set at either 26,000 or 55,000 rpm. At this point the fuel flow was started and timing for Skimmers No. 1 and No. 2 was begun. Fuel flow through the mixture-generator chamber skimmer was determined once or twice over timed intervals during the course of three test runs. Weight measurements over time intervals gave chamber skimmer rates. Weight measurements were also used to give rates at Skimmers No. 1 and No. 2, but the time interval was that for the three test runs.

Three test runs were run sequentially each time the flow system was operated. Each test run consisted of a gas sample taken at one location in the test section exit. Each test or gas sample was initiated by directing the take-off sample flow into the sampling bag after stopping the bag by-pass flow. Sample was drawn into the sample bags for about 5 minutes at a rate of $700 \text{ cm}^3/\text{min}$ (0.025 scfm) until pressure measurements indicated the bag was full. The by-pass flow was again started, the can containing the sample bag vented to the atmosphere and the sample directed through the hydrocarbon analyzer. After the sample had been analyzed the sample bag was completely collapsed and the lines to the bag evacuated to about 20 inches Hg vacuum in preparation for sampling from a new probe position.

Experimental Results

Experimental data obtained are presented in Tables 3 through 16. These data were all generated using the simple-tube probe, and earlier data obtained using probes with vapor/droplet impaction separators are not included. The data presented can be summarized as follows:

Tables 3 and 4 - Test-section inlet

Tables 5 and 6 - Straight test-section

Tables 7 and 8 - 30-degree-bend test-section

Tables 9 and 10 - 90-degree bend test-section with 4-inch bend radius

Tables 11 and 12 - 90-degree-bend test section with 0-inch
bend radius

Tables 13 and 14 - Rerun of one test condition with more
detailed traverse

Tables 15 and 16 - Rough-wall and heated test section.

The significance of the values presented in the above tables is generally self-evident, with some exceptions which require explanation.

The values for sample fuel concentration given in Column 13 of the odd-numbered tables above are for the total fuel concentration, liquid plus vapor, observed in the fuel-air samples collected by the traversing probe. The values for local total fuel rate, given in Column 22 of the even-numbered tables, are obtained by multiplying the observed total fuel concentration (Column 13) by the volumetric air-flow rate (Column 3) and the appropriate conversion factors. Thus, the local fuel rate to the probe is given in terms of the total fuel rate for the test section that would be consistent with the local fuel concentration. The average fuel rate for the test section (Column 25) can therefore be taken as the average of the local fuel rates (weighting the local fuel rates according to probe position).

The fuel vapor rate to the probe (Column 23) is computed by multiplying the vapor concentration at saturation corresponding to the observed test-section-exit wall fuel-film temperature by the air-flow rate. Thus, the amount of fuel in vapor form is computed and not measured directly. This procedure was necessitated by the difficulties in designing an effective vapor/droplet separating probe, as discussed previously. The amount of fuel present as entrained droplets at any probe position is computed as the difference between the observed total fuel rate sampled and computed fuel vapor rate.

Experimental Error Analysis

Mass Balance. From the experimental data, the fuel rate both entering and leaving the test section can be computed to provide a mass-balance check on the accuracy of the data. The flow rate to the mixture generator was the

TABLE 3. EXPERIMENTAL DATA FOR TEST-SECTION ENTRANCE

1	2	3	4	5	6	7	8	9	10	11	12	13
Run No.	Mean Drop Size, microns	Air Flow, scfm	Chamber Vacuum, in. Hg	Probe Position	Orifice Air Temperature, F	Test Section Wall Film Temperature, F Inlet	Outlet	Fuel Rate to Mixture Generator, lb/hr	Chamber Skimmer Flow, lb/hr	No. 1 Skimmer Flow, lb/hr	No. 2 Skimmer Flow, lb/hr	Sample Fuel Conc., $\mu\text{g}/\text{cm}^3$
250	14	20	11.0	Rear (2)**	77	66.5	--	20.6	17.0	--	--	16.1
251	"	"	"	Center (5)	76	66.0	--	"	--	0.19	--	15.5
252	"	"	"	Front (4)	74	65.0	--	"	17.9	--	--	14.8
226	14	40	8.5	Rear	76	78.5	--	20.6	15.8	--	--	16.4
227	"	"	"	Center	79	--	--	"	--	0.25	--	17.7
228	"	"	"	Front	79	77.5	--	"	16.7	--	--	16.7
276	14	70	2.0	Rear	66	57.0	--	20.6	--	--	--	11.5
275	"	"	"	Center	66	57.0	--	"	15.7	0.14	--	14.8
274	"	"	"	Front	66	57.5	--	"	--	--	--	9.5
271	14*	70	2.0	Rear	65	58.0	--	20.6	--	--	--	11.4
272	"	"	"	Center	66	57.0	--	"	15.3	0.12	--	15.2
273	"	"	"	Front	65	57.0	--	"	--	--	--	8.5

* Plus large drops.

** See Figure 20.

TABLE 4. REDUCED DATA FOR TEST-SECTION ENTRANCE

14	15	16	17	18	19	20	21	22	23	24	25	26	27
Run No.	Air Mass Flow, lb/hr	Net Fuel to Test Section, lb/hr	Entrained Air/Fuel Ratio	Saturated Air/Fuel Ratio	Test Section Air Velocity, average ft/sec	Test Section Air Density, lb/ft ³	Reynolds No.	Local Total Fuel Rate to Probe, lb/hr	Vapor Fuel Rate, lb/hr	Local Entrained Liquid Fuel Rate, lb/hr	Average Total Fuel Rate to Probe, lb/hr	Wall Film Fuel Rate, lb/hr	Total Sampled Fuel Rate, lb/hr
250		3.4	26	115	49	.0469		1.20	0.78	0.42			
251	90	--	--	118	"	"		1.17	0.77	0.40			
252		2.5	36	121	"	"		1.11	0.74	0.37			
226		4.5	40	79	87	.0530		2.48	2.29	0.19			
227	180	--	--	--	"	"		2.67	2.26	0.41			
228		3.6	50	81	"	"		2.51	2.22	0.29			
276		--	--	150	113	.0715		2.77	2.11	0.66			
275	315	4.8	66	150	"	"		3.92	2.11	1.81			
274		--	--	150	"	"		2.50	2.11	0.39			
271		--	--	148	113	.0715		3.00	2.13	0.87			
272	315	5.2	61	150	"	"		4.00	2.11	1.89			
273		--	--	150	"	"		2.25	2.11	0.14			

TABLE 5. EXPERIMENTAL DATA FOR STRAIGHT TEST SECTION

1	2	3	4	5	6	7	8	9	10	11	12	13
Run No.	Mean Drop Size, microns	Air Flow, scfm	Chamber Vacuum, in. Hg	Probe Position	Orifice Air Temperature, F	Test Section Wall Film Temperature, F		Fuel Rate To Mixture Generator, lb/hr	Chamber Skimmer Flow, lb/hr	No. 1 Skimmer Flow, lb/hr	No. 2 Skimmer Flow, lb/hr	Sample Fuel Conc. ug/cm ³
249	14	20	11.0	Rear	80	67.5	69.5	20.6	17.3	--	--	12.6
248	"	"	"	Center	80	--	--	"	--	0.16	0.15	13.0
247	"	"	"	Front	80	68.5	68.5	"	17.5	--	--	13.0
225	14	40	8.5	Rear	71	70.5	71.5	20.6	16.5	--	--	15.2
224	"	"	"	Center	71	70.5	70.5	"	--	0.27	0.27	15.2
223	"	"	"	Front	71	70.5	70.5	"	17.1	--	--	15.2
265	14	70	2.0	Rear	66	60.0	61.5	20.6	14.8	--	--	13.3
266	"	"	"	Center	65	58.5	60.5	"	--	0.07	0.37	13.3
267	"	"	"	Front	--	58.5	60.5	"	16.0	--	--	12.2
270	14*	70	2.0	Rear	66	57.5	59.5	20.6	--	--	--	13.6
269	"	"	"	Center	66	57.5	59.5	"	14.8	0.07	0.35	12.6
268	"	"	"	Front	66	57.5	59.5	"	--	--	--	10.7

* Plus large drops.

TABLE 6. REDUCED DATA FOR STRAIGHT TEST SECTION

14	15	16	17	18	19	20	21	22	23	24	25	26	27
Run No.	Air Mass Flow, lb/hr	Net Fuel to Test Section, lb/hr	Entrained Air/Fuel Ratio	Saturated Air/Fuel Ratio	Test Section Air Velocity, average ft/sec	Test Section Air Density, lb/ft ³	Reynolds No.	Local Total Fuel Rate to Probe, lb/hr	Vapor Fuel Rate, lb/hr	Local Entrained Liquid Fuel Rate, lb/hr	Average Total Fuel Rate to Probe, lb/hr	Wall Film Fuel Rate, lb/hr	Total Sample Fuel Rate, lb/hr
249								0.95	0.86	0.09			
248	90	3.1	29	111	48	.0475	19,400	0.98	0.85	0.13	0.97	0.15	1.12
247								0.98	0.82	0.16			
225								2.29	1.84	0.45			
224	180	3.6	50	102	86	.0536	39,300	2.29	1.77	0.52	2.29	0.27	2.56
223								2.29	1.77	0.52			
265								3.49	2.34	1.15			
266	315	5.2	61	146	113	.0715	68,800	3.49	2.29	1.20	3.42	0.37	3.79
267								3.22	2.29	0.93			
270								3.57	2.21	1.36			
269	315	5.8	55	150	113	.0715	68,800	3.32	2.21	1.11	3.25	0.35	3.60
268								2.82	2.21	0.61			

TABLE 7. EXPERIMENTAL DATA FOR 30-DEGREE-BEND SECTION

1	2	3	4	5	6	7	8	9	10	11	12	13
Run No.	Mean Drop Size, microns	Air Flow, scfm	Chamber Vacuum, in. Hg	Probe Position	Orifice Air Temperature, F	Test Section Wall Film Temperature, F	Inlet Outlet	Fuel Rate To Mixture Generator, lb/hr	Chamber Skimmer Flow, lb/hr	No. 1 Skimmer Flow, lb/hr	No. 2 Skimmer Flow, lb/hr	Sample Fuel Conc. $\mu\text{g}/\text{cm}^3$
246	14	20	11.0	Top (1)***	81	67.0	--	20.6	17.2	--	--	13.0
245	"	"	"	Center (5)	80	57.0	69.0	"	--	0.12	0.24	13.3
244	"	"	"	Bottom (3)	--	68.0	--	"	18.0	--	--	13.6
216	14	40	8.5	Top	75	68**	70**	20.6	--	--	--	14.8
215	"	"	"	Center	75	68**	70**	"	15.8	0.20	0.39	16.1
214	"	"	"	Bottom	75	68**	70**	"	--	--	--	18.3
280	14	70	2.0	Top	68	63.5	65.5	20.6	--	--	--	9.3
281	"	"	"	Center	68	63.5	65.5	"	15.6	0.08	0.71	10.1
282	"	"	"	Bottom	69	63.5	65.5	"	--	--	--	14.8
279	14*	70	2.0	Top	67	62.5	65.5	20.6	--	--	--	8.2
278	"	"	"	Center	66	62.5	64.5	"	15.6	0.06	0.77	9.2
277	"	"	"	Bottom	66	62.5	64.5	"	--	--	--	14.2

* Plus large drops.

*** See Figure 20.

** Approximate value.

TABLE 8. REDUCED DATA FOR 30-DEGREE-BEND TEST SECTION

14	15	16	17	18	19	20	21	22	23	24	25	26	27
Run No.	Air Mass Flow, lb/hr	Net Fuel to Test Section, lb/hr	Entrained Air/Fuel Ratio	Saturated Air/Fuel Ratio	Test Section Air Velocity, average ft/sec	Test Section Air Density, lb/ft ³	Reynolds No.	Local Total Fuel Rate to Probe, lb/hr	Vapor Fuel Rate, lb/hr	Local Entrained Liquid Fuel Rate, lb/hr	Average Total Fuel Rate to Probe, lb/hr	Wall Film Fuel Rate, lb/hr	Total Sampled Fuel Rate, lb/hr
246								0.98	0.85	0.13			
245	90	3.0	30	114	48	.0475	19,500	0.99	0.85	0.14	0.99	0.24	1.23
244								1.02	0.85	0.17			
216								2.22	1.75	0.47			
215	180	4.6	39	110	86	.0538	39,400	2.41	1.75	0.66	2.45	0.39	2.84
214								2.75	1.75	1.00			
280								2.43	2.63	--			
281	315	5.0	63	120	114	.0707	68,700	2.65	2.63	0.02	2.90	0.71	3.61
282								3.88	2.63	1.25			
279								2.15	2.63	--			
278	315	5.0	63	124	114	.0707	68,700	2.41	2.55	--	2.67	0.77	3.44
277								3.72	2.55	1.17			

TABLE 9. EXPERIMENTAL DATA FOR 90 DEGREE-BEND, 4-INCH RADIUS TEST SECTION

1	2	3	4	5	6	7	8	9	10	11	12	13
Run No.	Mean Drop Size, microns	Air Flow, scfm	Chamber Vacuum, in. Hg	Probe Position	Orifice Air Temperature, F	Test Section Wall Film Temperature, F		Fuel Rate To Mixture Generator, lb/hr	Chamber Skimmer Flow, lb/hr	No. 1 Skimmer Flow, lb/hr	No. 2 Skimmer Flow, lb/hr	Sample Fuel Conc. $\mu\text{g}/\text{cm}^3$
241	14	20	11.0	Top	76	68.5	70.5	20.6	17.3	--	--	13.3
242	"	"	"	Center	--	--	--	"	--	0.18	0.21	13.6
243	"	"	"	Bottom	77	68.5	71.5	"	17.6	--	--	15.2
231	14	40	8.5	Top	79	75.5	74.5	20.6	17.7	--	--	14.9
230	"	"	"	Center	79	76.5	74.5	"	--	0.15	0.76	14.9
229	"	"	"	Bottom	79	78.0	73.0	"	16.8	--	--	15.5
286	14	70	2.0	Top	70	64.5	65.5	20.6	--	--	--	9.8
287	"	"	"	Center	70	64.5	66.0	"	15.7	0.10	1.14	9.5
288	"	"	"	Bottom	70	--	--	"	--	--	--	10.0
285	14*	70	2.0	Top	70	63.5	64.5	20.6	--	--	--	8.2
284	"	"	"	Center	70	63.5	65	"	15.9	0.06	1.01	8.1
283	"	"	"	Bottom	69	64.0	65.5	"	--	--	--	8.5

* Plus large drops.

TABLE 10. REDUCED DATA FOR 90-DEGREE-BEND, 4-INCH-RADIUS TEST SECTION

14	15	16	17	18	19	20	21	22	23	24	25	26	27
Run No.	Air Mass Flow, lb/hr	Net Fuel to Test Section, lb/hr	Entrained Air/Fuel Ratio	Saturated Air/Fuel Ratio	Test Section Air Velocity, average ft/sec	Test Section Air Density, lb/ft ³	Reynolds No.	Local Total Fuel Rate to Probe, lb/hr	Vapor Fuel Rate, lb/hr	Local Entrained Liquid Fuel Rate, lb/hr	Average Total Fuel Rate to Probe, lb/hr	Wall Film Fuel Rate, lb/hr	Total Sampled Fuel Rate, lb/hr
241								0.98	0.89	0.09			
242	90	3.0	30	109	49	.0474	19,800	1.02	0.90	0.12	1.04	0.21	1.25
243								1.14	0.91	0.23			
231								2.23	2.01	0.22			
230	180	3.2	56	84	87	.0532	39,400	2.23	2.01	0.22	2.25	0.76	3.01
229								2.32	1.93	0.39			
286								2.57	2.63	--			
287	315	4.8	66	124	114	.0705	68,400	2.50	2.69	--	2.55	1.14	3.69
288								2.62	2.69	--			
285								2.15	2.55	--			
284	315	4.7	67	128	114	.0705	68,400	2.11	2.61	--	2.15	1.01	3.16
283								2.23	2.63	--			

TABLE 11. EXPERIMENTAL DATA FOR 90-DEGREE BEND, 0-INCH-RADIUS TEST SECTION

1	2	3	4	5	6	7	8	9	10	11	12	13
Run No.	Mean Drop Size, microns	Air Flow, scfm	Chamber Vacuum, in. Hg	Probe Position	Orifice Air Temperature, F	Test Section Wall Inlet	Test Section Film Outlet	Fuel Rate To Mixture Generator, lb/hr	Chamber Skimmer Flow, lb/hr	No. 1 Skimmer Flow, lb/hr	No. 2 Skimmer Flow, lb/hr	Sample Fuel Conc. $\mu\text{g}/\text{cm}^3$
240	14	20	11.0	Top	70	70.5	69.0	20.6	16.8	--	--	11.4
239	"	"	"	Center	70	70.5	69.0	"	--	0.20	0.26	10.7
238	"	"	"	Bottom	70	--	--	"	17.8	--	--	9.8
232	14	40	8.5	Top	78	78.5	75.0	20.6	15.6	--	--	14.9
233	"	"	"	Center	79	--	--	"	--	0.28	0.45	15.2
234	"	"	"	Bottom	79	77.5	75.0	"	16.2	--	--	18.3
292	14	70	2.0	Top	69	63.5	65.5	20.6	--	--	--	9.8
293	"	"	"	Center	70	63.5	65.5	"	14.8	0.05	0.95	9.8
294	"	"	"	Bottom	--	--	--	"	--	--	--	12.3
291	14*	70	2.0	Top	70	--	--	20.6	--	--	--	9.5
290	"	"	"	Center	70	63.5	65.0	"	15.7	0.05	1.01	9.5
289	"	"	"	Bottom	70	65.5	65.5	"	--	--	--	12.3

* Plus large drops.

TABLE 12. REDUCED DATA FOR 90-DEGREE-BEND, 0-INCH-RADIUS TEST SECTION

14	15	16	17	18	19	20	21	22	23	24	25	26	27
Run No.	Air Mass Flow, lb/hr	Net Fuel to Test Section, lb/hr	Entrained Air/Fuel Ratio	Saturated Air/Fuel Ratio	Test Section Air Velocity, average ft/sec	Test Section Air Density, lb/ft ³	Reynolds No.	Local Total Fuel Rate to Probe, lb/hr	Vapor Fuel Rate, lb/hr	Local Entrained Liquid Fuel Rate, lb/hr	Average Total Fuel Rate to Probe, lb/hr	Wall Film Fuel Rate, lb/hr	Total Sampled Fuel Rate, lb/hr
240								0.85	0.85	--			
239	90	3.0	30	102	49	.0474	19,800	0.80	0.85	--	0.80	0.26	1.06
238								0.73	0.85	--			
232								2.23	2.06	0.17			
233	180	4.4	41	80	87	.0530	39,300	2.28	2.06	0.22	2.38	0.45	2.83
234								2.74	2.06	0.68			
292								2.57	2.64	--			
293	315	5.8	54	127	114	.0705	68,500	2.57	2.64	--	2.73	0.95	3.68
294								3.22	2.64	0.58			
291								2.49	2.61	--			
290	315	4.9	64	127	114	.0705	68,500	2.49	2.61	--	2.67	1.01	3.68
289								3.22	2.64	0.58			

TABLE 13. EXPERIMENTAL DATA FOR REPLICATION TEST WITH 90-DEGREE-BAND,
4-INCH-RADIUS TEST SECTION

1	2	3	4	5	6	7	8	9	10	11	12	13
Run No.	Mean Drop Size, microns	Air Flow, scfm	Chamber Vacuum, in. Hg	Probe Position	Orifice Air Temperature, F	Test Section Wall Film Temperature, F	Inlet Outlet	Fuel Rate To Mixture Generator, lb/hr	Chamber Skimmer Flow, lb/hr	No. 1 Skimmer Flow, lb/hr	No. 2 Skimmer Flow, lb/hr	Sample Fuel Conc. $\mu\text{g}/\text{cm}^3$
298	14	40	8.5	Top	(1)*	73	75	20.6	15.7	0.03	0.81	16.1
299				Top center	(6)	73	75					16.4
296				Center	(5)	73	75					16.1
297				Bottom center	(8)	73	75					15.5
295				Bottom	(3)	73	75					17.5
301				East	(4)	74	76					17.7
303				East center	(9)	77	79					16.4
302				West center	(7)	74	76					15.8
300				West	(2)	74	76					16.4

* See Figure 20.

TABLE 14. REDUCED DATA FOR REPLICATION TEST WITH 90-DEGREE-BEND, 4-INCH RADIUS TEST SECTION

14	15	16	17	18	19	20	21	22	23	24	25	26	27
Run No.	Air Mass Flow, lb/hr	Net Fuel to Test Section, lb/hr	Entrained Air/Fuel Ratio	Saturated Air/Fuel Ratio	Test Section Air Velocity, average ft/sec	Test Section Air Density, lb/ft ³	Reynolds No.	Local Total Fuel Rate to Probe, lb/hr	Vapor Fuel Rate, lb/hr	Local Entrained Liquid Fuel Rate, lb/hr	Average Total Fuel Rate to Probe, lb/hr	Wall Film Fuel Rate, lb/hr	Total Sampled Fuel Rate, lb/hr
298	180	4.9	37	86	87	.0531	39,300	2.41	2.05	0.36	2.46	0.81	3.27
299					87	"		2.46	"	0.41			
296					87	"		2.41	"	0.36			
297					87	"		2.31	"	0.26			
295					87	"		2.62	"	0.57			
301					87	.0530		2.65	2.11	0.54			
303					87	.0528		2.46	2.30	0.16			
302					87	.0530		2.37	2.11	0.26			
300					87	"		2.46	"	0.36			

TABLE 15. EXPERIMENTAL DATA FOR ROUGH-WALL AND HEATED TEST SECTIONS

1	2	3	4	5	6	7	8	9	10	11	12	13
Run No.	Mean Drop Size, microns	Air Flow, scfm	Chamber Vacuum, in. Hg	Probe Position	Orifice Air Temperature, F	Test Section Wall Temperature, F	Section Film Inlet Outlet	Fuel Rate To Mixture Generator, lb/hr	Chamber Skimmer Flow, lb/hr	No. 1 Skimmer Flow, lb/hr	No. 2 Skimmer Flow, lb/hr	Sample Fuel Conc., ug/cm ³
<u>Rough Wall</u>												
312	14	40	8.5	Top	69	67	67	20.6	16.7	0.25	1.62	12.35
311	"	"	"	Center	69	66	66	"	--	--	--	12.35
313	"	"	"	Bottom	71	67	66	"	16.0	0.11	1.28	13.35
<u>Heated Inlet Air</u>												
319	14	40	8.5	Top	125	99	95	20.6	--	--	--	32.4
318	"	"	"	Center	120	97	94	"	13.3	0.08	0.19	31.2
317	"	"	"	Bottom	125	99	93	"	--	--	--	30.2
<u>Heated Wall</u>												
322	14*	40	8.5	Top	80	--	--	20.6	16.2	--	--	20.6
320	"	"	"	Center	80	78	141	"	--	0.11	0.07	18.9
321	"	"	"	Bottom	80	77	146	"	16.4	--	--	21.0

* All runs with 90-degree, 4-inch-bend-radius test sections.

TABLE 16. REDUCED DATA FOR ROUGH-WALL AND HEATED TEST SECTIONS

Run No.	Air Mass Flow, lb/hr	Net Fuel to Test Section, lb/hr	Entrained Air/Fuel Ratio	Saturated Air/Fuel Ratio	Test Section Air Velocity, average, ft/sec	Test Section Air Density, lb/ft ³	Reynolds No.	Local Total Fuel Rate to Probe, lb/hr	Vapor Fuel Rate, lb/hr	Local Entrained Liquid Fuel Rate, lb/hr	Average Total Fuel Rate to Probe, lb/hr	Wall Film Fuel Rate, lb/hr	Total Sampled Fuel Rate, lb/hr
<u>Rough Wall</u>													
312		3.3	54	94	85	.0540	39,100	1.85	1.91	--			
311	180	--	--	97	"	"	"	1.85	1.85	--	1.90	1.45	3.35
313		4.5	40	94	"	"	"	2.00	1.85	0.15			
<u>Heated Inlet Air</u>													
319		--	--	49	90	.0512	37,500	4.85	3.39	1.46			
318	180	7.3	25	51	"	"	"	4.67	3.34	1.33	4.68	0.19	4.87
317		--	--	49	"	"	"	4.53	3.27	1.26			
<u>Heated Wall</u>													
322		4.4	41	--	92(2)	.0499	37,500	3.09	?	0			
320	180	--	--	80(1)	"	"	"	2.83	?	0	3.02	0.07	3.09
321		4.2	43	82(1)	"	"	"	3.15	?	0			

Note: All runs with 90-degree, 4-inch-bend radius test sections.

(1) At inlet.

(2) Average.

same for all tests, 20.6 lb/hr. A major fraction of the fuel to the mixture generator is removed by the chamber skimmer--this is the fuel that is not entrained by the air in the mixture generator and which impacts on the mixture-generator-chamber wall and must be removed. A small amount of additional fuel impacts on the wall of the transition section between the mixture generator and the test section and is removed by the No. 1 skimmer just upstream of the test-section entrance. The net fuel rate entering the test section should equal the average entrained fuel rate sampled by the probe at the exit plus the fuel rate to the No. 2 skimmer at the test-section exit.

Mass-balance data are presented in Table 17, from which it is evident that a good mass balance was not obtained. On the average, there is a systematic error of 1.4 lb/hr of fuel not accounted for--about 7 percent of the gross fuel rate to the mixture generator, but a much higher percentage of the net fuel delivered to the test section.

TABLE 17. FUEL MASS-BALANCE SUMMARY

Air Flow, cfm		Test Section			
		Straight Section	30-Degree Bend	90-Degree Bend, 4-inch radius	90-Degree Bend, 0-inch radius
20	Fuel input, lb/hr	3.1	3.0	3.0	3.0
	Fuel collected, lb/hr	<u>1.1</u>	<u>1.2</u>	<u>1.3</u>	<u>1.1</u>
	Difference, lb/hr	2.0	1.8	1.7	1.9
	Percent collected	36	41	42	36
40	Fuel input, lb/hr	3.6	4.6	3.2	4.4
	Fuel collected, lb/hr	<u>2.6</u>	<u>2.9</u>	<u>3.0</u>	<u>2.9</u>
	Difference, lb/hr	1.0	1.7	0.2	1.5
	Percent collected	71	62	95	66
70	Fuel input, lb/hr	5.2	5.0	4.8	5.8
	Fuel collected, lb/hr	<u>3.8</u>	<u>3.7</u>	<u>3.7</u>	<u>3.8</u>
	Difference, lb/hr	1.4	1.3	1.1	2.0
	Percent collected	73	75	77	65

An obvious possible source of error is the result of computing the net fuel flow to the test section as the relatively small difference between the fuel to the generator and the fuel removed by the chamber skimmer. Other possible errors include the following:

- Nonrepresentative or nonisokinetic sampling of the entrained fuel
- Overloading the No. 2 Skimmer at the test-section exit, thus not collecting all of the wall-film fuel
- Errors in the determination of the fuel concentration in the mixture sampled by the probe.

A three-point sampling traverse would not be expected to yield a precise mass balance; also, no mathematical correction for nonisokinetic sampling conditions was attempted because of the unreliability of such corrections for pulsating flow. However, such errors could hardly have been large enough to account for the mass imbalance.

In examining the data, it is apparent that the values for the total amount of fuel sampled, as a function of the air-flow rate, are reasonably consistent, while the data for the fuel removed by the chamber skimmer are not. It has been concluded, therefore, that the chamber skimmer data are not accurate, and the cause of the erratic data is believed to be carry-over of fuel out of the trap used to measure the skimmer flow rate. Consequently, we are inclined to disregard the computed values for fuel input rate to the test section, and rely on the observed values of fuel rate at the test-section exit.

Total Sampled Fuel Rate. It is believed that the No. 2 Skimmers effectively remove all of the fuel flowing as the wall film, and that the simple volumetric measurement of this fuel rate is relatively accurate--on the order of ± 2 to 5 percent.

The values for the fuel concentration in the samples collected by the probe are obtained in a less direct manner, and are therefore possibly subject to greater error. As a check on this, as described previously, samples of the same concentration were run directly to the hydrocarbon analyzer and through the probe sampling system. The main probable source of error would be "hangup" of hydrocarbon within the sampling system, and the checks indicated that this was not a problem. Values for the total fuel collected by the probes are estimated to be accurate within ± 5 percent.

Vapor Flow Rate. The computed vapor flow rate is subject to errors in measuring the mixture temperature at the test-section exit and is also subject to the validity of the assumption that the vaporized fuel is in equilibrium with the liquid fuel. A 2 F error in mixture temperature measurement is equivalent to an error in vapor flow rate of 0.06 lb/hr at 20 cfm, 0.12 lb/hr at 40 cfm, and 0.22 lb/hr at 70 cfm. Comparing these possible errors to the observed flow rates indicated that up to 20 percent error in values for vapor flow and errors up to 50 percent in entrained liquid fuel flow rate could be anticipated. Accordingly, values given for entrained fuel should be considered qualitative at best.

Replication Results. The data presented in Tables 13 and 14 were obtained to provide more precise information on mixture stratification by traversing with 9 points instead of the usual 3. These data also provide a check on one data set, the 40-cfm air-flow runs with the 90°-bend, 4-inch-radius test section presented in Tables 9 and 10. A comparison of the two sets of data indicates that fuel-transport behavior is substantially the same in terms of total fuel entrained, wall fuel-film flow rate, and degree of entrained-fuel stratification. Only the values for absolute amount of entrained liquid fuel are substantially different.

Overall Accuracy. Measurements of total entrained fuel and wall fuel-film flow rate are believed to be sufficiently accurate to characterize the fuel transport in the experiments. Determination of the relative amounts of entrained fuel occurring as liquid and vapor is subject to substantial errors; nevertheless, the results are believed to provide a valid qualitative indication of fuel-droplet transport characteristics.

Test-Section Flow Conditions

Test-section average air velocities in the experiments conducted range from about 50 to 115 ft/sec; the resulting Reynolds numbers range from about 10,000 to 69,000. Thus, air flow is well into the turbulent regime under all experimental conditions. Since there is a sharp contraction and a short round-to-square transition section just upstream of the test section,

it is unlikely that anything approaching a fully established flow condition is established at the test-section inlet.

Columns 22 and 24 of Table 4 indicate that there is some stratification of the entrained fuel at the test section inlet, particularly at the higher air velocities. A higher concentration of fuel in the center of the section is indicated, which could be caused by the upstream sharp contraction. The variation in entrained fuel is reasonably symmetrical.

In all cases, the observed test-section wall temperature is a few degrees colder than the surrounding air temperature. Consequently, the flow is not adiabatic, although the heat gain should be negligible because the plastic test-section material is not a good heat conductor. As discussed previously, it is believed that the liquid and vapor fuel components are substantially in equilibrium. Because of the low volatility of the test fluid, compared to gasoline, air-fuel ratios at saturation range from 80 to 150, depending upon the fuel temperature.

Droplet Impaction

Figure 23 shows the amount of liquid fuel impacted on the test-section wall as a function of air-flow rate and test-section geometry. As would be expected, the least amount of fuel was impacted in the straight section, and increasingly larger amounts of fuel were impacted in the 30-degree and 90-degree bends.

The fact that a greater amount of fuel was impacted in the long-radius 90-degree bend than in the sharp-cornered 90-degree bend is a surprising result; however, there is some reason to believe that reentrainment is responsible for the apparently lower impaction in the sharp-cornered test section. There is additional support for this hypothesis in later discussion.

Figure 24 shows the same data as Figure 23, expressed as a fraction of the total liquid fuel flow. The lower curve shows a surprisingly large fraction of the liquid fuel impacted in the straight test section--over 50 percent at 20 cfm, decreasing to 23 percent at 70 cfm. From this, it is apparent that flow-induced turbulence plays a significant role in droplet

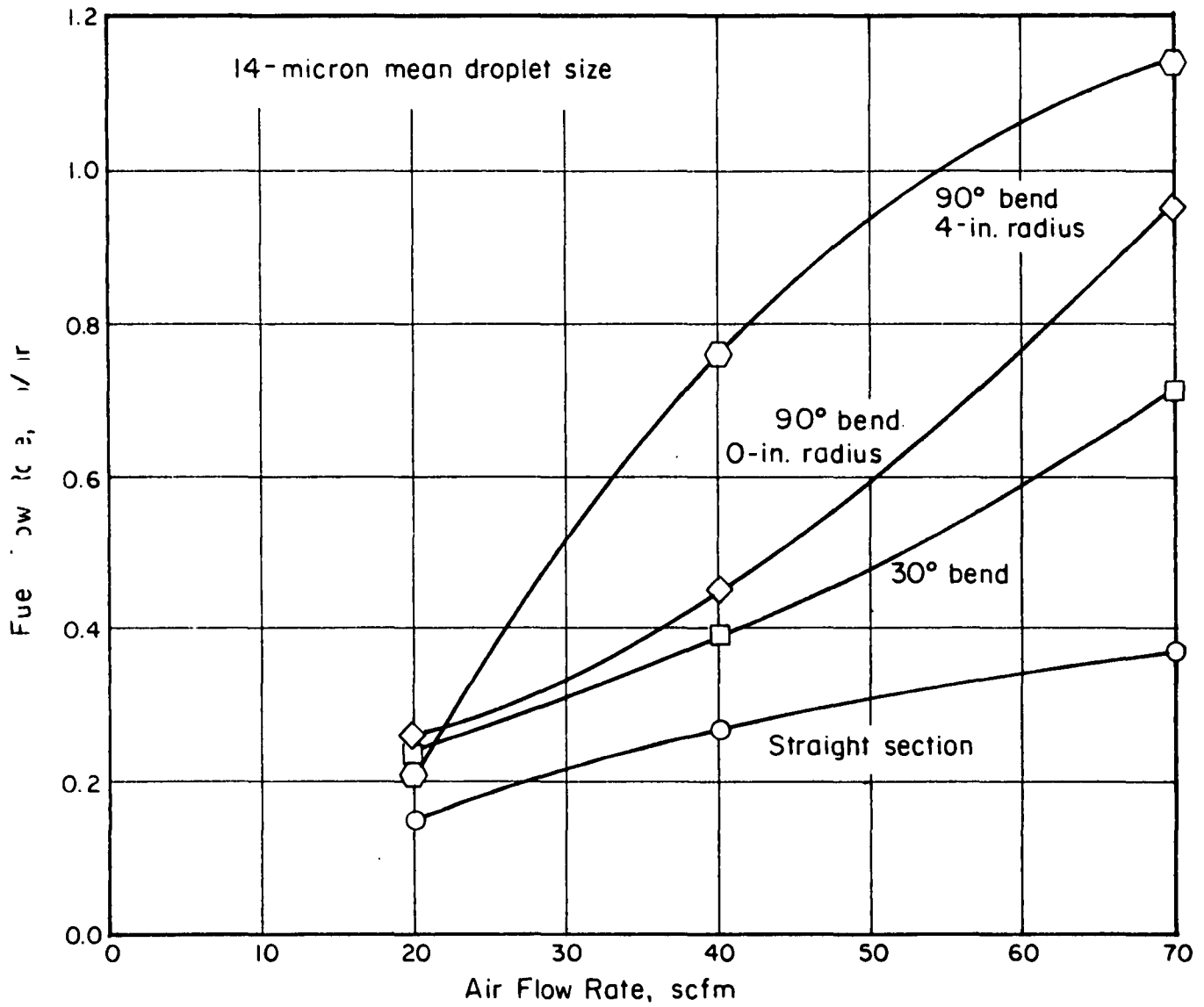


FIGURE 23. WALL FUEL-FILM FLOW RATE AS A FUNCTION OF AIR FLOW RATE AND TEST-SECTION GEOMETRY

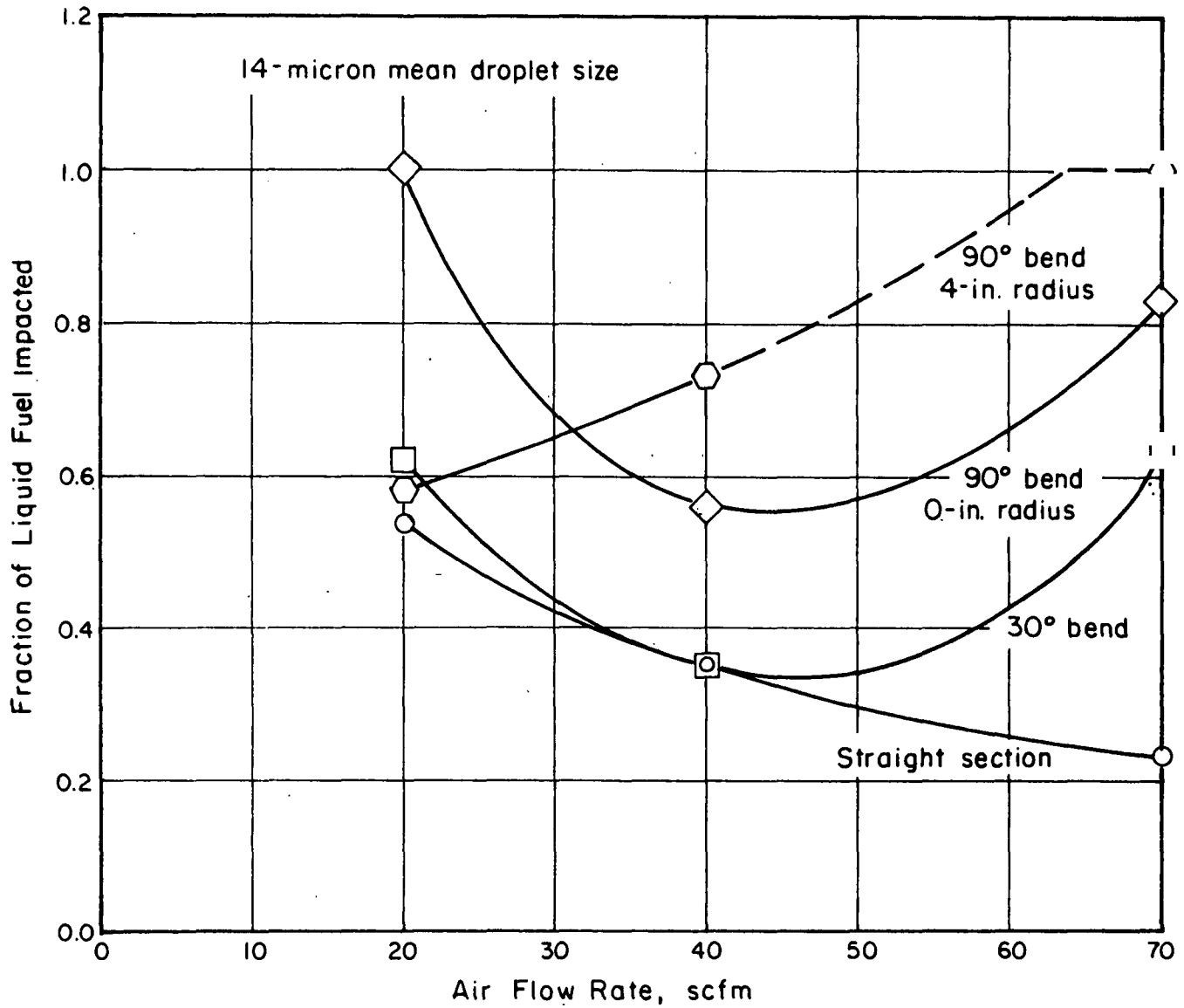


FIGURE 24. FRACTION OF LIQUID FUEL IMPACTED AS A FUNCTION OF AIR FLOW RATE AND TEST-SECTION GEOMETRY

impaction. The fact that a lower fraction of fuel is impacted in a straight section as air velocity is increased is not necessarily surprising if an analogy to heat transfer is made. As air velocity is increased in a duct, the amount of heat transferred per degree of temperature difference increases, but less than in proportion to the mass flow of air. Since heat transfer and droplet impaction occur by analogous physical mechanisms, one could expect the fraction of droplets impacted to decrease as air flow increased.

From the curve for the 30-degree bend in Figure 24, it can be inferred that at the lower air velocities, turbulence is more important than turning angle in causing droplet deposition. However, at 70 cfm, the effect of turning predominates. The curve for the 90-degree, 4-inch-radius bend indicates that the high-air-flow-rate effect of turning is greater, as would be expected.

The curve for the 90-degree sharp-cornered bend shows a departure from the trend of the other three curves, with 100 percent impaction at 20 cfm and lesser impaction at higher air flow rates. Again, reentrainment is believed to be a significant factor in this departure. At flows above 20 cfm, it is possible that 100 percent droplet impaction is still experienced, but that reentrainment is negligible at flow rates below 20 cfm.

Figures 25 through 28 show how the entrained fuel droplets are distributed at the test-section exit, as a function of air-flow rate and test-section geometry. Figure 25 shows a reasonably flat fuel-droplet-flow distribution at all air flow rates with the straight test section. This could be expected because of the apparent high degree of turbulent mixing occurring within the test section. Figure 26 indicates a flat fuel-droplet-flow profile at 20 cfm for the 30-degree-bend section, but with increasing stratification toward the outside of the bend (bottom) at higher air-flow rates.

Figure 27 shows a somewhat increased degree of stratification with the 90-degree, 4-inch-bend test section at 20 and 40 cfm, as would be expected. No curve is shown for 70 cfm in Figure 27 since all the droplets were impacted at that condition.

Figure 28, for the sharp-cornered bend, shows no entrained liquid fuel at 20 cfm, highly stratified droplets at 40 cfm, and an extreme degree of stratification at 70 cfm with droplets only along the outer wall of the bend.

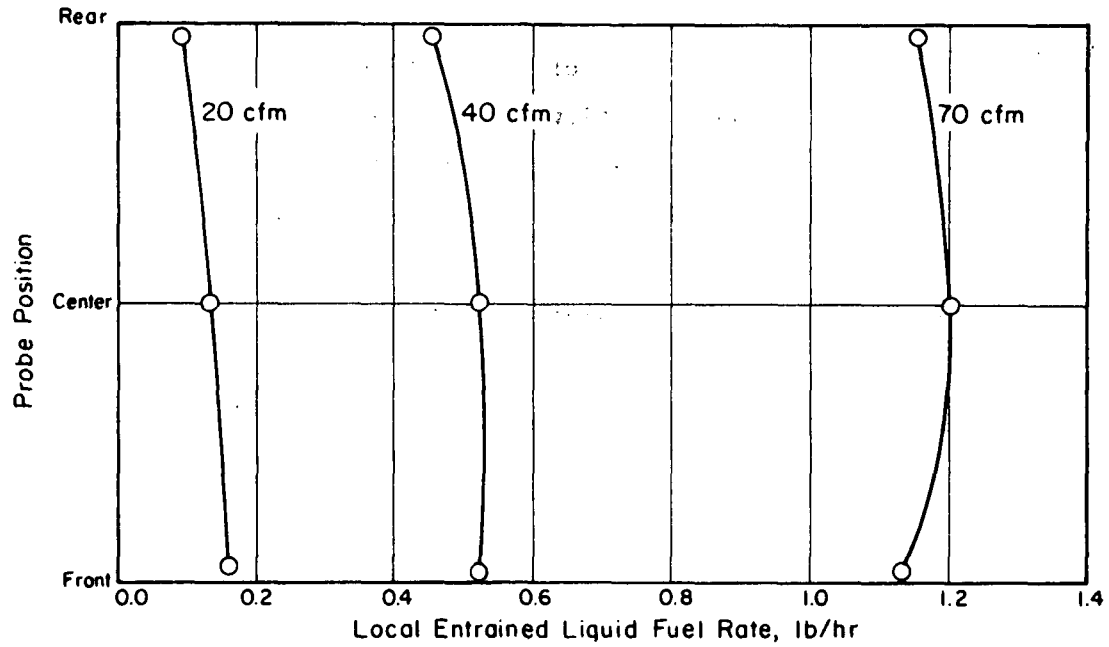


FIGURE 25. ENTRAINED-FUEL-DROPLET STRATIFICATION AT STRAIGHT TEST-SECTION EXIT

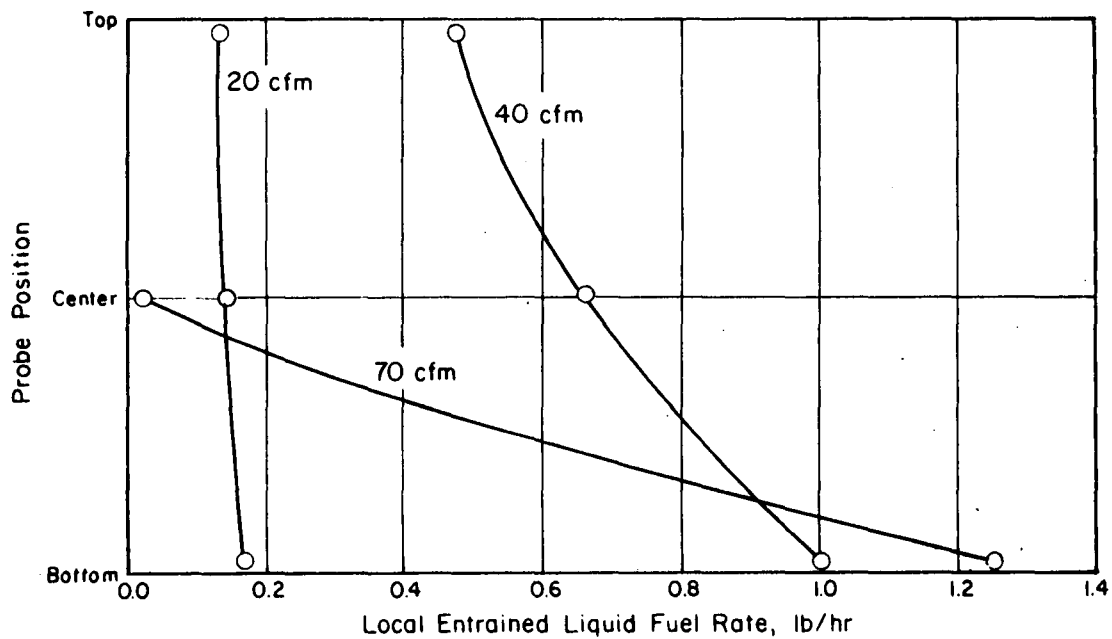


FIGURE 26. ENTRAINED-FUEL-DROPLET STRATIFICATION AT 30-DEGREE-BEND TEST-SECTION EXIT

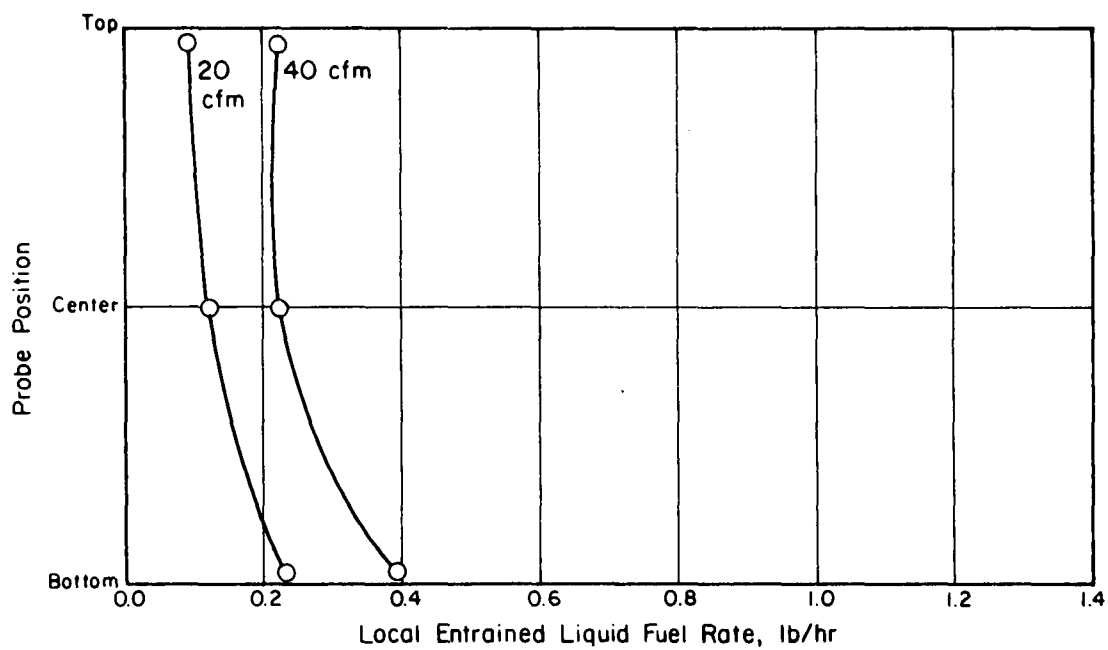


FIGURE 27. ENTRAINED-FUEL-DROPLET STRATIFICATION AT 90-DEGREE, 4-INCH-RADIUS-BEND TEST-SECTION EXIT

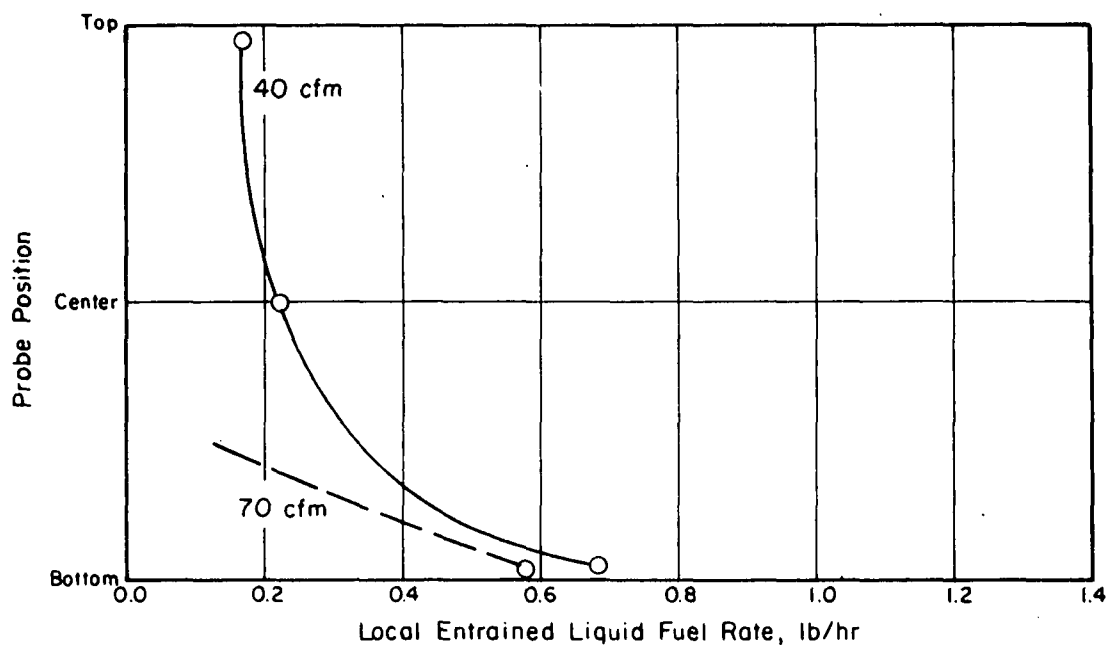


FIGURE 28. ENTRAINED-FUEL-DROPLET STRATIFICATION AT 90-DEGREE, 0-INCH-RADIUS-BEND TEST-SECTION EXIT

This figure does not strongly support the hypothesis that reentrainment is a significant factor, nor does it particularly detract from it.

From the droplet-impaction experiments, it is clear that ultrafine atomization does not make it possible to avoid fuel-droplet impaction because of the role of flow-induced turbulence in causing impaction. Nevertheless, it appeared possible to avoid impacting at least half the fuel under the range of air-flow rates investigated with a 14-micron mean-droplet size in both straight and 30-degree-bend test sections. The effects of bend turning angle are more significant at higher velocities and predominate over turbulence-caused effects at 70 cfm. Over half the fuel was impacted in the 90-degree-bend test sections under all conditions with 14-micron mean-droplet size.

The fact that the sharp-cornered 90-degree bend resulted in less net fuel impaction, possibly due to reentrainment, should not necessarily be used to indicate that the sharp-bend configuration is superior to the long-radius bend for intake manifolds. In this case, the reentrainment is probably the result of greater liquid-fuel hold-up in the bend--a condition leading to time variations in mixture ratio and poor response to transients.

Runs 311-313 were run with a rough-walled test section (90-degree, 4-inch-radius bend) to check for possible effects of wall surface on droplet impaction. Data for these runs are presented in Tables 15 and 16, and can be compared to Runs 229-231, in Tables 9 and 10 for equivalent test conditions for a smooth-walled section. This comparison shows about twice the fuel skimmed off the wall with the rough surface-- a surprising result in that no difference in the rate of droplet impaction was anticipated. No explanation for this result is available, nor is the significance of the result apparent at this time, except for one possibility. There is the possibility that reentrainment is significant in all the tests conducted on droplet impaction, and the rough wall inhibits reentrainment. It should be emphasized that there is no evidence that this is the case. However, if it were true, smooth-walled intake manifolds could be expected to produce superior engine response characteristics.

Generally, then, it can be concluded that ultrafine atomization, minimum manifold-passage turning angle, long bend radii, and low air velocity are all conducive to low droplet impaction; however, some impaction will occur under any circumstances if there are fuel droplets in the air stream. It is

therefore further concluded that nearly complete vaporization in the mixture generator of auto-engine induction systems is highly desirable.

Wall Fuel-Film Transport

Wall fuel-film transport observations were made purely on a visual basis, and the information so obtained relates mainly to flow patterns and areas of liquid holdup. Figures 29, 30, and 31 are sketches illustrating the observed flow patterns. The patterns for the 30-degree bend and the long-radius 90-degree bend were similar and did not vary appreciably with air-flow rate. Liquid deposition on the walls was apparently uniform upstream of the bend; at the bend, liquid was observed to move across the side walls from the outer wall to the inner wall. It is highly likely that this flow pattern is the result of secondary air flows along the side walls of the bend which are caused by the higher static air pressure along the outside wall of the bend.

Liquid swept toward the inside of the bend accumulates at the center of the inside wall, where the liquid film is noticeably thicker. The increased droplet deposition along the outer wall is apparently well distributed.

Figure 31 shows the wall fuel-film patterns observed in the sharp-cornered 90-degree bend. With this geometry, there are pockets of liquid-fuel holdup on both inner and outer walls. Intuitively, it would seem that such a flow condition is highly conducive to reentrainment.

These observations were made with transparent, smooth-walled test sections, while intake manifolds are typically rough surfaced sand castings. We believe that the general flow patterns will be similar for both smooth and rough-walled passages; however, film thicknesses and velocities would be altered. Also, the possibility for reentrainment might be different with a rough surface. No conclusions have been drawn in this study regarding absolute film thickness and velocity.

The character of the fuel-film surface on smooth-walled test sections in most cases would be described as "rippled", but not thick enough to become "wavy".

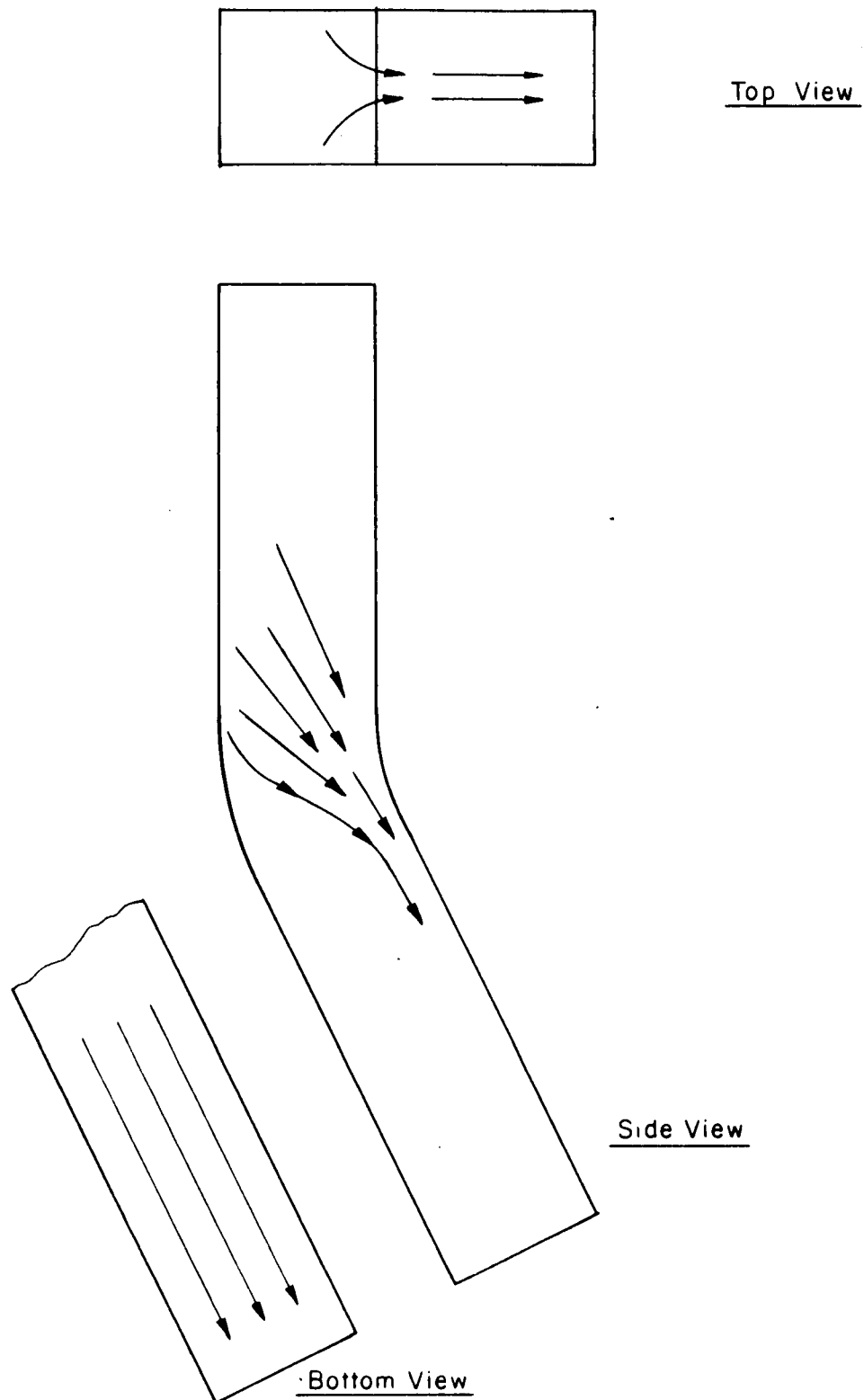


FIGURE 29. WALL FUEL-FILM FLOW PATTERN IN 30-DEGREE TEST SECTION

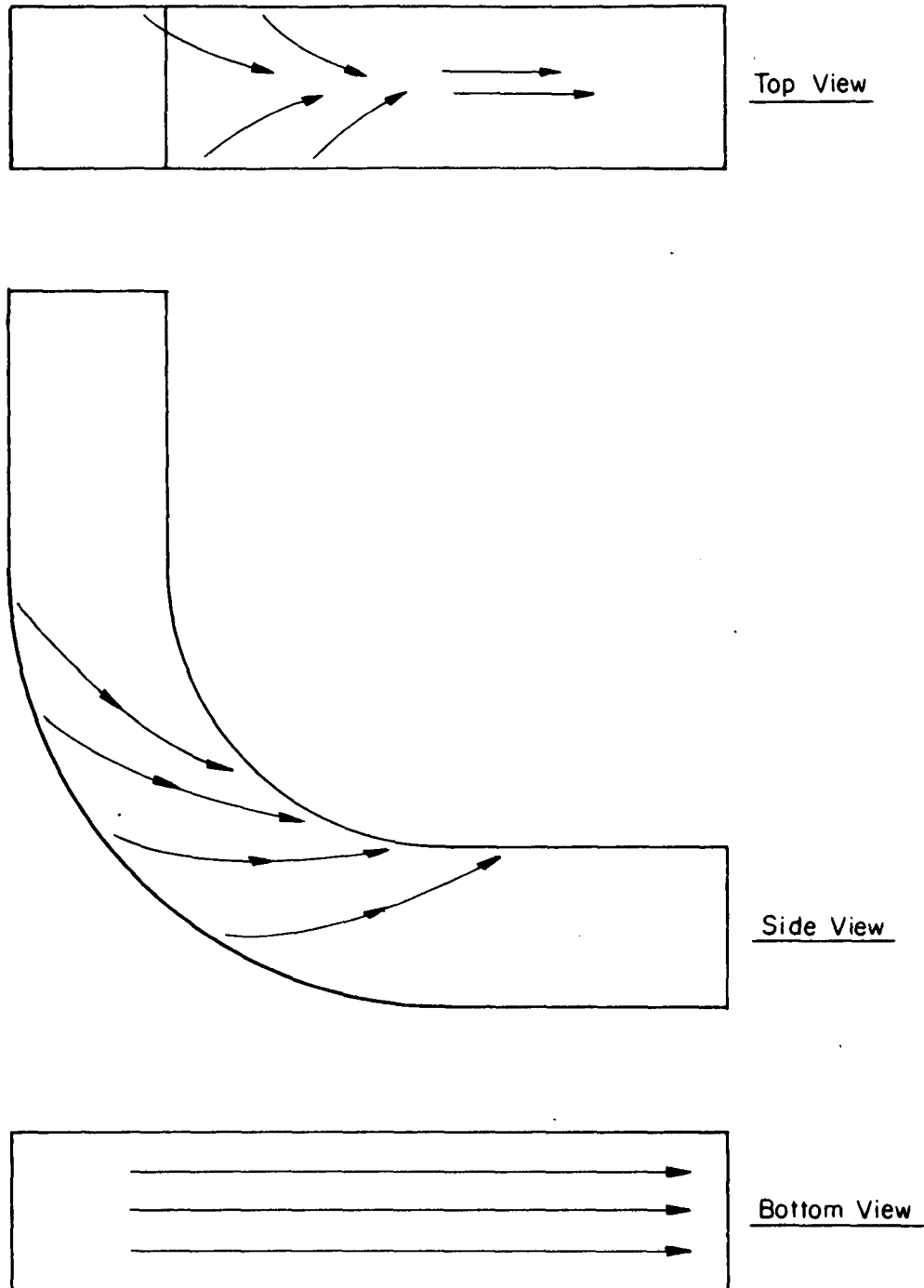


FIGURE 30. WALL FUEL-FILM FLOW PATTERN IN 90-DEGREE,
4-INCH RADIUS TEST SECTION

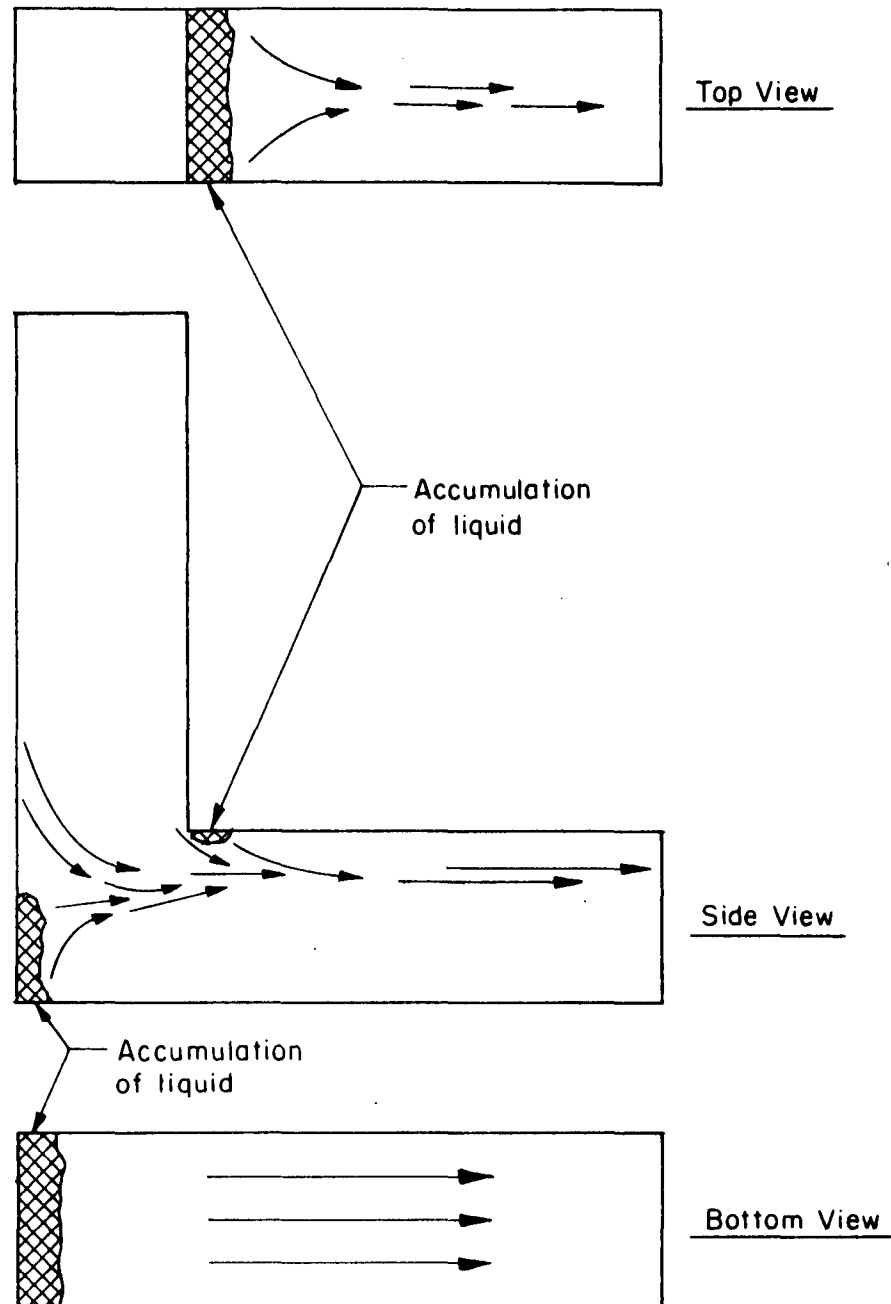


FIGURE 31. WALL FUEL-FILM FLOW PATTERN IN 90-DEGREE,
0-INCH RADIUS TEST SECTION

Vaporization

The results of the experimental work provided information on vaporization both from liquid-fuel droplets and from the liquid wall film. For the case of droplet vaporization, this information is largely qualitative, since rate of vaporization could not be measured directly in the experimental apparatus. As far as the authors could determine, existing literature information on droplet and film vaporization cannot be applied to compute rates of vaporization that might be occurring in the experiments conducted.

Droplet Vaporization. In conducting experiments on droplet dynamics, it was desirable to have test conditions that would result in a constant droplet size. This could be achieved by two possible circumstances: (1) droplet vaporization in the mixture generator so rapid that equilibrium conditions are established in the test section, or (2) droplet vaporization so slow that the amount of vaporization in the test section is negligible. As has been discussed previously in this report, the former alternative prevailed and necessitated the use of a test fuel of low volatility in order to establish droplets in the test section.

Accordingly, we know droplet vaporization was rapid; unfortunately, we cannot characterize accurately how rapid. However, the calculated residence time of the air in the mixture generator provides a lower bound on the vaporization rate. At 70 cfm air rate, this residence time is approximately 0.24 second. Mixture residence times in current conventional induction systems are on the order of 10 to 100 milliseconds; consequently, the residence time in the mixture generator of the experimental apparatus represents from 2-1/2 to 25 times the residence time in a typical induction system.

The data for Runs No. 317-319 in Tables 15 and 16 were taken with air entering the mixture generator heated to 125 F. Data for the same test section without preheated air are given for Runs 229-231 in Tables 9 and 10. A comparison of these data shows that about 60 percent more fuel was captured by the air in the mixture generator with the heated air. If aerodynamic entrainment was the principal mechanism by which the air captures the fuel, the effect of inlet air temperature on the amount captured should be slight, and the main effect of temperature would be to vaporize a greater fraction of the entrained fuel.

The fact that more fuel is captured with the heated air indicates that vaporization during the aerodynamic entrainment is appreciable. The zone in which entrainment occurs is of small volume relative to the overall volume of the mixture generator, consequently, it can be inferred that substantial vaporization occurs in a fraction of the total residence time of the air in the mixture generator.

Therefore, although quantitative data on rate of vaporization were not obtained, there is reason to expect that fuel droplets in the vicinity of 14 microns size would essentially approach equilibrium vaporization in air in milliseconds, and could vaporize appreciably in times as short as 10 milliseconds.

Heated-Wall Tests. Data for tests at 40 cfm with a heated-wall test section (90-degree, 4-inch-radius bend) are given in Tables 15 and 16, Runs 320-322. Wall-temperature data are presented in Table 18. Compared to Runs 229-231 in Tables 9 and 10 for the same conditions with an unheated test section, it is seen that the amount of wall-film fuel captured by the No. 2 skimmer is 0.07 lb/hr with the heated section and 0.76 lb/hr without heat. Thus, it is indicated that the effect of heating the test-section wall to 190 F is to vaporize about 90 percent of the fuel that would otherwise impact and remain on the test-section wall.

Another effect is that the mixture temperature rises about 64 F in the test section; thus, the mixture, which was saturated with fuel vapor at the test-section inlet, is not saturated at the exit. This leaves us with no information on whether there is entrained liquid fuel at the exit under these conditions.

Heating the test-section walls can reduce the fuel-film flow rate by two possible mechanisms: (1) by causing the entrained droplets to vaporize before they impact, or (2) by vaporizing the wall-film fuel.

The wall-temperature data presented in Table 18 show that the outside-of-bend wall temperatures downstream of the bend are a few degrees lower than the average, indicating that impacted fuel droplets are probably cooling the wall. Consequently, it seems unlikely that all or most fuel droplets are being vaporized before they impact. The residence time of the mixture in the test section at 40 cfm air input is about 16 milliseconds, and it is likely that

TABLE 18. WALL-TEMPERATURE DATA FOR
HEATED TEST SECTION

Thermocouple Location	Thermocouple Number	Temperature, F
Inside wall	2	202
"	3	191
Side wall	6	196
"	1	187
"	8	186
"	9	187
Outside wall	4	194
"	5	198
"	7	180
"	10	180

Thermocouple locations are shown in Figure 10.

14-micron fuel-droplet vaporization is not complete within that duration. There is no good measure of whether droplet vaporization is appreciable in the test section with the heated wall.

The amount of heat transferred from the wall in vaporizing the fuel is small compared to the sensible heat transferred to the air. Assuming 0.7 lb/hr of fuel is vaporized and that the latent heat of vaporization is 150 Btu/lb, 105 Btu/hr are transferred to vaporizing the wall fuel-film. Estimating that the air is heated 64 F in the test section, a heat input to the air of 2770 Btu/hr is computed.

Although the mechanisms by which the fuel is vaporized in the heated test section is not clear, it is clearly significant that the wall fuel-film was virtually eliminated by the effect of the 190 F wall temperature.

Overall Conclusions

It is apparent that, with fine atomization, minimum manifold-passage turning angle, long bend radii, and low air velocities, fuel-droplet impaction can be kept low, but it cannot be avoided. Fortunately, ultra-fine atomization is also highly conducive to rapid droplet vaporization, and indications are that droplet vaporization with droplet sizes below 20 microns occurs rapidly enough to achieve near-equilibrium vapor concentration in a practical mixture generator at moderate engine speeds, and possibly to achieve appreciable vaporization at higher engine speeds.

Even though some droplet impaction is apparently unavoidable, it is evident that, with fine fuel atomization, the wall fuel-film can be virtually avoided by the use of moderately heated intake-manifold passages.

DESIGN CONCEPTS

The original objective of this part of the study was to design, construct, and demonstrate a laboratory prototype fuel-induction system having the capability of improved fuel-air mixing and distribution. This system was to include a mixture generator, a vaporization section, and an intake manifold.

While the prototype fuel-induction system was intended for initial use as a laboratory apparatus, one of the design constraints was that the mixture-generator and intake-manifold should be within size limitations that would ultimately permit use in the space available in standard automobiles. The vaporization system, on the other hand, was considered for use only as a laboratory tool for providing a fully vaporized-fuel-air mixture to an engine.

As previously mentioned, the scope of this part of the study was amended to include conceptual design studies; and the detail design, fabrication, and demonstration tasks were deleted.

Induction System Concept

General Description

Figures 32 and 33 are layout sketches of the proposed fuel atomization system and intake manifold. The system consists of an air inlet and filter housing, a fuel atomizer, a mixing chamber, a throttle, and a manifold. The air cleaner diameter and its height above the engine have been made approximately the same as for conventional induction systems so that this system would fit under the hood of standard automobiles. The air cleaner is also designed to house a standard filter element.

The configuration shown in Figures 32 and 33 will fit a Ford 351 CID V-8 engine. This engine is available in both automotive and industrial/marine versions, and was selected for the primary application because the inlet ports on the cylinder heads are spaced uniformly. The uniform inlet-port spacing simplifies the layout of intake passages around the circular manifold plenum.

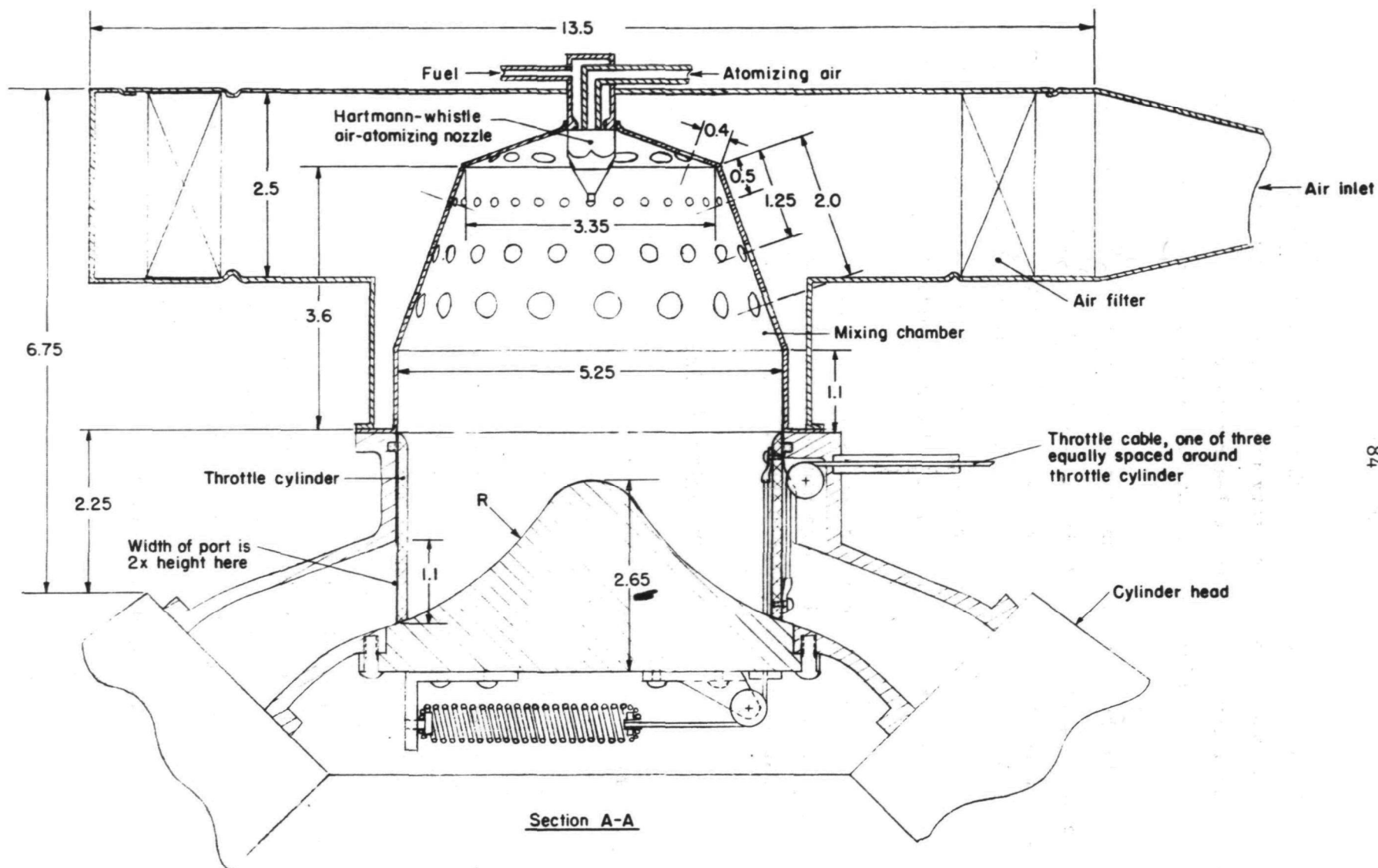


FIGURE 32. SKETCH LAYOUT OF PROTOTYPE IMPROVED INDUCTION SYSTEM-SECTION VIEW

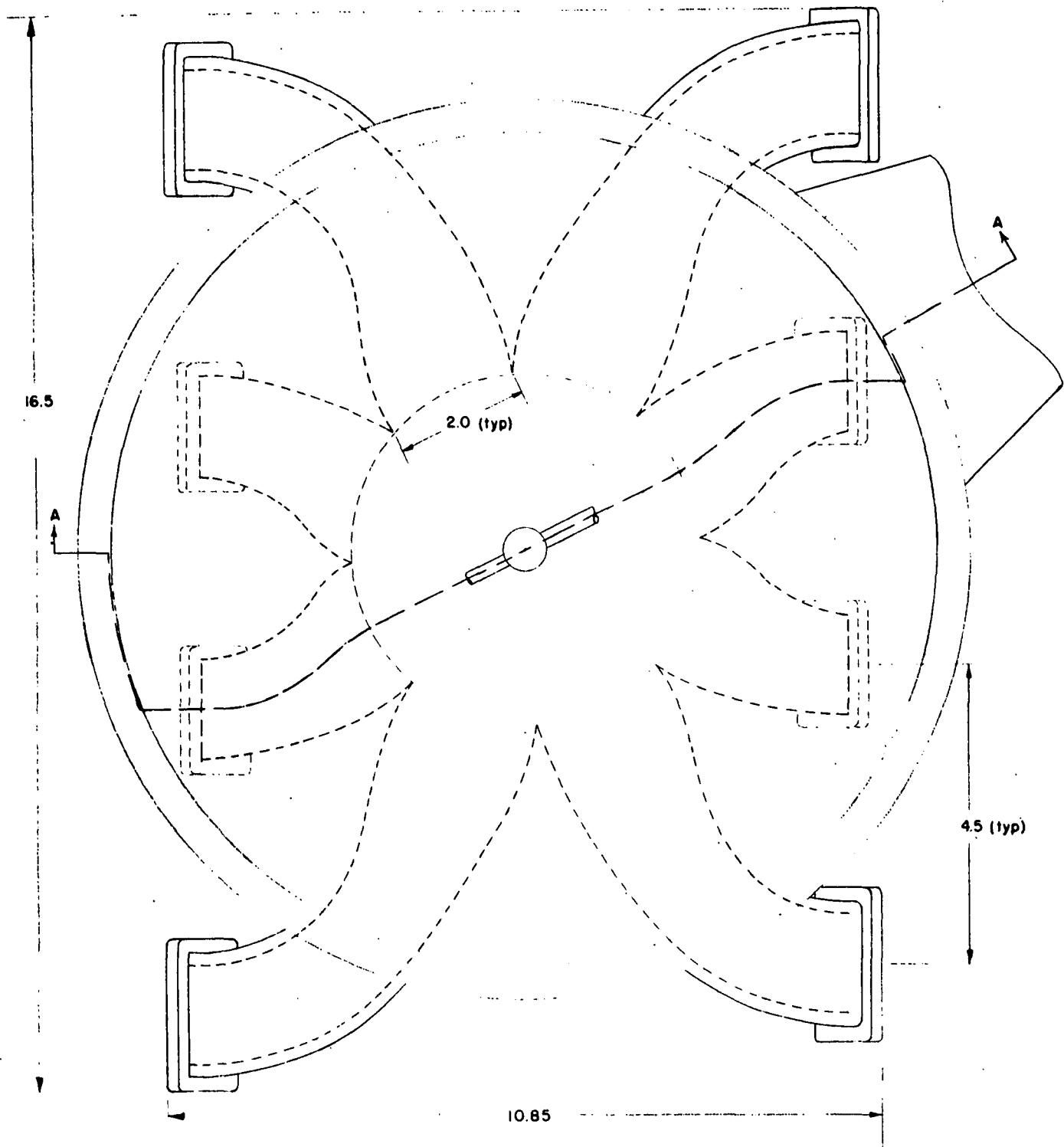


FIGURE 33. SKETCH LAYOUT OF PROTOTYPE IMPROVED INDUCTION SYSTEM-PLAN VIEW

Figures 34 and 35 are sketches of a proposed intake-passage layout for an engine with paired inlet ports in the cylinder head, such as the Chrysler 318 CID and 340 CID engines. The passages to the middle two ports on each side are more tortuous than those for the spaced-port manifold previously illustrated. However, the bends are not quite as sharp as they appear to be in Figure 35 because there is an elevation change of about 1-3/4 inches from the manifold plenum to the cylinder head port.

The dimensions given in these and subsequent figures in this section of the report are the more important or critical dimensions. Dimensions not given are generally arbitrary.

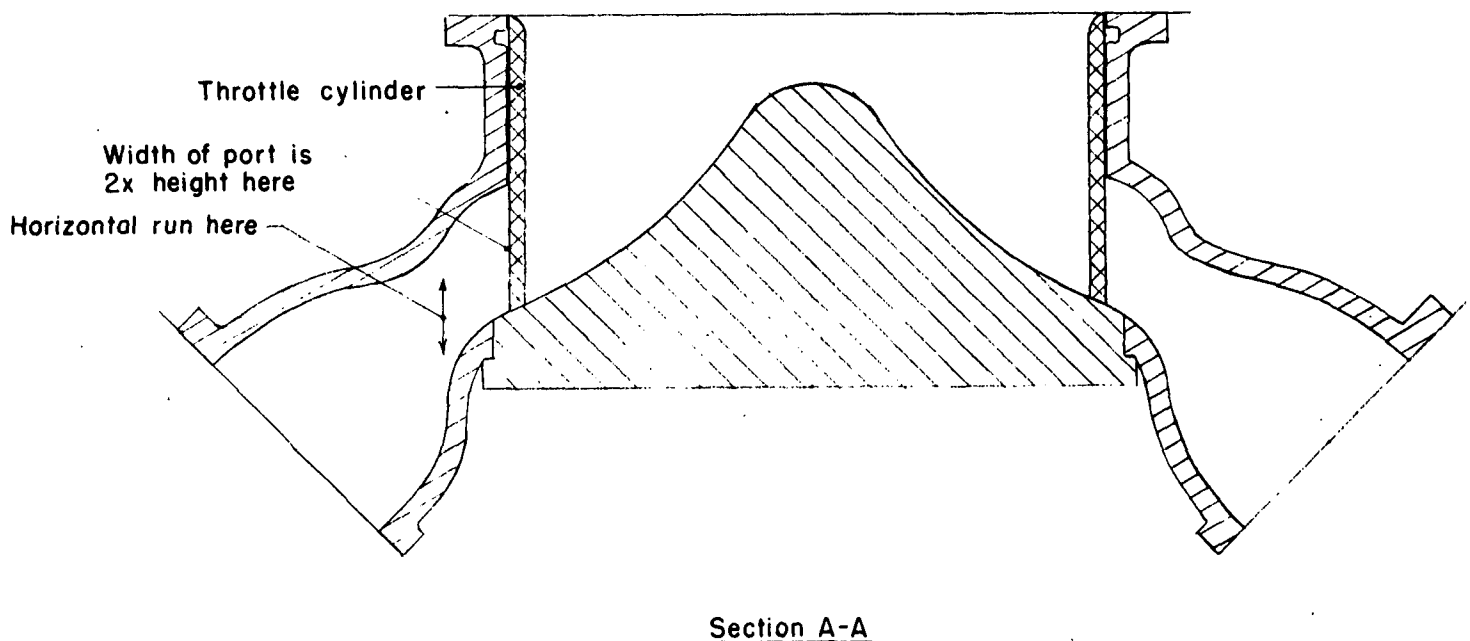


FIGURE 34. SKETCH LAYOUT OF INTAKE-PASSAGE CONFIGURATION FOR PAIRED-PORT ENGINE - SECTION VIEW

87

9.55

12.6

7.95

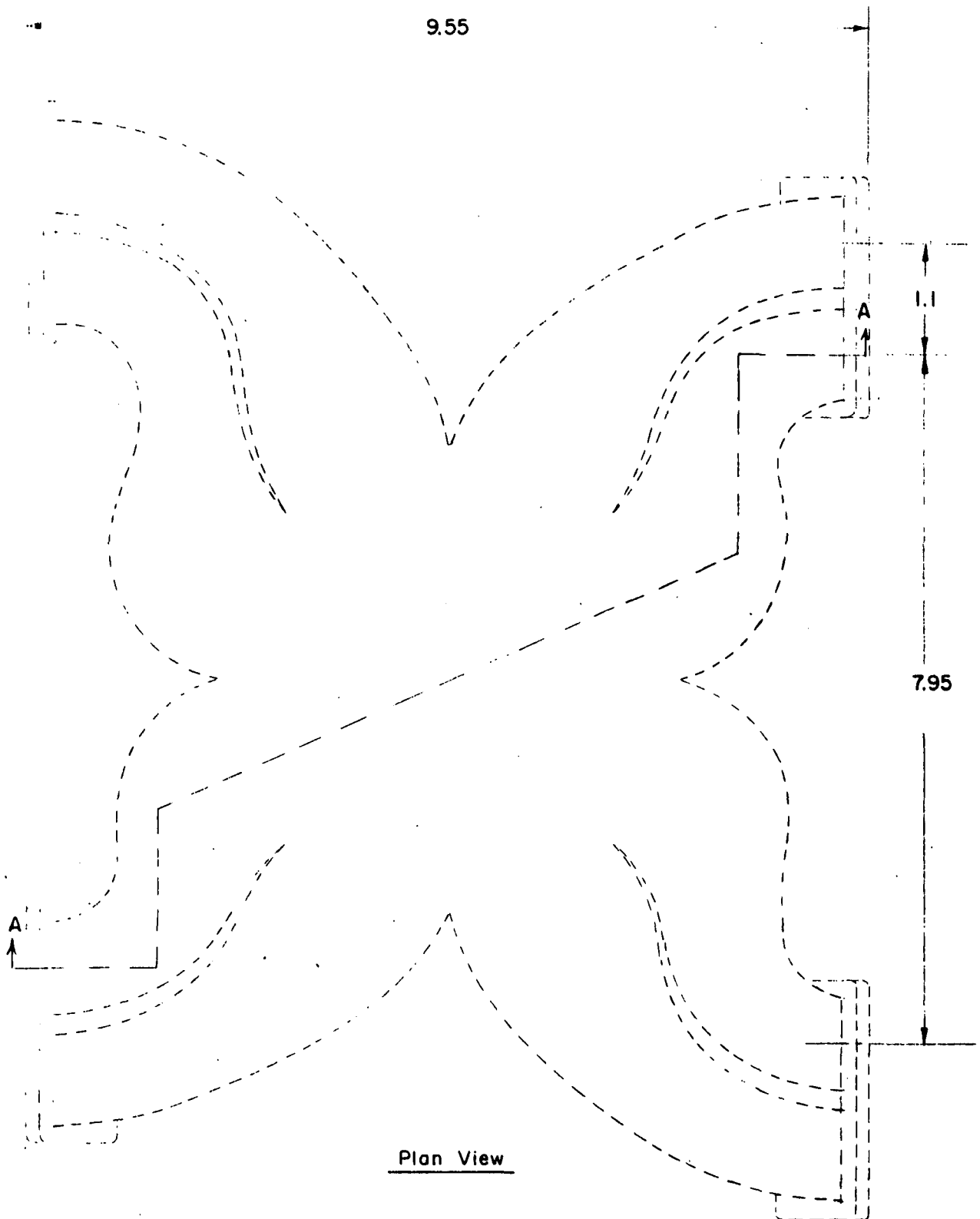


FIGURE 35. SKETCH LAYOUT OF INTAKE-PASSAGE CONFIGURATION FOR PAIRED-PORT ENGINE - PLAN VIEW

Fuel Atomizer

Several alternative atomization systems appeared promising for the automotive application. These were: the piezoelectric ultrasonic atomizer, the impinging-jet air atomizer, the Hartmann-whistle-type atomizer, and the spinning-disk atomizer.

In the ultrasonic atomizer, liquid fuel flows over a vibrating surface and is atomized by forces generated in the fluid by mechanical agitation. The piezoelectric ultrasonic atomizer consists of an electronic power supply which drives a piezoelectric disk. Attached to the disk is a cylindrical horn with a sharp outer edge which vibrates in a radial mode. Fuel flowing down the outer surface of the horn is atomized off the sharp edge.

The mean droplet size of liquid atomized ultrasonically is dependent on the frequency of vibration. A practical frequency range for units intended to deliver substantial flow rates is 25 to 100 KHz. An atomizer operating at 100 KHz can deliver droplet sizes in the range of 10 to 20 microns⁽⁷⁾.

The power requirement for ultrasonic atomization varies from about 5 watts for 2.1 lb/hr of fuel oil⁽⁸⁾ to about 23 watts for 160 lb/hr of water⁽⁹⁾.

In the impinging-jet air atomizer the energy of compressed air is used to atomize the fuel. In a simple configuration, a high-speed air flow is directed around the outside and approximately perpendicular to a jet of fuel.

Small droplet sizes can be obtained with impinging-jet atomization because the energy contained in the air stream can be independent of the quantity of fuel being atomized; that is, a large high-velocity air jet can be used to atomize a small amount of fuel. The power requirement for impinging-jet atomization is essentially the pumping work of the air.

The Hartmann-whistle-type atomizer involves a jet of high-velocity air which is impinged upon the open end of a small cavity⁽¹⁰⁾. This jet whistles with such intensity as to provide strong local shock waves in the space between the air nozzle and the cavity. Fuel introduced around the periphery of the air jet is atomized in the highly turbulent flow pattern around this cavity.

Droplet size capability of the Hartmann-whistle-type atomizer is of the same order as the piezoelectric ultrasonic atomizer. Air consumption is generally higher in this type of atomizer than in the impinging-jet atomizer, but smaller droplet sizes are attainable.

Spinning-disk atomization is based on the centrifugal acceleration of the fuel to a high velocity and subsequent discharge into the air stream. The fuel is introduced at the center of the disk, flows radially across the surface of the disk under the action of centrifugal force, and leaves the disk in a thin liquid sheet which immediately breaks up into uniformly sized droplets. Droplet size is dependent on disk radius and disk speed. Power requirements are dependent on fuel feed rate, disk speed, and disk radius.

Spinning-disk atomizers are capable of producing droplet sizes well under 20 microns, and energy requirements are in the 400 to 500 watt range for maximum fuel flow.

Each of the promising alternative fuel atomization systems was evaluated on the basis of simplicity, compactness, energy requirements, and minimum-droplet-size capabilities. Although a desirable droplet size of under 20 microns has been indicated by both theoretical considerations and experimental data, it has been stipulated that the fuel atomizer to be proposed as a prototype should be capable of producing a range of droplet sizes. With this capability, the propotype can be used to investigate the effects of droplet size on performance in an actual engine.

Table 19 summarizes the results of the fuel-atomizer evaluation. The Hartmann-whistle-type atomizer appeared to be the most promising, as it is fairly well developed in this application, is simple and compact, and can be designed for a wide range of droplet sizes and fuel flow rates.

The actual fuel nozzle selected for the prototype induction system is similar to a commercially available unit which is being used in a modified form in a low-emission-burner development program at Battelle. The nozzle operates on the Hartmann whistle principle, with an air and fuel jet directed at sonic velocity against a cup-like deflector. A cone-shaped spray pattern of finely atomized fuel results.

Figure 36 is a sketch of the proposed nozzle showing the spray pattern.

TABLE 19. COMPARISON OF ALTERNATIVE ATOMIZATION SYSTEMS

	Piezo-Electric Ultrasonic	Impinging Jet	Hartmann Whistle	Spinning Disk
Lowest practically attainable mean drop size	20 μ	<20 μ	<<20 μ	20 μ
Fuel flow rate capacity	Adequate with possible limitations	Adequate	Adequate	Adequate if stacked disks used
Energy required for maximum fuel flow rate of 36 lb/hr	~15 watts	~500 watts	~450 watts	~500 watts
Components required	Piezo crystal Power supply Fuel control	Nozzle Air pump Fuel control	Nozzle Air pump Fuel control	Disk(s) High-speed motor Fuel control
Space requirements	Medium	Small	Small	Large

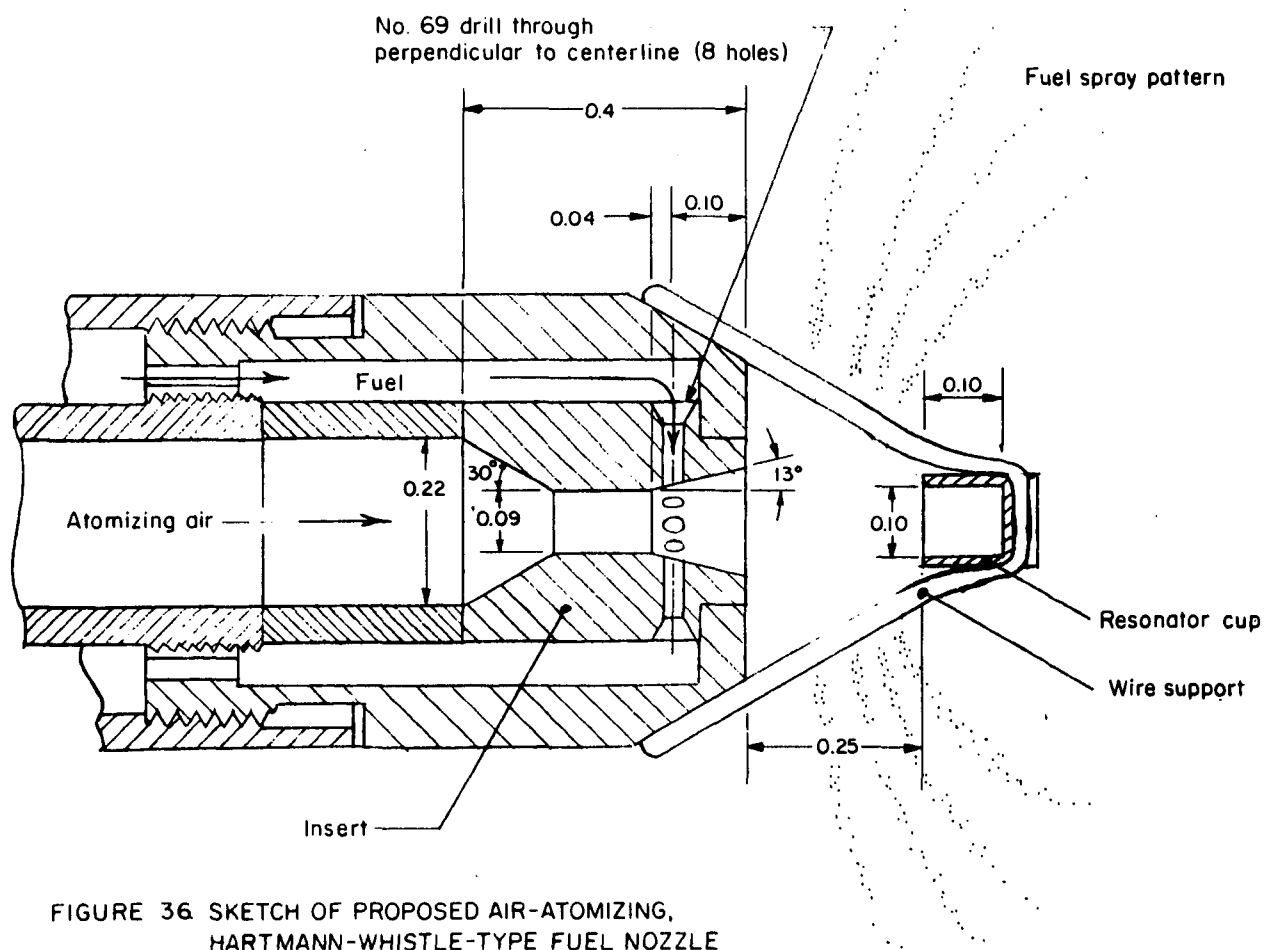


FIGURE 36 SKETCH OF PROPOSED AIR-ATOMIZING, HARTMANN-WHISTLE-TYPE FUEL NOZZLE

According to data supplied by the nozzle manufacturer⁽¹⁰⁾ and to Battelle's experience in the low-emission-burner development program, an atomizing air supply of about 7.1 scfm at 22 psig is required for the full mixture flow rate of the engine (36 lb/hr). At this condition the air pump power requirement would be about 0.6 hp. The fuel droplet size in a Hartmann-whistle-type fuel atomizer is a function primarily of the ratio of atomizing-air flow rate to fuel flow rate. Larger ratios produce smaller droplets. There are no reliable data available concerning the specific droplet size range capability of the nozzle selected. However, the manufacturer has reported achieving 50-micron-size droplets with water at low levels of pressure and flow, and droplets considerably smaller than 20 microns at high pressures and flow rates with water. Given the differences in physical characteristics between water and gasoline, it is reasonable to assume that the Hartmann-whistle-type air atomizing nozzle illustrated in Figure 36 can be operated to produce a droplet size range of 15 to 100 microns. The dimensions given on the sketch have been selected with this objective in mind.

Besides the nozzle, this atomization system requires an air supply and a fuel supply. The atomizing air can be supplied by an air pump similar to those used for AIR (air injection reactor) emission control systems. This air pump is belt driven from the engine, and delivers about 10 scfm at idle and 50 scfm at 100 mph. Corresponding delivery pressures are 1/2 psi at idle and 15 psi at 100 mph. Fuel can be supplied to the proposed atomizer using a regular automotive diaphragm-type fuel pump.

Mixing and Vaporization Chamber

The purpose of the mixing chamber is to promote fuel vaporization and good mixing between the air and the fuel while minimizing the deposition of fuel droplets on the walls. As with the fuel atomizer, space limitations are important.

In the mixing chamber configuration selected for the prototype induction system, the inlet air is introduced through holes in the chamber walls from an annulus passage outside the chamber. The hole sizes and pattern illustrated are intended to produce a symmetrical non-swirling turbulence

pattern. Air flow through large holes at the very top would penetrate to the center of the chamber and mix with a portion of the fuel spray. Fifteen 0.45-inch diameter holes would be required in this row. The row of small holes near the top should produce low-momentum jets which would be deflected down along the chamber wall. Thirty-two 0.30-inch diameter holes would be required in this row. The other two rows of holes provide additional air for mixing with the air and fuel mixture in the region between the center and the walls of the chamber. Twenty-one 0.30-inch diameter and seventeen 0.45-inch diameter holes would be required in these two rows. The pressure drop across the mixing chamber at full flow will be about 4 inches of water.

It should be emphasized that the optimum mixing chamber configuration can only be arrived at by trial and error. The configuration shown is considered a good starting point.

The volume of the mixing chamber as described in Figure 32 is about 0.046 cu ft, which will result in mixture residence times of about 0.14 sec at idle and 0.009 seconds at maximum speed. This range of residence times can be expected to produce a high degree of fuel vaporization, at least at low engine speeds.

Throttle

The throttle as shown in Figure 32 is a cylindrical "sleeve" which controls the openings between the inlet manifold plenum and the manifold passages. The throttle sleeve moves vertically to increase or decrease the openings through which the fuel and air mixture must pass to reach the engine cylinders. The movement can be effected by cables as shown (3 would be used to avoid binding) or by pins and a cam or levers from below. When fully closed, V-shaped slots in the sleeve, one located at each manifold passage, would allow the fuel and air mixture at idle to pass through.

Figure 37 illustrates an alternative to the sleeve throttle shown in Figure 32. In this alternative, the central section of the manifold, or "plug" is moved up and down to control the mixture flow. The movable element could be centrally supported and actuated from below.

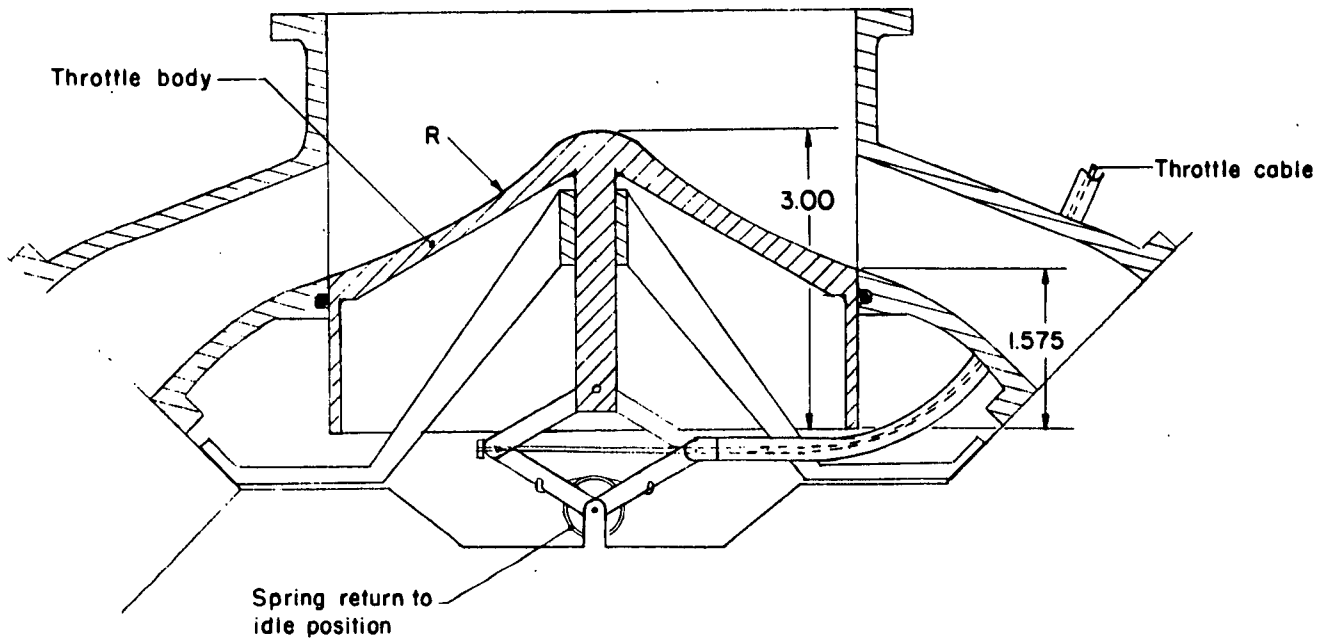


FIGURE 37. SKETCH OF PROPOSED INDUCTION SYSTEM WITH PLUG THROTTLE

The relative merits of the sleeve and plug throttle configurations are difficult to assess without conducting further studies. In both cases at part throttle opening there is a potential for fuel impacting on surfaces of the throttle and then becoming reentrained in the manifold passage in an unstable manner. Furthermore, in both configurations the part throttle position will result in downstream eddies (in the manifold passages) which may have some detrimental influence on time-based cylinder-to-cylinder distribution. However, either configuration should be a significant improvement over the conventional butterfly throttle plate. Mechanical design will also play an important role in selection of a suitable mixture throttle.

It must be acknowledged that the sleeve valve presents potential difficulties in both design and manufacturing. The actuating mechanisms shown cannot be considered practical designs, and the required tolerances for the sleeve valve and its seat and guide could involve considerable manufacturing expense. The plug valve presents similar problems.

An alternative to sleeve-valve or plug-valve throttling schemes shown in Figures 32 and 37 is to move the throttle to the entrance of the mixture generator. In this location, the valve imposes no fuel-impaction problems, and, therefore, a conventional butterfly-type throttle could be used. This approach necessitates designing the mixture generator as a pressure vessel. It also introduces a minor complication in the design of the fuel-metering system in that the system must discharge into a variable-pressure zone instead of a constant-pressure zone.

Figures 38 and 39 are layout sketches of the prototype induction system showing a suggested configuration for inlet-air throttling. An inlet-air chamber with 10-gage (approximately 1/8-inch thick) walls surrounds the mixing and vaporization chamber, and both are bolted directly to the intake manifold. A circular-cross-section throttle passage is welded to the side of the inlet chamber. A baffle at the inlet-air chamber entrance distributes the air more uniformly around the mixing chamber. The air filter housing fits essentially air-tight at the throttle-passage entrance by overlapping edges. A standard air filter is used.

Inlet Manifold

Design of the inlet manifold for low impaction was based on reducing the number of 90-degree bends in each passage and providing minimum turning angle consistent with available space in the remaining bends. A single-plane central-plenum configuration offered the best approach to achieve these objectives. With the single-plane plenum, individual manifold passages can be made fairly short, providing the diameter of the central plenum can be made large. A large-diameter central plenum is compatible with the design of the mixing and vaporization chamber and with the use of an air atomizing fuel nozzle.

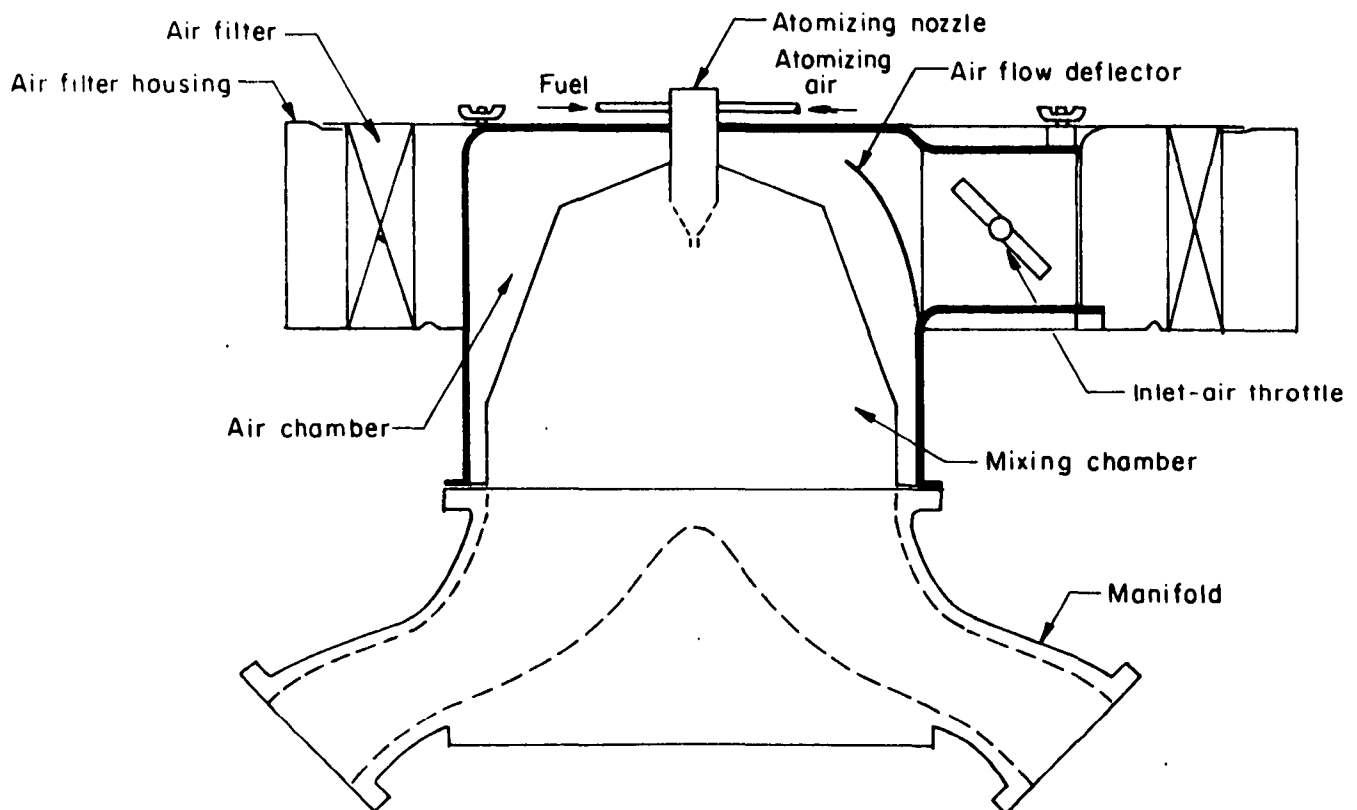


FIGURE 38. SKETCH LAYOUT OF PROPOSED INDUCTION SYSTEM WITH ALTERNATIVE INLET-AIR THROTTLE - SECTION VIEW

The inlet manifold configurations shown in Figures 33 and 35 consist of a central cylindrical plenum, equally spaced ports around the circumference of the plenum, and passages of varying lengths between these ports and the engine cylinder-head ports. The manifold passages were designed with bend radii (measured to the outside passage surface) no less than four times the passage width. At the central plenum the passage ports are about 1 inch high and 2 inches wide. At the cylinder head the passage ports are approximately square to match the cylinder-head ports.

The conical hump in the center of the manifold plenum is designed to provide guidance to the mixture flow entering the manifold passages through the sleeve throttle opening. The optimum height and shape of this hump would be experimentally determined.

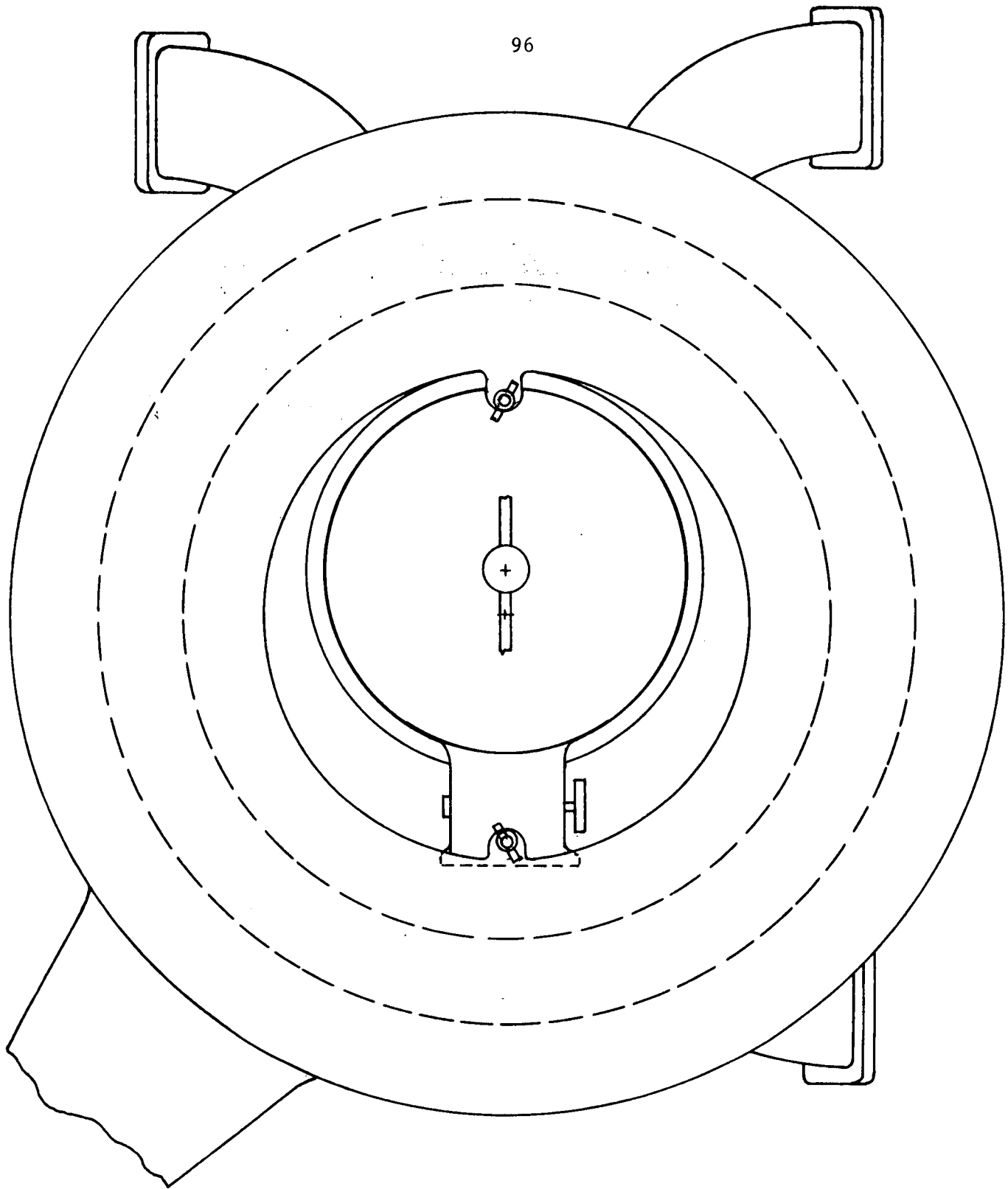


FIGURE 39. SKETCH LAYOUT OF PROPOSED INDUCTION SYSTEM
WITH ALTERNATIVE INLET-AIR THROTTLE - PLAN VIEW

Idle Capability

With systems using the sleeve- or plug-valve throttle, the idle fuel-and-air mixture flow can be provided for by notching the throttle sleeve (or throttle plug) at each manifold-passage port. The fuel atomizing nozzle and mixing chamber should be able to provide a homogeneous mixture of finely atomized fuel and air even under idle conditions because the fuel droplet size depends only on the ratio of atomizing air flow to fuel flow and not on total air flow. By proper design of the atomizing air supply system, this ratio can be maintained high enough at idle to achieve the fine atomization necessary for good mixing and low impact losses. Thus, it is anticipated that a separate idle fuel system would not be necessary.

Acceleration Enrichment

The air atomizing or Hartmann-whistle-type nozzle does not lend itself well to acceleration enrichment. Thus, if acceleration enrichment is required, it will be necessary with this induction system concept to provide for this enrichment separately. One method of doing this would be simply to provide an accelerator pump, as most carburetors have, to inject an extra amount of fuel into the mixing chamber when the accelerator is depressed. The quantity of fuel injected in this manner should be proportional to the speed of movement and distance of travel of the accelerator. This accelerator pump could be designed so that gradual movement of the accelerator did not cause an injection of excess fuel.

The fuel could be either injected from a point near the atomizing nozzle or from a nozzle in the center of the hump in the manifold plenum. The latter injection point might provide the quickest response characteristics.

Specific configurations for control of idle operation and acceleration enrichment have not been provided in this study. The aim of the proposed prototype fuel induction system is to demonstrate the potential of improved fuel atomization, improved mixing and distribution, and reduced droplet impaction for reducing exhaust emissions, particularly NO_x . If this potential is successfully demonstrated, then the idle and acceleration enrichment requirements would be tackled next.

Fuel Metering System

In the proposed induction system, fuel would be supplied to the atomizer nozzle by a fuel pump. The pressure generated by the fuel pump at any engine speed would have to be in excess of that required for the maximum fuel flow rate anticipated for that speed. Control of the actual fuel flow by a throttling valve would provide the fuel metering.

To insure precise air/fuel ratio control at any speed and load condition a means would be required to sense air flow. One such method would be to provide a venturi in the air inlet and to use the venturi pressure differential as an air flow signal to control the fuel metering. Another approach would be to measure engine speed, intake manifold air pressure, and air temperature, and to electrically combine these signals in conjunction with a predetermined engine volumetric efficiency curve. The resulting output signal would set the fuel rate.

The fuel metering control would also have to be designed to provide enrichment for cold-weather starting -- equivalent to the effect of the choke in conventional carburetors.

Fuel Vaporization

Effect of Fuel Vaporization on Maximum-Power Capability

Vaporization of the fuel potentially results in a decrease in the partial pressure of the air in the fuel-air mixture, which, in turn, can result in reduced engine air breathing and reduced maximum-power capability. However, a cursory analysis indicates that this will not be a problem and that a power increase is a more likely result.

If it is assumed that the fuel can be represented by n-heptane, and if it is further assumed that the mixture is at 100 F and one atmosphere absolute pressure, the volume of 1 lb of air is 14.1 ft^3 while the volume of 0.067 lb of fuel vapor (stoichiometric ratio) is 0.27 ft^3 (assuming perfect-gas-law relationships are valid). The additional volume of the fuel is

equivalent to only 2 percent of the air volume; therefore a 2-percent power loss is the most that could be anticipated.

However, if the cooling effect of fuel vaporization is considered, an increase in the air density of the fuel-air mixture can be anticipated. Assuming the average heat of vaporization to be 150 Btu/lb, and assuming that both air and liquid fuel are initially at the same temperature, a 37.5 F drop in mixture temperature can be expected as a result of the fuel vaporization. If the air and fuel are initially at 100 F, the resulting drop is about 6 percent of the absolute temperature. The net result of vaporization considering effects on both mixture temperature and air partial pressure is an anticipated 4 percent increase in engine air flow, assuming an adiabatic intake manifold. Since the manifold is not adiabatic, something less than a 4-percent increase would be anticipated in a real engine.

Hot-Spot Vaporization in Manifold

Although ultra-fine atomization of the fuel should preclude the necessity for a high-temperature manifold hot spot, there may still be some need for providing moderate, uniform heat in the manifold for vaporizing any fuel which does deposit out of the mixture. The cone-shaped hump in the center of the proposed manifold plenum offers a suitable surface for manifold heating. The interior of this cone could be hollow with passages to the cavity through the intake manifold mating with exhaust passage ports on the cylinder heads.

In the case of the alternative "plug" throttle with the movable cone, it would be more difficult but not impossible to provide the cavity and passages for exhaust gas flow.

Fuel Vaporization Chamber Concept

The proposed induction system concept, with or without manifold heating, may under some conditions still deliver a mixture containing fuel droplets to the engine. Thus, it is expected that geometric and time-based distribution of the mixture will not be perfect. To provide a means by which

to evaluate the improvement in distribution that can be achieved with complete vaporization of the fuel, and to obtain a measure of the amount of heat required to accomplish this, a separate vaporization chamber was designed for use as a laboratory device.

The design criterion for this vaporization chamber was that it have the capacity for completely vaporizing the fuel at maximum air/fuel mixture flow rate when used either in conjunction with the proposed induction system prototype or with conventional induction system components.

After consideration of several alternatives, the approach selected to vaporize the fuel in an induction system was to seek a design in which a majority of the fuel droplets could be caused to impact on heated surfaces regardless of the mixture flow rate. Two important additional criteria in the design sought were compactness and low pressure loss. No attempt was made to design a system what could fit under the hood of a car.

Several approaches to the design of the vaporization chamber were investigated before arriving at the final design. For instance, fuel could be vaporized in a length of heated pipe. From previous experience with heating air in such an arrangement, it was found that a length of about 20 feet would be required to heat the air from 70 to 140 F. With such an arrangement, the air should be preheated before entering the vaporization section in order to minimize the length of pipe required.

One means of increasing the contact time of the air with the hot walls of a heated-pipe vaporization chamber would be to induce swirl with a twisted tape. The tape would perform a second beneficial function of centrifuging large fuel droplets out to the heated walls. However, a mixing section would have to be provided to break up the overly rich mixture at the walls caused by vaporization of the large droplets. Large droplets would probably impinge on the cool twisted tape at high flows. The resulting fuel film on the tape would probably be reentrained by the air in an irregular manner. Vaporization effectiveness of this arrangement would be a function of the mixture flow rate. At low flows, large droplets may not impact on the heated walls.

It was felt that a better approach would be to look for a design in which a majority of the fuel droplets would be likely to impact on heated surfaces regardless of the mixture flow rate. The first impaction-type

vaporization chamber investigated had Thermek tubes. Thermek tubes are produced by a process whereby the surface of a tube is mechanically lifted to form spiraled spines completely surrounding the tube. Fuel droplets introduced perpendicular to a bank of these tubes would surely impact. However, insufficient heat-transfer information was available on this type of extended surface for predicting air-heating rates.

A number of standard-type heating coils were then investigated. A heat exchanger configuration was found which combined compactness with high surface area. This heat exchanger is a McQuay Model 5BB hot water booster coil with closely spaced fins that are corrugated to produce a tortuous flow path.

Figure 40 is a sketch of a section of this coil showing the fin and tube geometry. An arrangement with 14 fins to the inch, a face area 6 inches wide by 12 inches high, and a 3-1/2 inch thickness was selected.

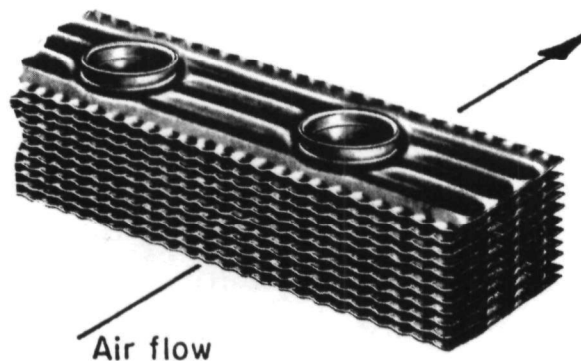


FIGURE 40. FIN AND TUBE GEOMETRY FOR FUEL VAPORIZATION CHAMBER

Figure 41 is a design layout of the vaporization chamber. The heating coil is shown mounted in a housing with inlet and outlet plenum chambers to provide for uniform mixture distribution with minimum pressure loss. The coil is tilted at an angle from the axis of the inlet and outlet ports so as to maximize the fin area exposed to the droplets. The housing would be constructed with sufficient strength and rigidity to withstand maximum inlet manifold vacuum. The inlet and outlet flanges of this configuration are designed to be compatible with the proposed prototype induction system. Simple adaptors could be made to fit the vaporization chamber to conventional induction system components. The overall dimensions of this vaporization chamber are: height 16 in., width 7 in., and length 11 in.

Figure 42 is a sketch of the vaporization chamber mounted on a 351 CID V-8 engine with the prototype induction system components. Shown also in this sketch are the auxiliary components required. In operation, hot water is circulated through the coil by a pump. The water is heated by the addition of steam in a mixing chamber, the water absorbing the latent heat of the condensing steam. Surplus water accumulating in the system by the condensing steam will be drained off at the standpipe to maintain a constant level in the circulation loop.

With an inlet temperature of 70 F, the system should be capable of achieving a mixture temperature of 140 F at the outlet at full flow conditions. This mixture temperature was selected for coil design from a consideration of dew point temperatures expected in an operating engine. The dew point temperature is the lowest temperature at which all of the fuel will remain in vapor form in equilibrium with the combustion air. This temperature is a function of the air-fuel ratio of the mixture and the manifold vacuum.

The mixture temperature at the inlet manifold will be controlled by varying the temperature of the water being circulated through the coil. A steam rate of about 36 lb/hr of saturated steam at atmospheric pressure (about 4-1/2 gal/hr of water) will be required to vaporize the fuel and heat the combustion air at full flow conditions. A hot-water circulation rate of 4.0 gal/min will be used, giving a water-side pressure drop in the coil of 1.2 ft of water. The gas-side pressure differential across the coil at full mixture flow of 300 cfm (at 2 in. Hg vacuum and 70 F) will be about 0.4 inches of water.

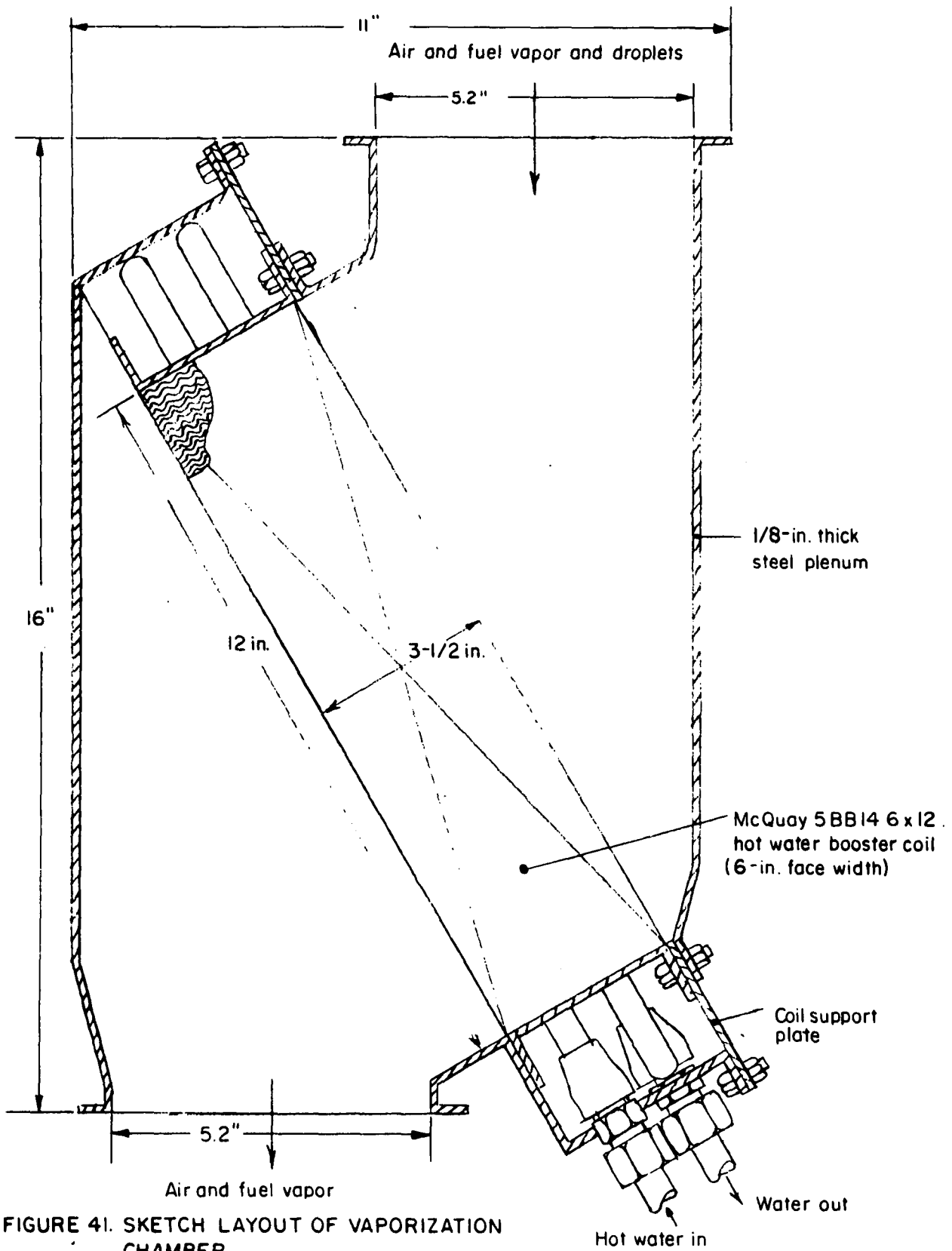


FIGURE 41. SKETCH LAYOUT OF VAPORIZATION CHAMBER

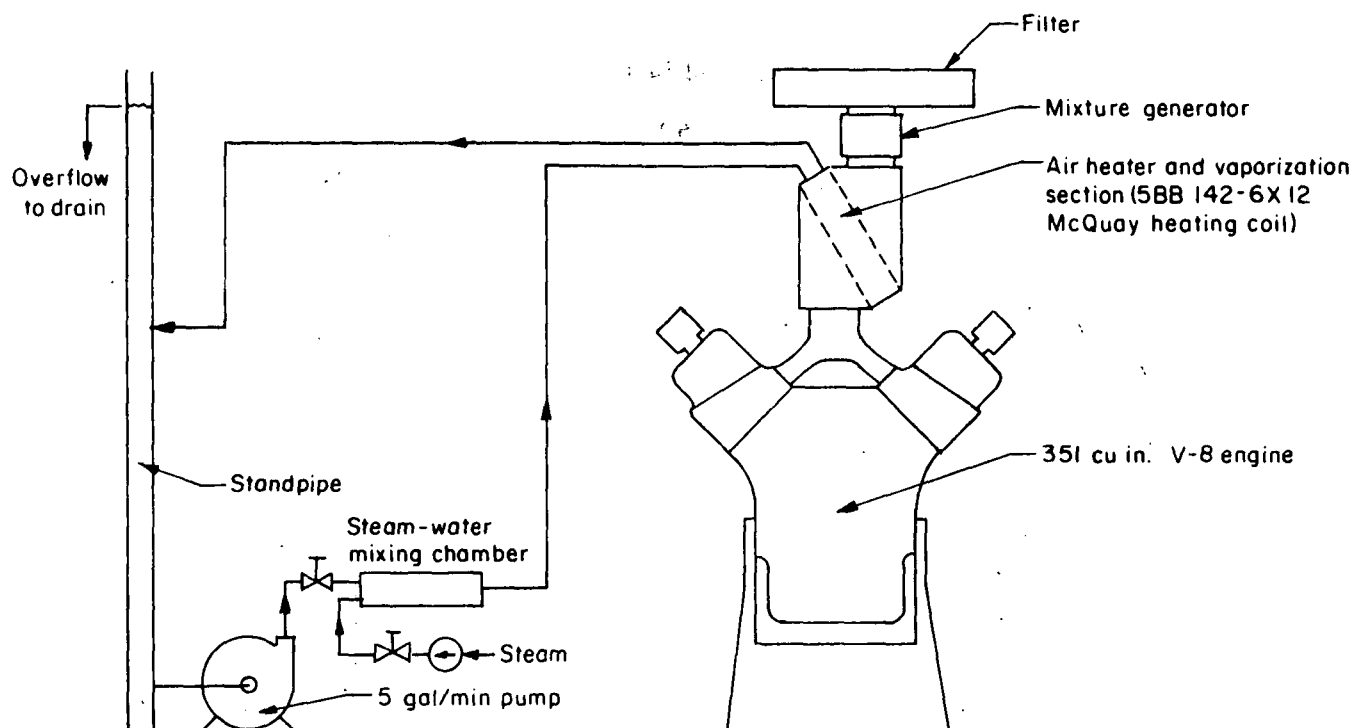


FIGURE 42. FUEL VAPORIZATION APPARATUS

The system can be made to respond to a step increase in heating load with little delay by greatly increasing the steam input, momentarily. However, the system is expected to respond to a step decrease in heating load rather slowly because heat is removed from the water only in the coil. Fifteen minutes or more may be required to achieve a stable inlet manifold temperature at idle, following operation at full heating load.

ACKNOWLEDGEMENTS

This study was conducted under the sponsorship of the Office of Air Programs, Environmental Protection Agency. The project Officer was Mr. Jeffrey L. Raney, originally and, later, Dr. Jose L. Bascunana of the Characterization and Control Development Branch of the Division of Emission Control Technology, with Mr. George D. Kittredge as Branch Chief.

LIST OF REFERENCES

- (1) Trayser, D. A., et al, "A Study of the Influence of Fuel Atomization, Vaporization, and Mixing Processes on Pollutant Emissions from Motor-Vehicle, Power Plants", Phase Report from Battelle-Columbus Laboratories to National Air Pollution Control Administration (April 30, 1969).
- (2) Fluid Meters - Their Theory and Application, Fifth Edition, The American Society of Mechanical Engineers, New York City (1959).
- (3) Ranz, W. E., "Principles of Inertial Impaction", Department of Engineering Research, Pennsylvania State University, Bulletin No. 66 (1956).
- (4) Technical Data Book - Petroleum Refining, American Petroleum Institute, Division of Refining, 1966 (with later revisions).
- (5) Obert, E. F., Internal Combustion Engines, Second Edition, International Textbook Co., Scranton (1950), Chapter 8, pp 233-235.
- (6) Gieseke, J. A., and Mitchell, R. I., "Size Measurement of Collected Drops", J. Chem. Engr. Data, Vol 10 (No. 4), p 350 (1965).
- (7) Doyle, A. W., Perron, R. R., and Shanley, E. S., "A Study of New Means for Atomization of Distillate Fuel Oil", API Publication 1725 (1967).
- (8) Hazard, H. R., and Hunter, H. H., "A Miniature Ultrasonic Burner for a Multifueled Thermoelectric Generator", API Conference Paper CP66-3, API Publication 1705 (1966).
- (9) Martner, J. G., "An Ultrasonic Atomizer Capable of High Rates", API Conference Paper CP66-5, API Publication 1705 (1966).
- (10) Hartmann, J., and Trolle, B., "A New Acoustic Generator, The Air-Jet Generator", Journal of Scientific Instruments, Vol 4 (No. 101), 1926-27.
- (11) "Development of a Low Emission Burner for Rankine-Cycle Engine", EPA Contract No. EHS 70-117.
- (12) Personal correspondence with Sonic Development Corporation of America.
- (13) Mitchell, R. I., and Pilcher, J. M., "Improved Cascade Impactors for Measuring Aerosol Particle Sizes in Air Pollutants, Commercial Aerosols and Cigarette Smoke", Ind. & Eng. Chemistry, Vol 51, No. 9 (1959).

APPENDIX A

IMPACTOR STAGE DESIGN FOR VAPOR/DROPLET SAMPLERS

APPENDIX A

IMPACTOR STAGE DESIGN FOR VAPOR/DROPLET SAMPLERS

The design procedures for the three impactor geometries (vapor/droplet samplers) were all similar. The design was based on known and measured efficiencies for a similar impactor design. The relationship governing the design of an impactor stage can be expressed as

$$\frac{d_j \mu}{\rho_p V_j D_p^2} = K_I \quad . \quad (A-1)$$

where

- d_j = diameter of jet
- ρ_p = density of droplet liquid
- V_j = gas velocity through the jet
- D_p = droplet diameter
- K_I = impactor design constant
- μ = gas viscosity

A further consideration is that the distance from the jet to the impaction surface should be about 0.4 times the jet diameter.

The value of the constant, K_I , in Equation A-1 is available from the design for the Battelle cascade impactor ⁽¹²⁾ which has been calibrated. This value can be taken as

$$K_I = 6.92 \times 10^{-11} \text{ in/lb}$$

The density of Stoddard Solvent is 49.3 lb/ft³ and the maximum velocity in the test sections was expected to correspond to 100 scfm through a cross section of 1.25 x 1.25 inches giving a velocity of 164 ft/sec at atmospheric pressure. The sampling rate was chosen to be 0.71 scfm which gives a velocity of 167 ft/sec through a jet with a diameter of 0.113 inch. If this jet diameter is chosen, the sampling probe under the highest expected flow conditions would

be the same size as the jet. This jet size was therefore chosen for these reasons and also because the cut-off size for the impactor would be 1.35 microns as calculated with Equation A-1 which was assumed to be a small enough droplet size for the purposes of separating drops from the vapor.

The vapor/droplet samplers were calibrated by measuring the size distribution of drops passing through the impactor on the gas side. The calibrations were performed using water droplets containing a dissolved fluorescent tracer (sodium fluorescein dye). The water was atomized from a DeVilbiss D-40 atomizer operated with an air supply at 5 psig. The DeVilbiss D-40 atomizer is a simple dip-tube aspirating atomizer available at many drug stores for use in inhalation therapy. The spray was directed into a duct four inches in diameter and two feet long, and two-minute samples were taken from the duct exit with the vapor/droplet sampler. The size distribution of droplets produced by the atomizer is presented as Figure A-1. The data points on this graph are averages of five measurements made with the Battelle cascade impactor.

Measurements of sampling flow rates were made with calibrated rotameters. The total sampling rate was 0.75 scfm, with each half, vapor and droplet, being 0.375 scfm. The gas flow through the vapor side was sampled into a cascade impactor to determine the droplet size cutoff point. On the droplet side both the liquid collected in the sampler and that collected on a backup filter following the sampler were measured. All measurements were of fluorescence, which is proportional to liquid mass, and were made with a fluorophotometer.

The mathematical procedure for determining the impactor efficiency can be explained in terms of mass flows of droplets of different sizes. Figure A-2 illustrates the sampler calibration arrangement and the mass flows of droplets. The desired information to be derived is the efficiency of the vapor/droplet sampler, ϵ_i , for different droplet sizes noted by the subscript i . This fractional efficiency can be defined as:

$$\epsilon_i = m_i / M_i$$

where

M_i = mass of droplets of size i entering the vapor/droplet sampler

m_i = mass of droplets of size i collected in the vapor/droplet sampler.

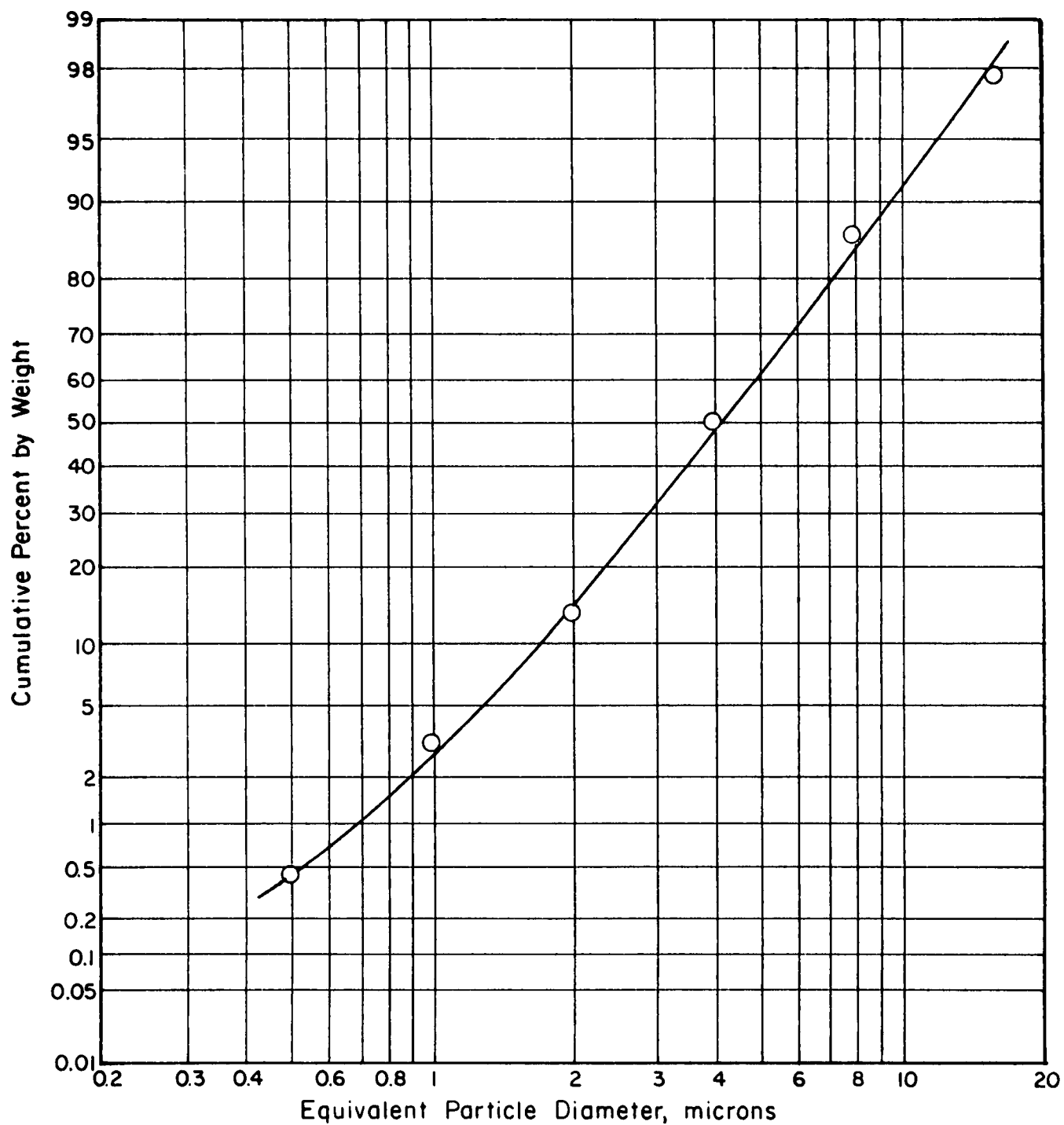


FIGURE A-1. DROPLET SIZE DISTRIBUTION USED FOR CALIBRATION OF THE VAPOR/DROPLET SAMPLER

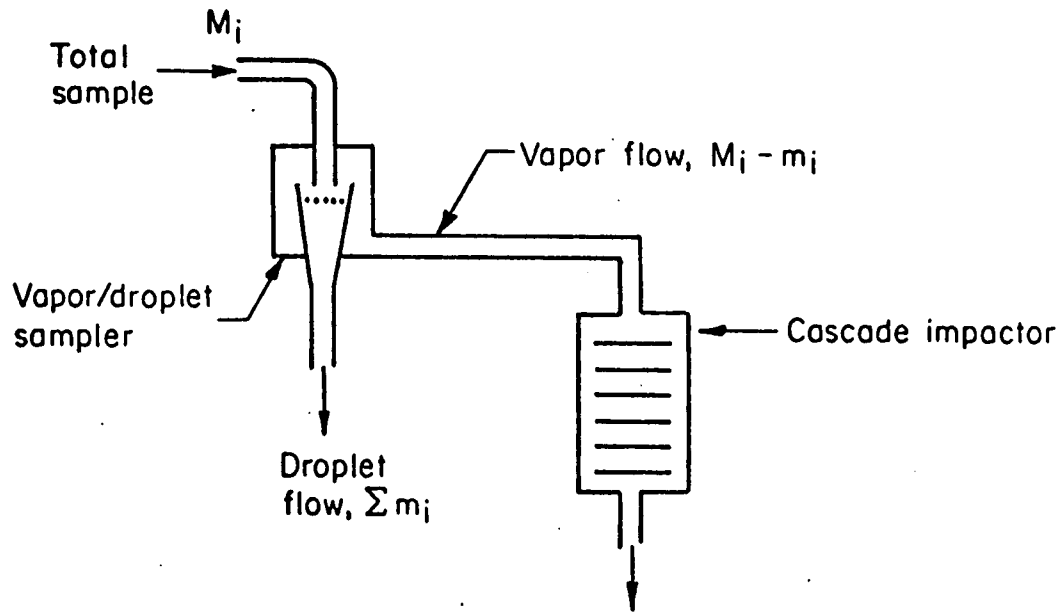


FIGURE A-2. VAPOR/DROPLET SAMPLER CALIBRATION ARRANGEMENT

The cascade impactor separates the droplets into size fractions (with average size i) with the mass fraction of each size noted by $x_i = M_i / \sum M_i$. When the cascade impactor is preceded by the vapor/droplet sampler the measured fraction in each size range is given by $y_i = (M_i - m_i) / \sum (M_i - m_i)$. Rearranging this equation gives:

$$\frac{m_i}{M_i} = 1 - \frac{y_i \sum (M_i - m_i)}{M_i} \quad (\text{A-3})$$

or

$$\epsilon_i = 1 - \frac{y_i \sum (M_i - m_i)}{x_i \sum M_i} \quad (\text{A-4})$$

The total mass of all sizes sampled, $\sum M_i$, is measured as the total mass collected in the vapor/droplet sampler and the cascade impactor, or

$$\sum M_i = \sum M_i + \sum (M_i - m_i) \quad (\text{A-5})$$

Then in values measured experimentally,

$$\epsilon_i = 1 - \left(\frac{y_i}{x_i} \right) \left[\frac{\Sigma(M_i - m_i)}{\Sigma m_i + \Sigma(M_i - m_i)} \right] \quad . \quad (A-6)$$

The experimental calibration procedure is to sample with the cascade impactor alone to obtain x_i . Then the vapor/droplet sampler is inserted ahead of the cascade impactor and the droplet distribution sampled again. From this sample values for y_i , $\Sigma(M_i - m_i)$, and Σm_i are determined and the efficiency, ϵ_i , calculated.

Figure A-3 shows the efficiency of the vapor/droplet sampler as a function of droplet size for sampler Designs 2 and 3. The fact that the fractional efficiency does not go below 0.5 reflects the sampling situation where one-half of the total vapor and small-droplet flow passes through the impaction stage along with any larger droplets. In other words, even if there is no inertial impaction of the smaller droplets they are carried along with the larger droplet flow. Impaction is seen to be 90 percent effective for drops of 2 microns, and more efficient for larger drops. Although this is less efficient than predicted, it is still sufficient.

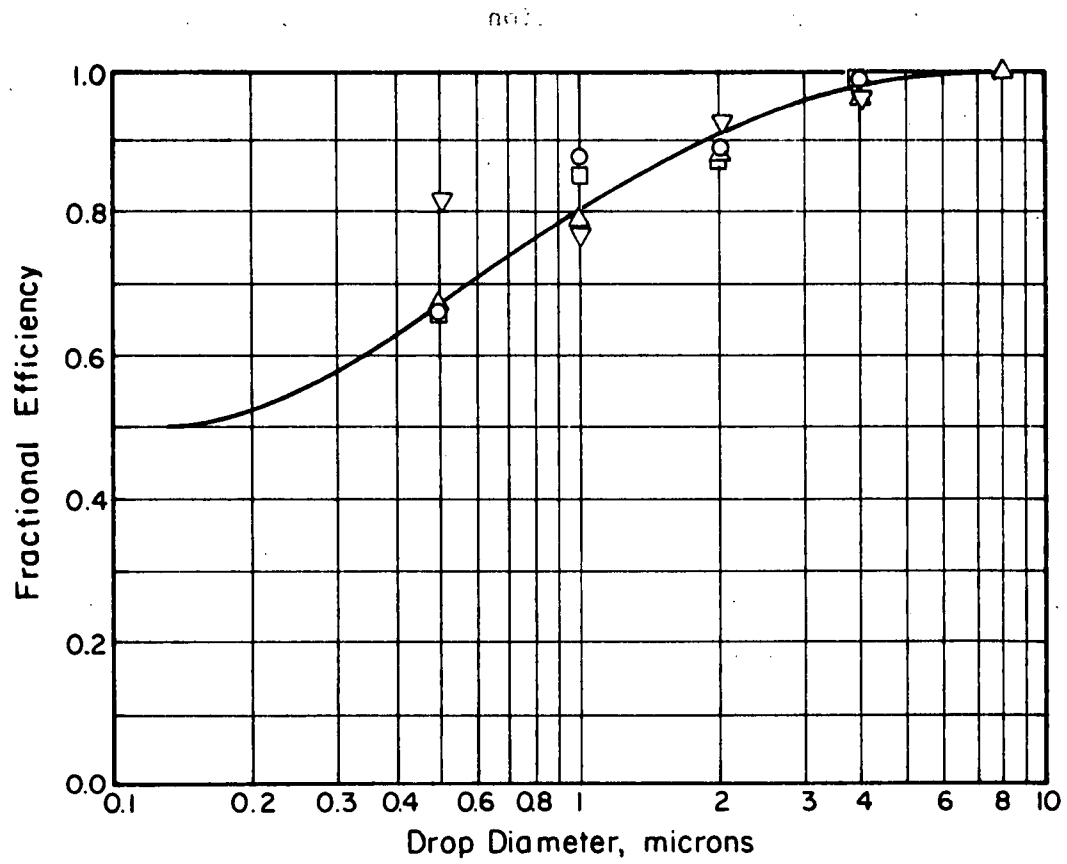


FIGURE A-3. COLLECTION EFFICIENCY OF THE VAPOR/DROPLET SAMPLER AS A FUNCTION OF DROPLET SIZE

APPENDIX B

CALIBRATION CURVES

APPENDIX B

CALIBRATION CURVES

The significance of the curve sheets presented in this Appendix should be self explanatory, with the exception of Figures B-3 through B-14. These figures indicate the droplet sizes produced by the spinning-disk atomizer, used in the laboratory apparatus, in free air, as a function of fuel feed rate and disk speed. Actual drop-size distribution entering the test section was somewhat smaller, as shown in Figure 22.

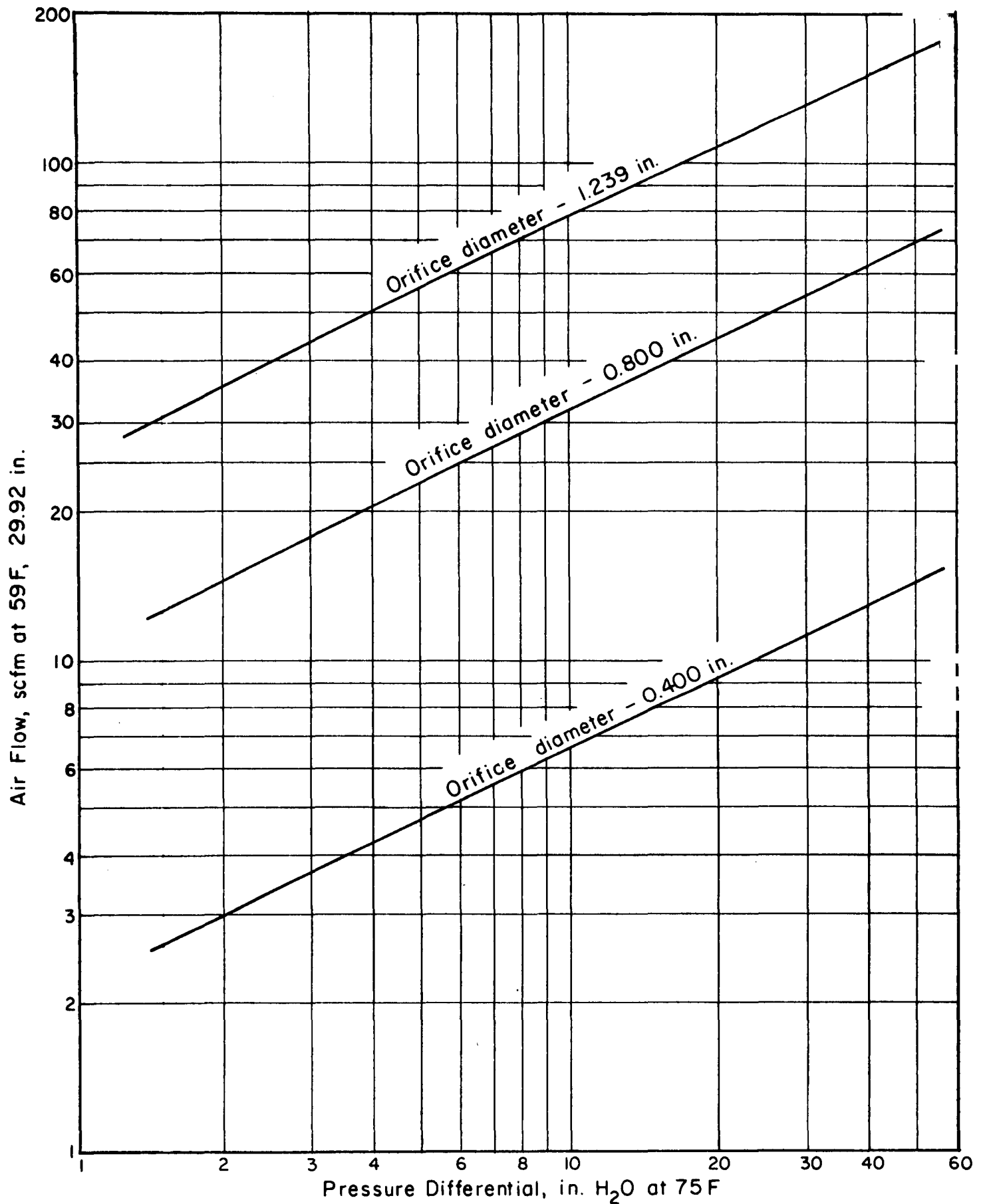


FIGURE B-1. COMPUTED FLOW VERSUS PRESSURE DIFFERENTIAL DATA FOR SQUARE-EDGED ORIFICE FLOW METER WITH 1-D AND 1/2-D TAPS

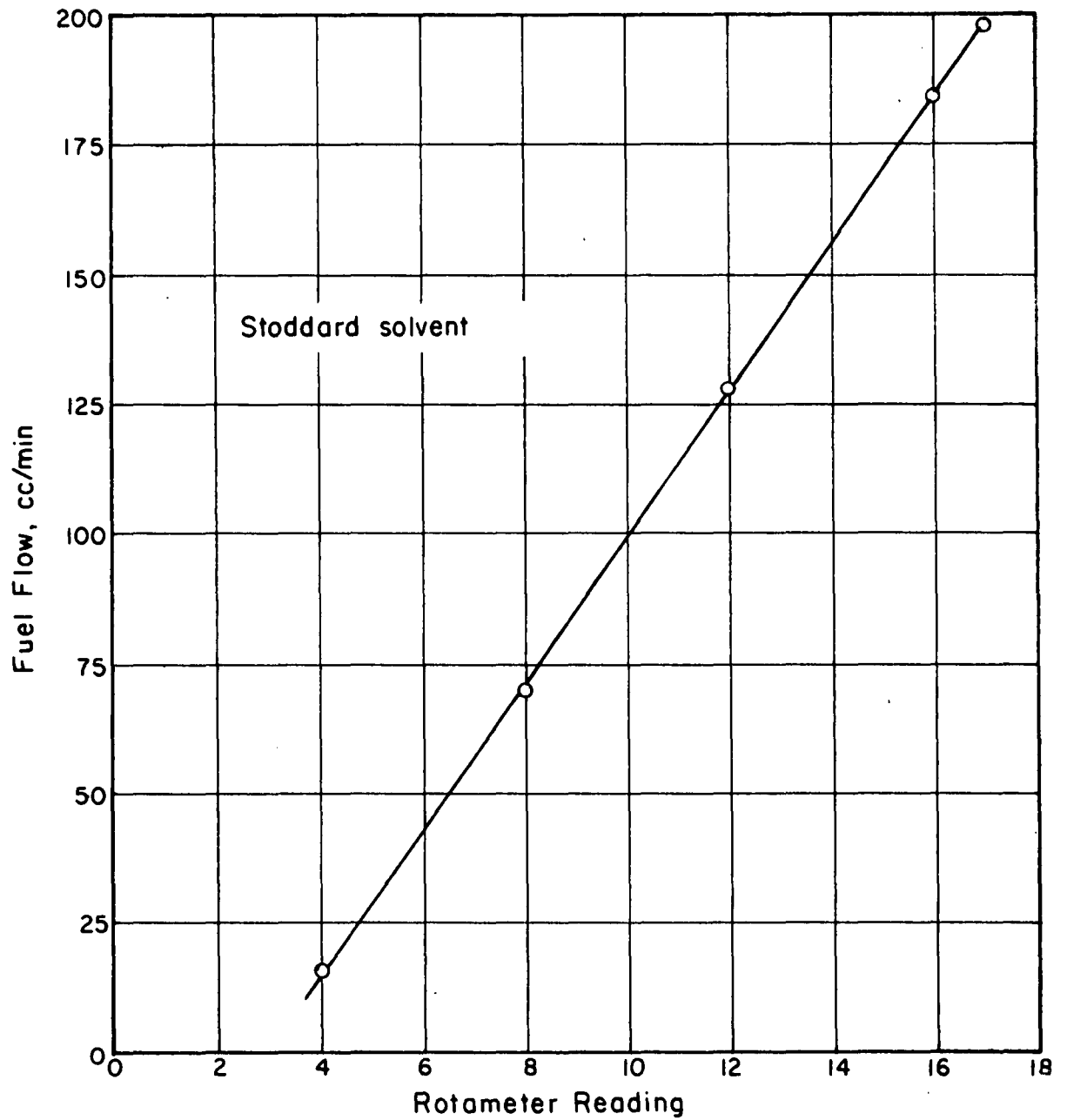


FIGURE B-2. CALIBRATION CURVE FOR FUEL SYSTEM
FLOW METER

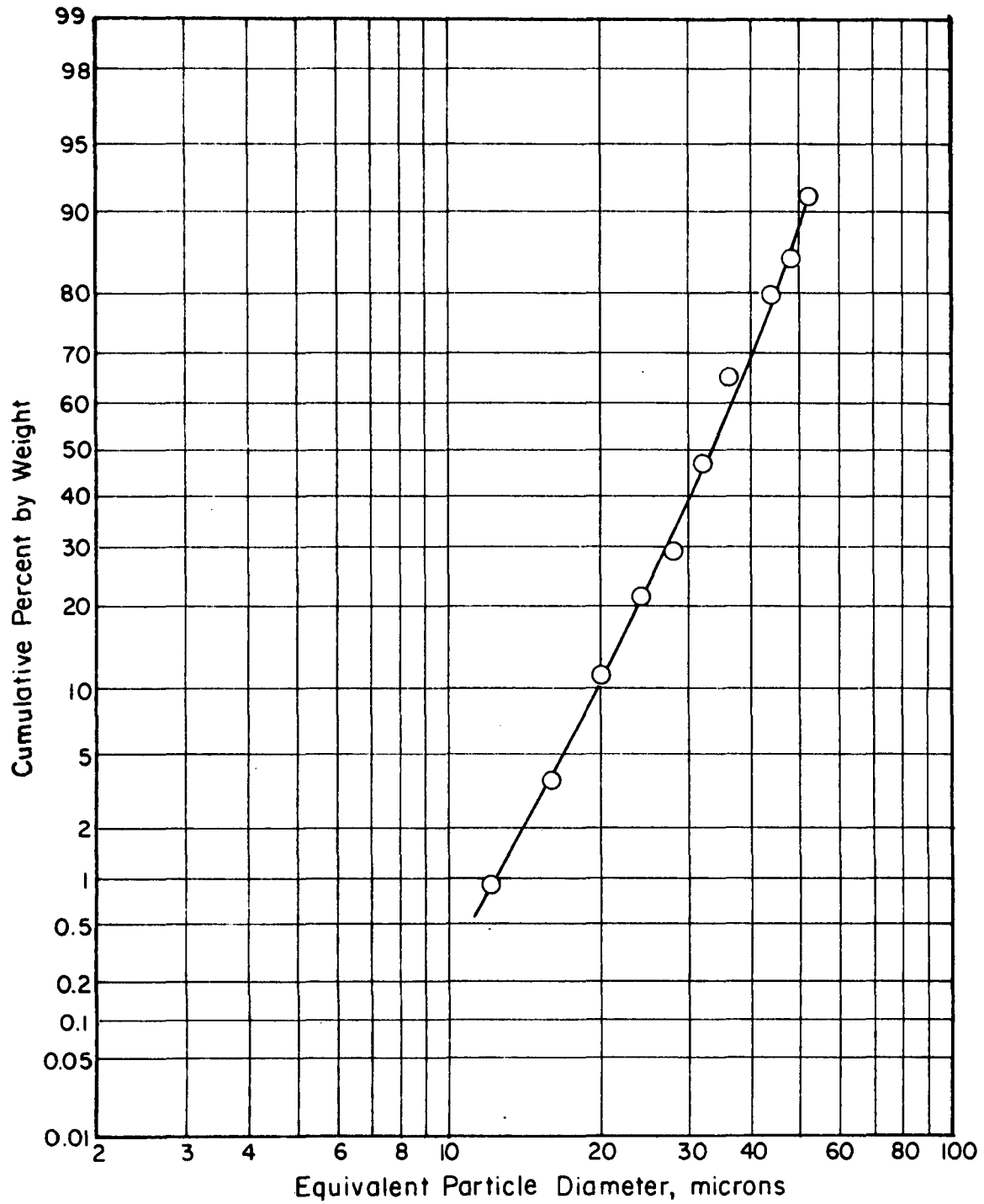


FIGURE B-3. DROP SIZE DISTRIBUTION AT 28,000 RPM AND
1 CM³/SEC

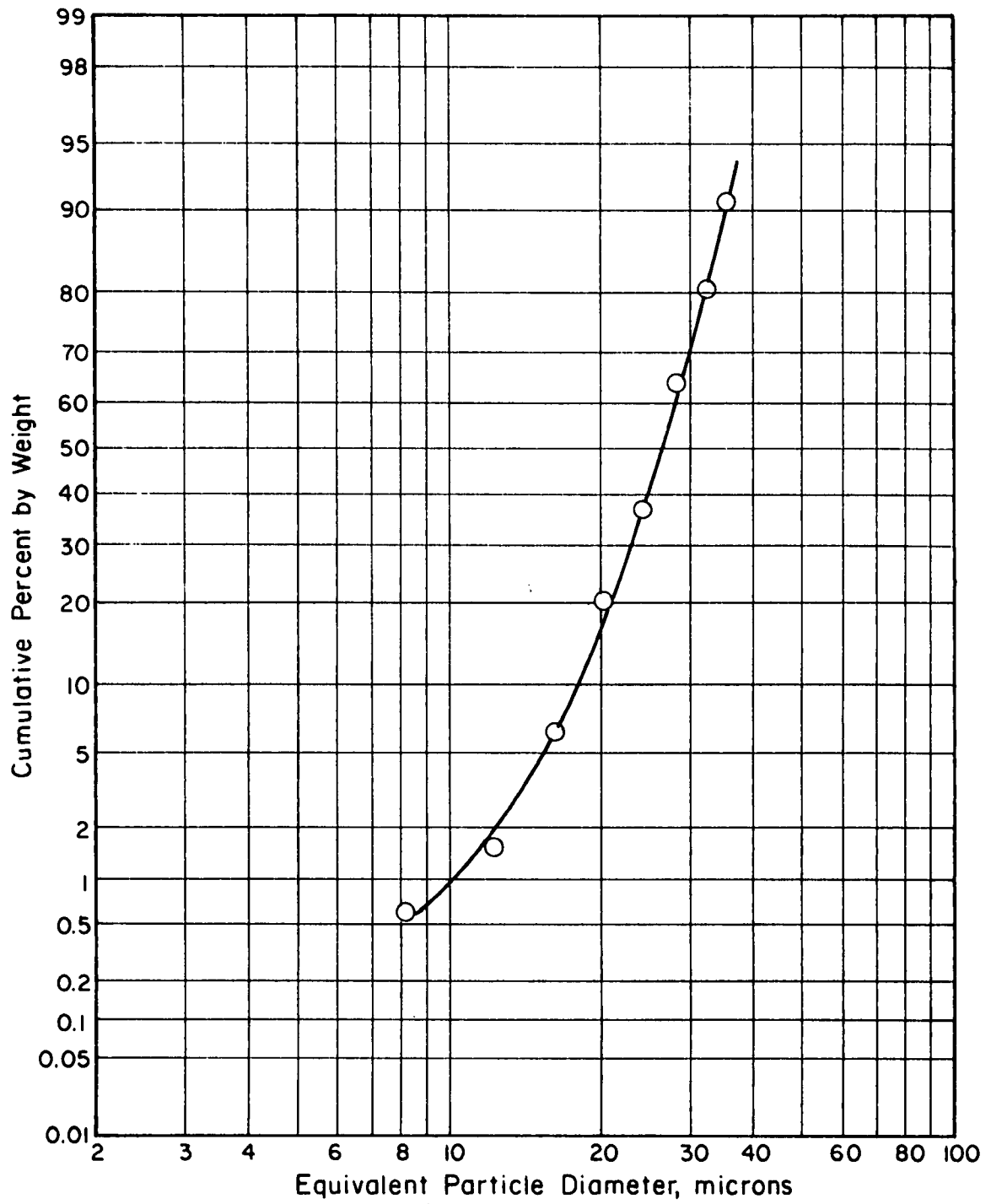


FIGURE B-4. DROP SIZE DISTRIBUTION AT 40,000 RPM AND
1 CM³/SEC

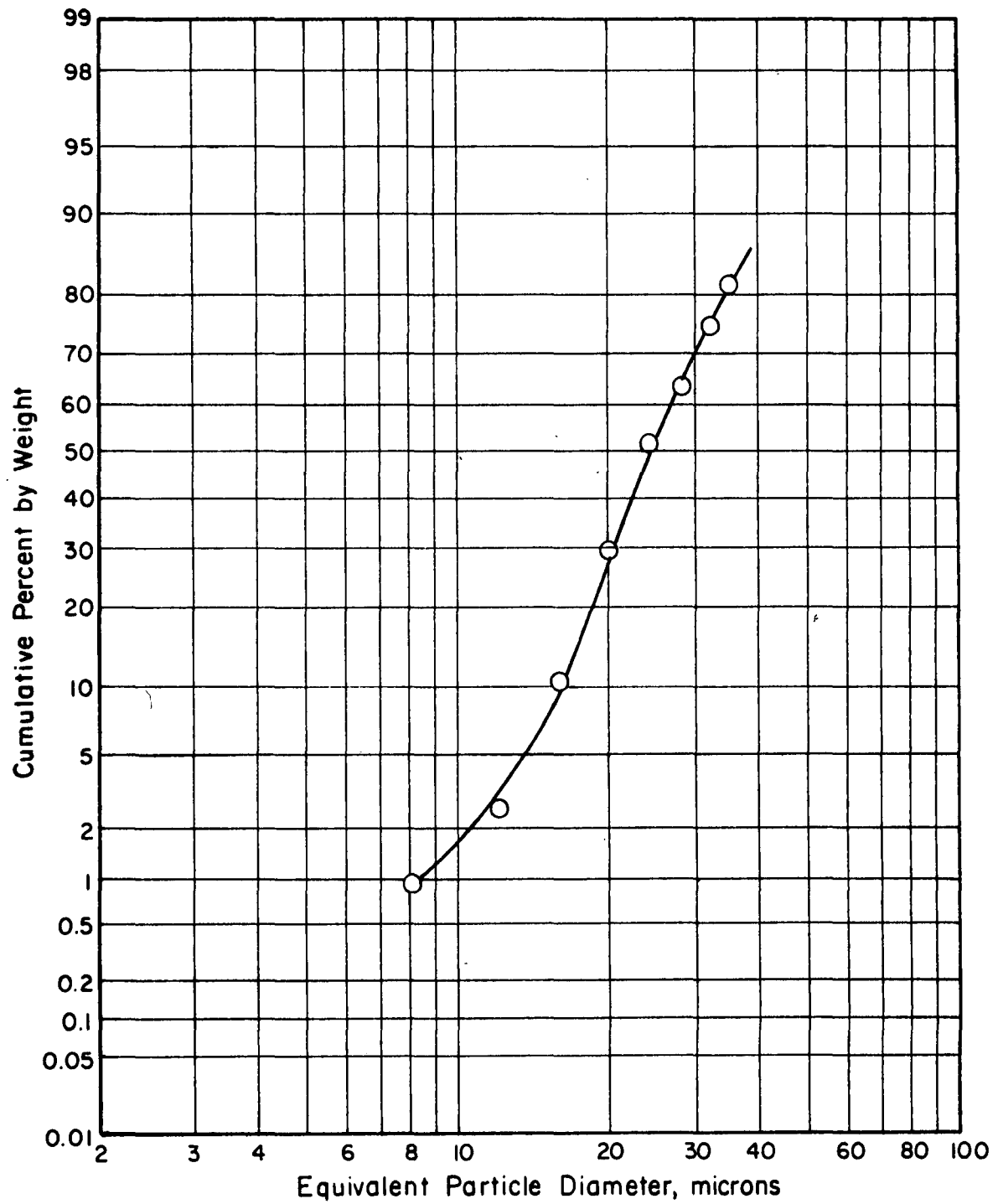


FIGURE B-5. DROP SIZE DISTRIBUTION AT 46,000 RPM AND
1 CM³/SEC

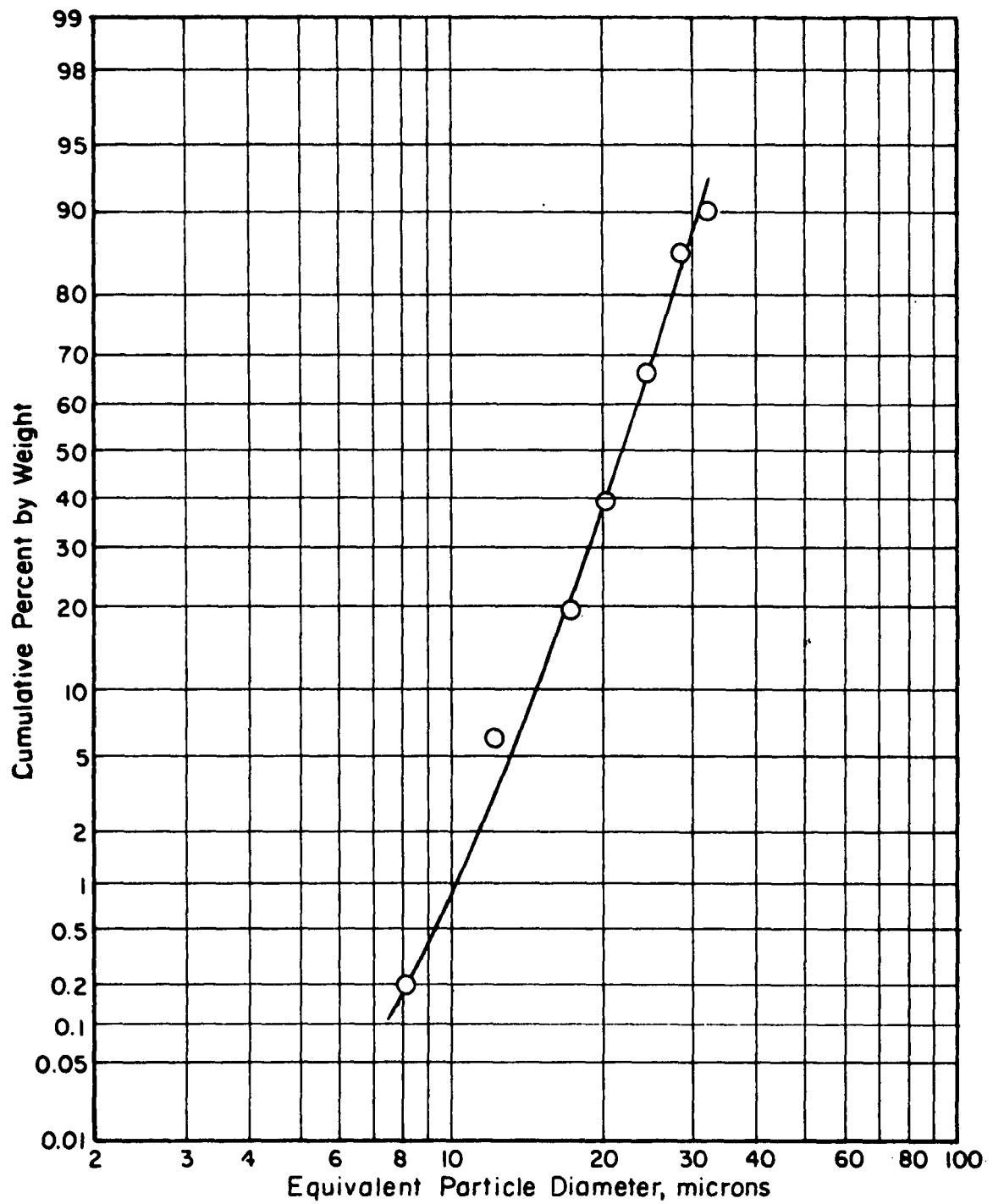


FIGURE B-6. DROP SIZE DISTRIBUTION AT 53,000 RPM AND
1 CM³/SEC

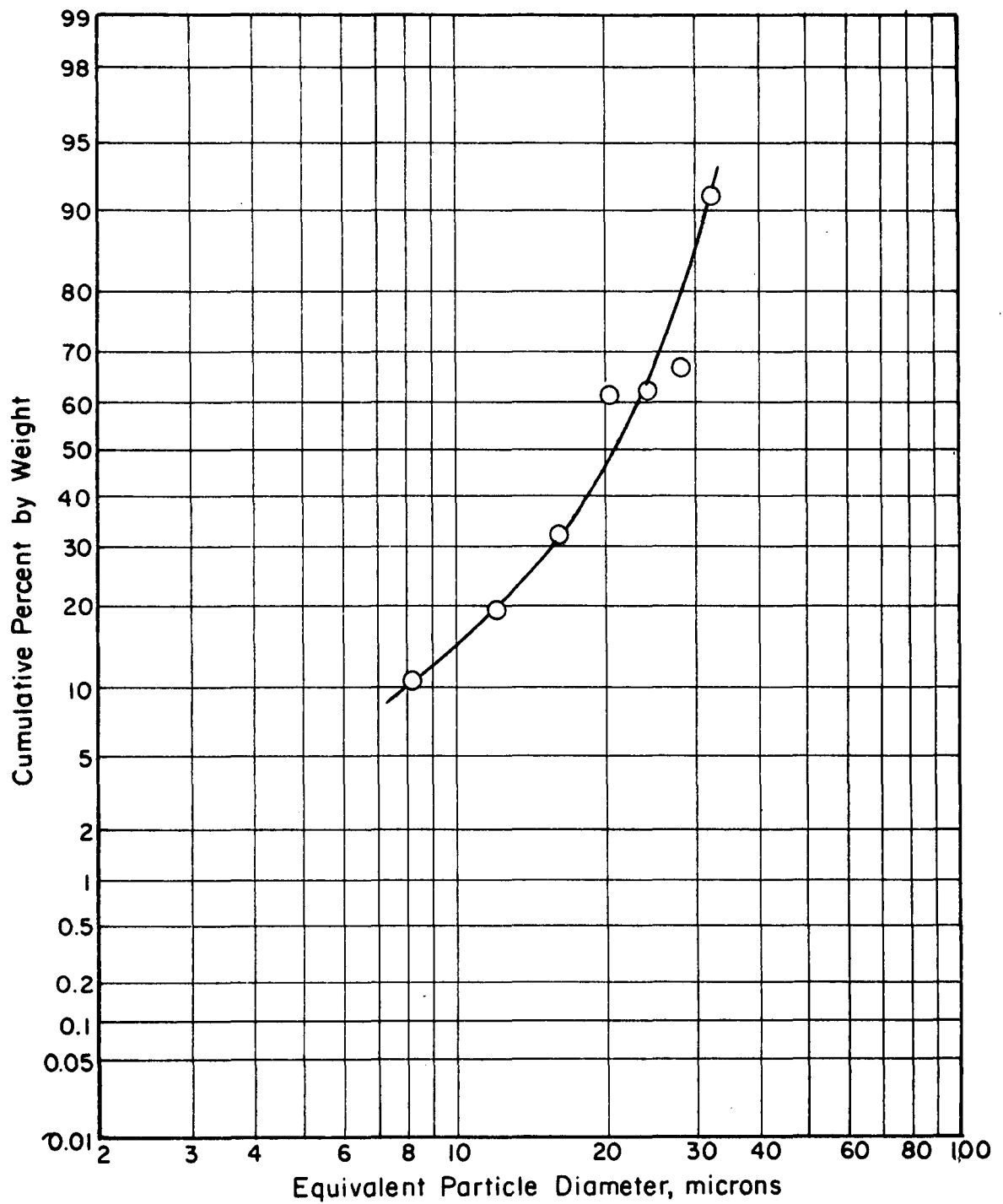


FIGURE B-7. DROP SIZE DISTRIBUTION AT 59,000 RPM AND 1 CM³/SEC

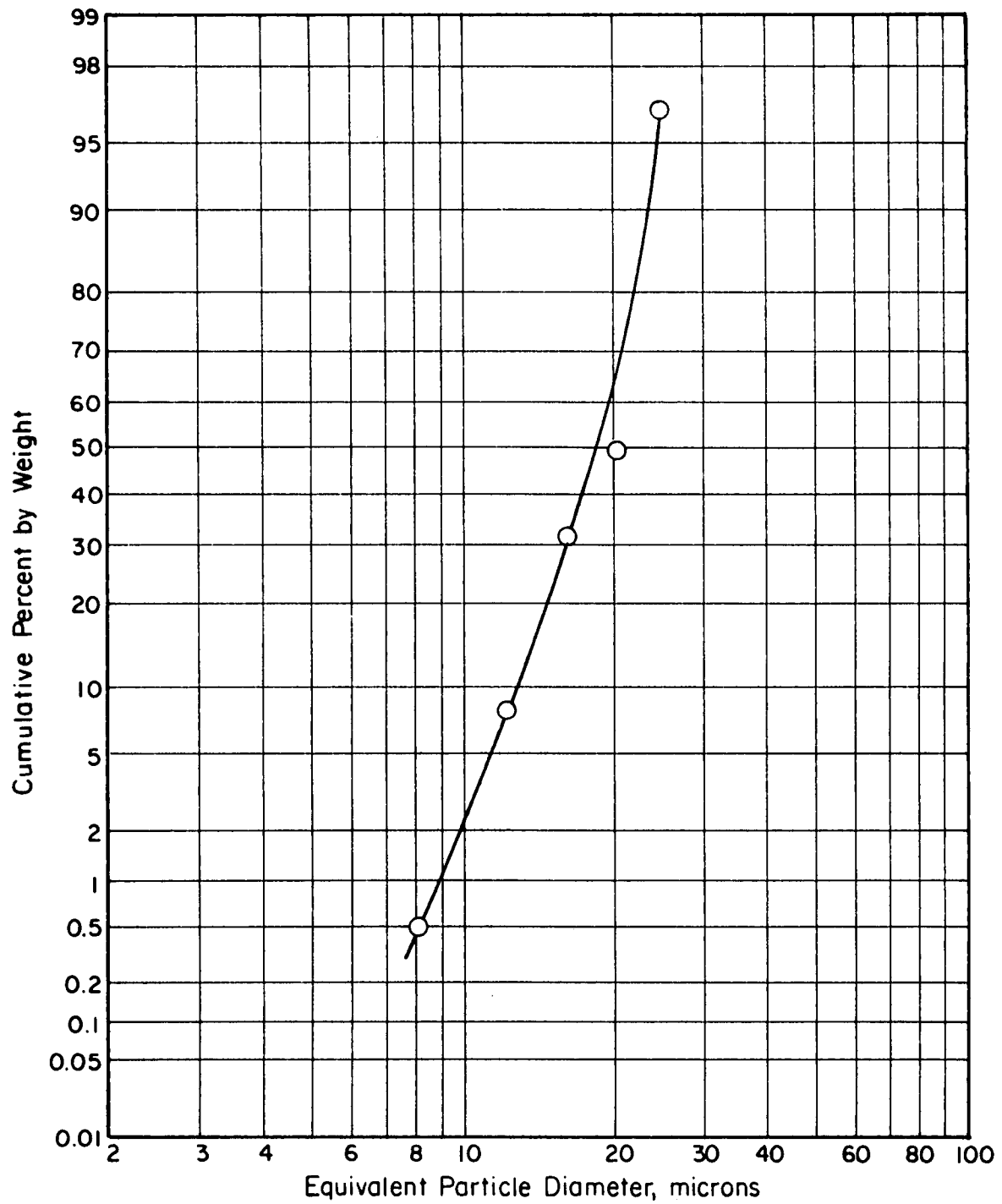


FIGURE B-8. DROP SIZE DISTRIBUTION AT 64,000 RPM AND
1 CM³/SEC

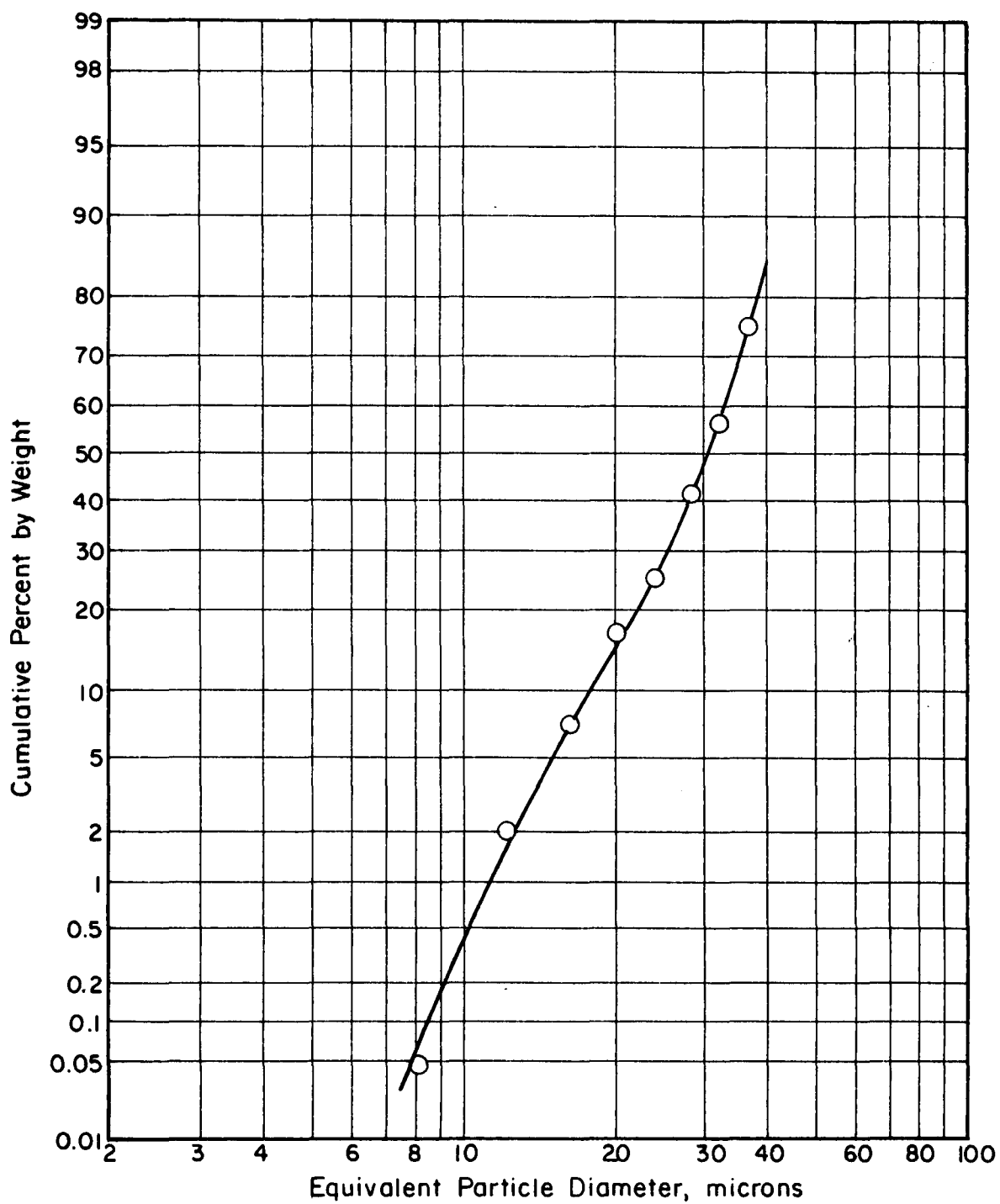


FIGURE B-9. DROP SIZE DISTRIBUTION AT 32,000 RPM AND 0.5 CM³/SEC

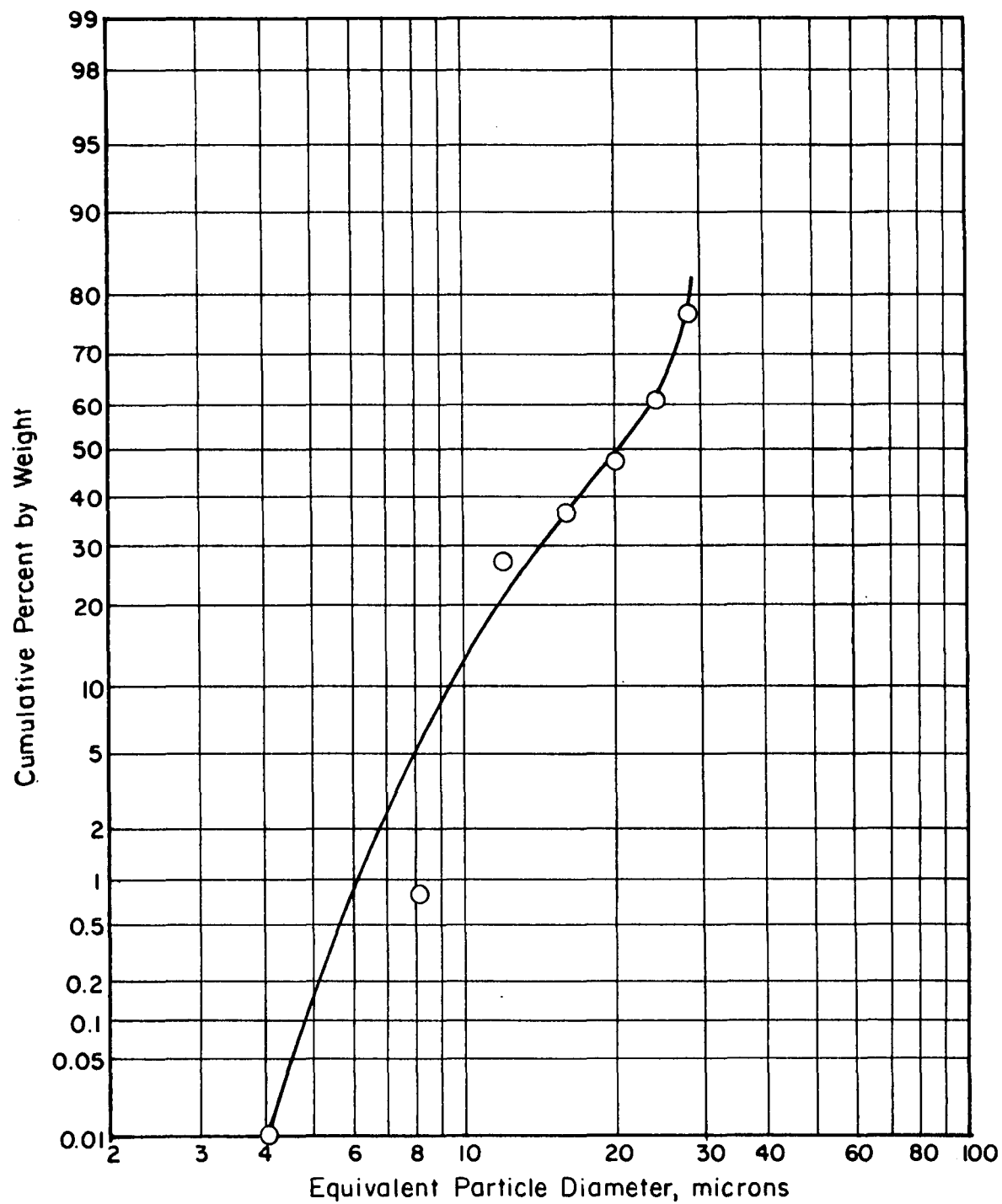


FIGURE B-10. DROP SIZE DISTRIBUTION AT 43,000 RPM AND $0.5 \text{ CM}^3/\text{SEC}$

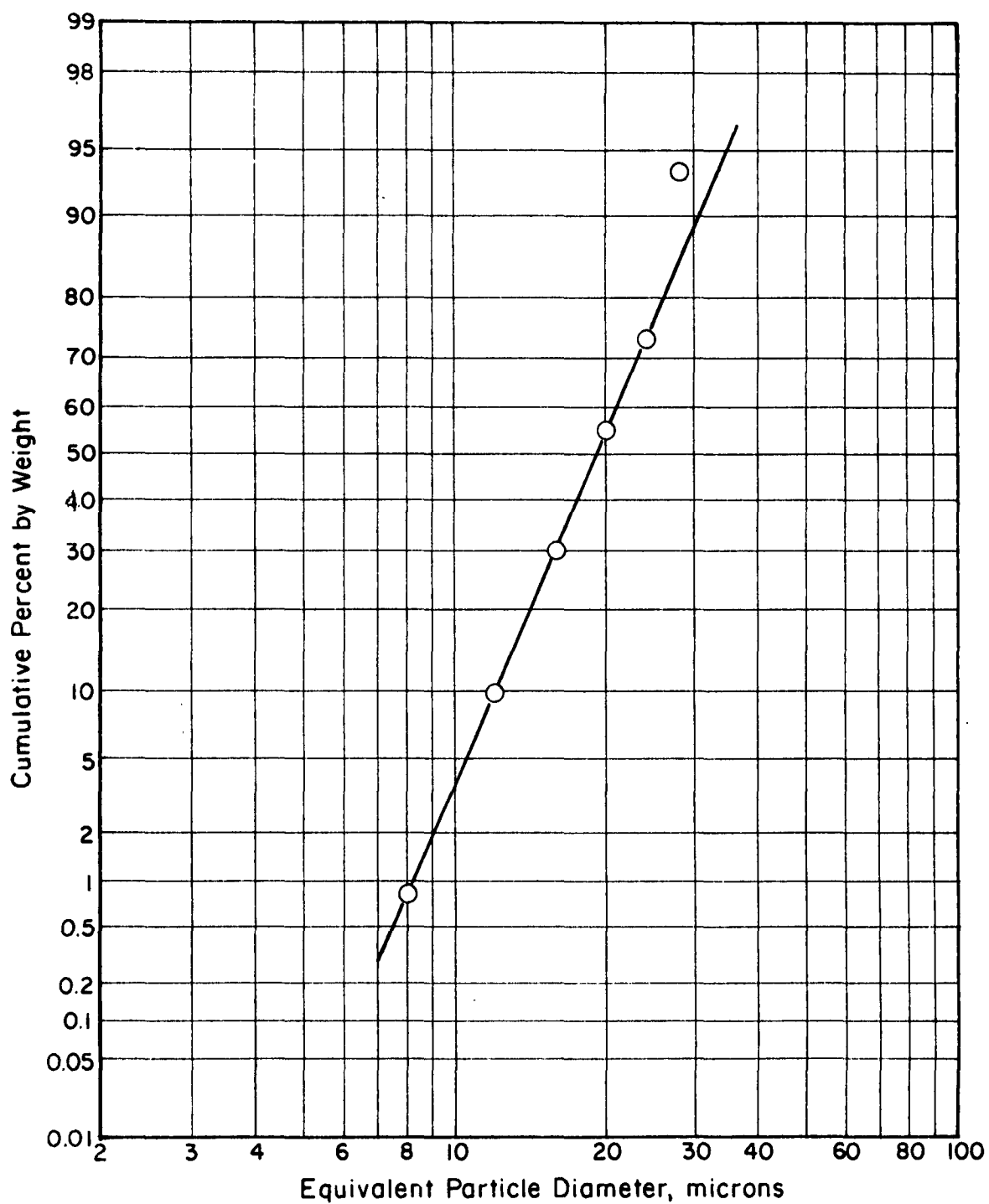


FIGURE B-II. DROP SIZE DISTRIBUTION AT 50,000 RPM AND 0.5 CM³/SEC

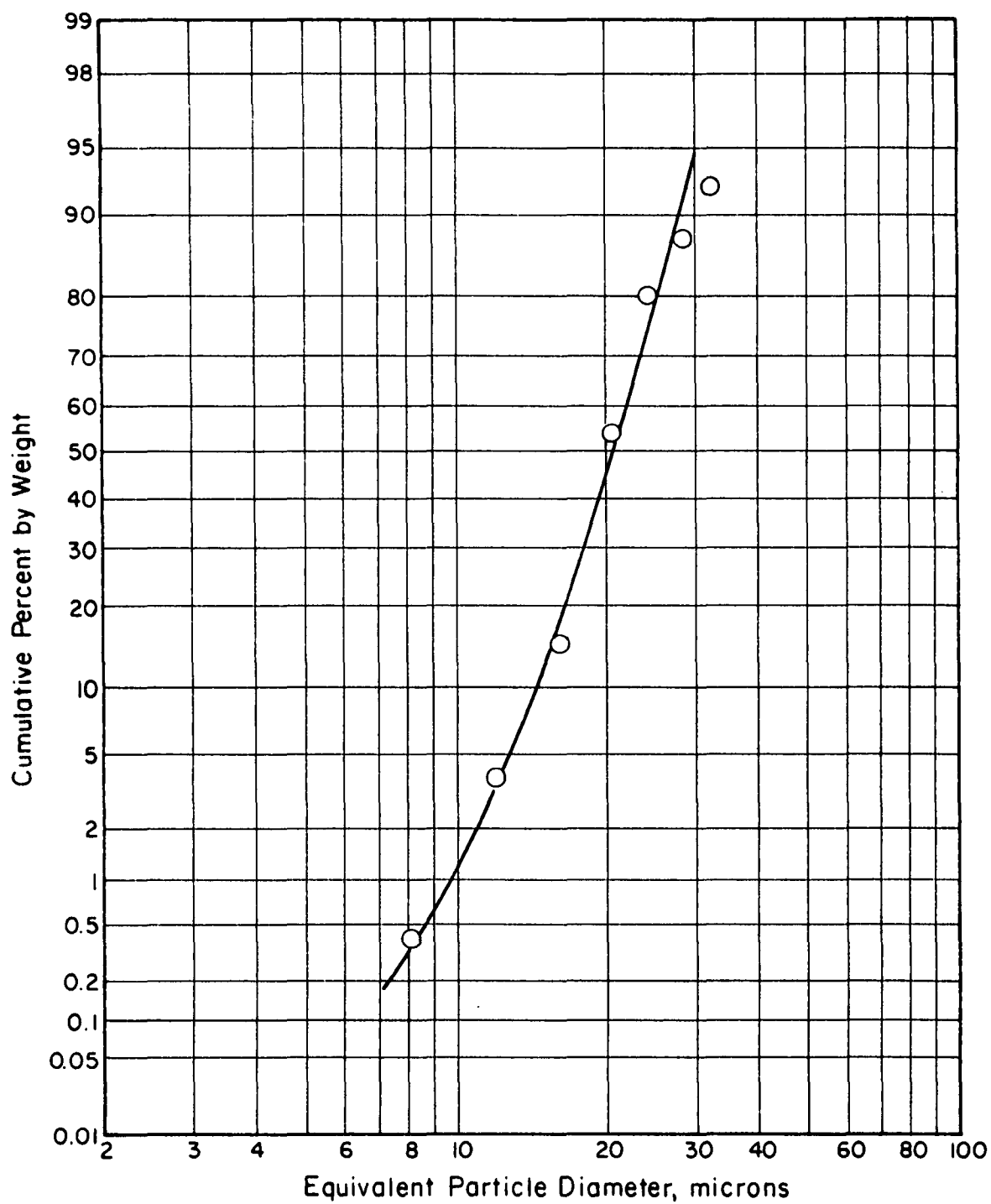


FIGURE B-12. DROP SIZE DISTRIBUTION AT 56,000 RPM AND 0.5 CM³/SEC

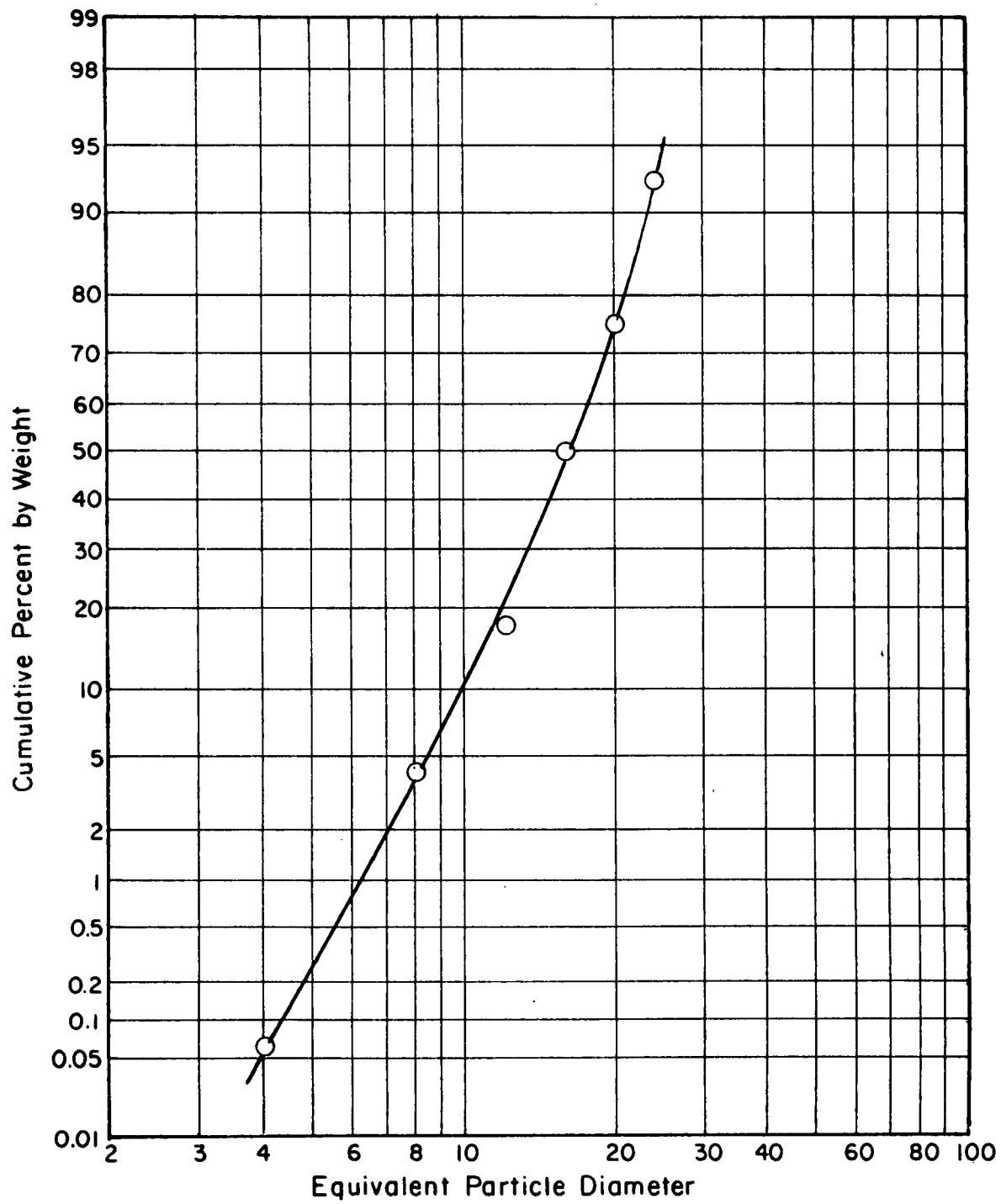


FIGURE B-13. DROP SIZE DISTRIBUTION AT 61,000 RPM AND $0.5 \text{ CM}^3/\text{SEC}$

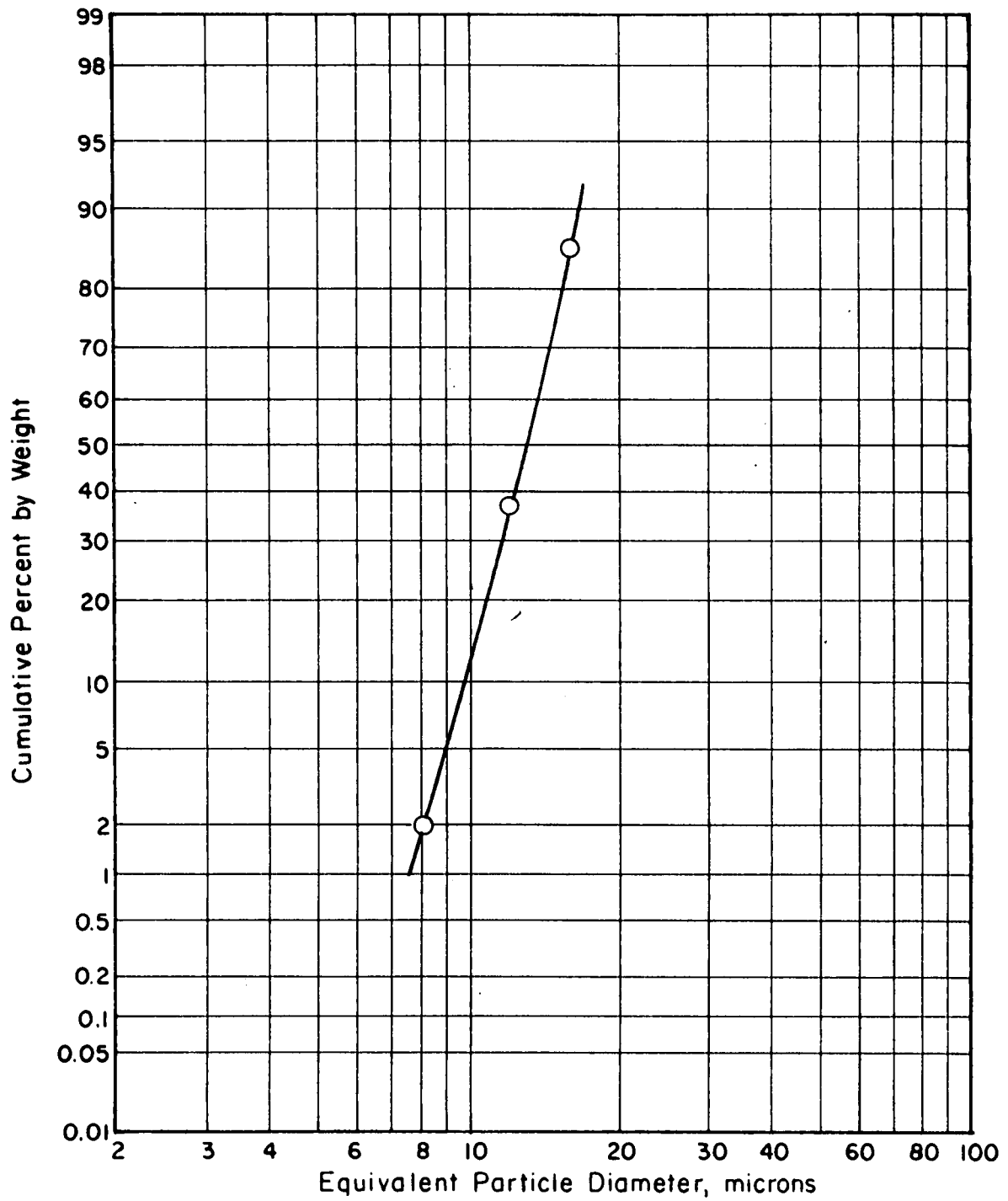
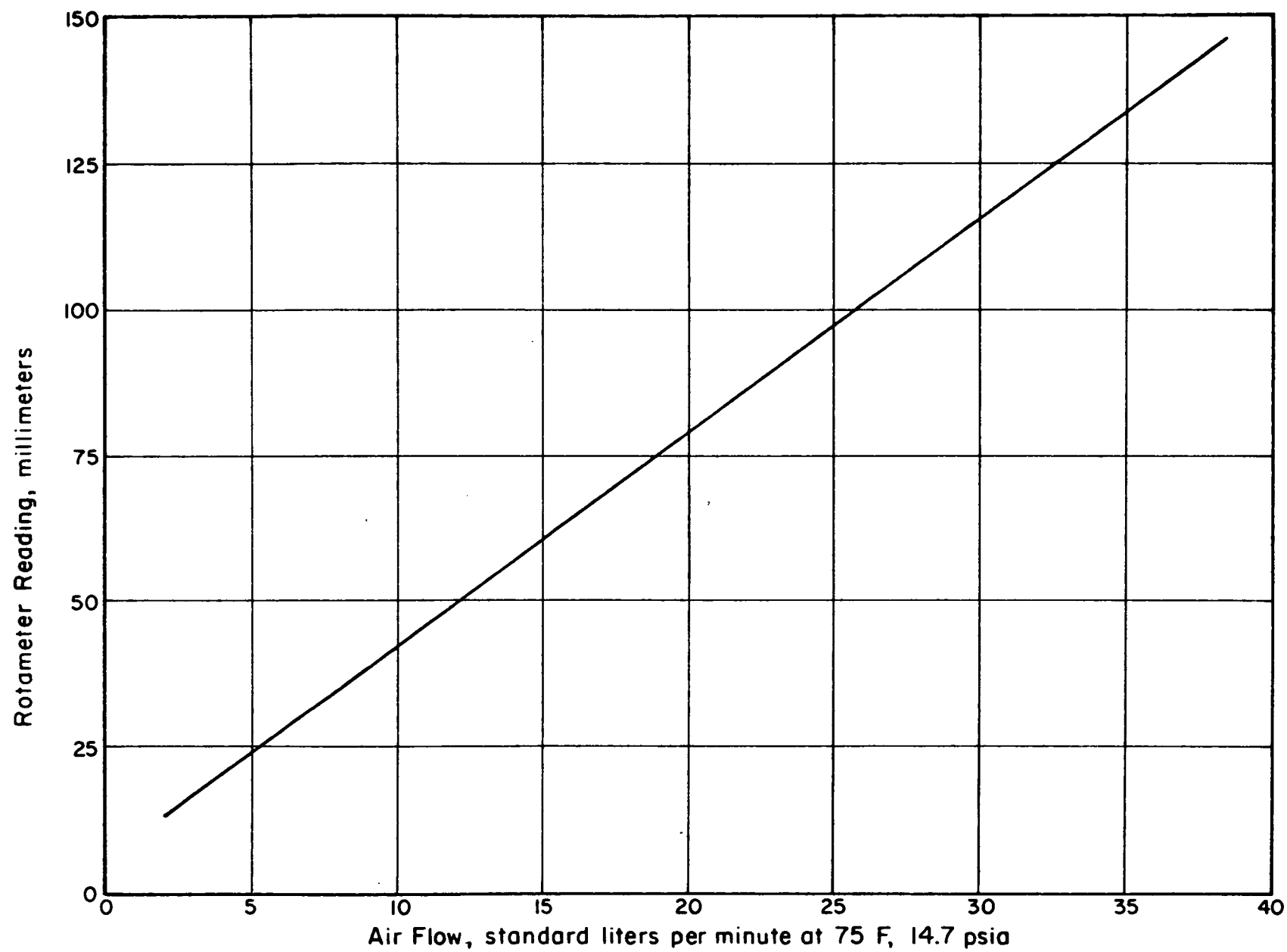


FIGURE B-14. DROP SIZE DISTRIBUTION AT 65,000 RPM AND 0.5 CM³/SEC



B-16

FIGURE B-15. STANDARD CALIBRATION OF PRIMAR SAMPLING ROTAMETERS

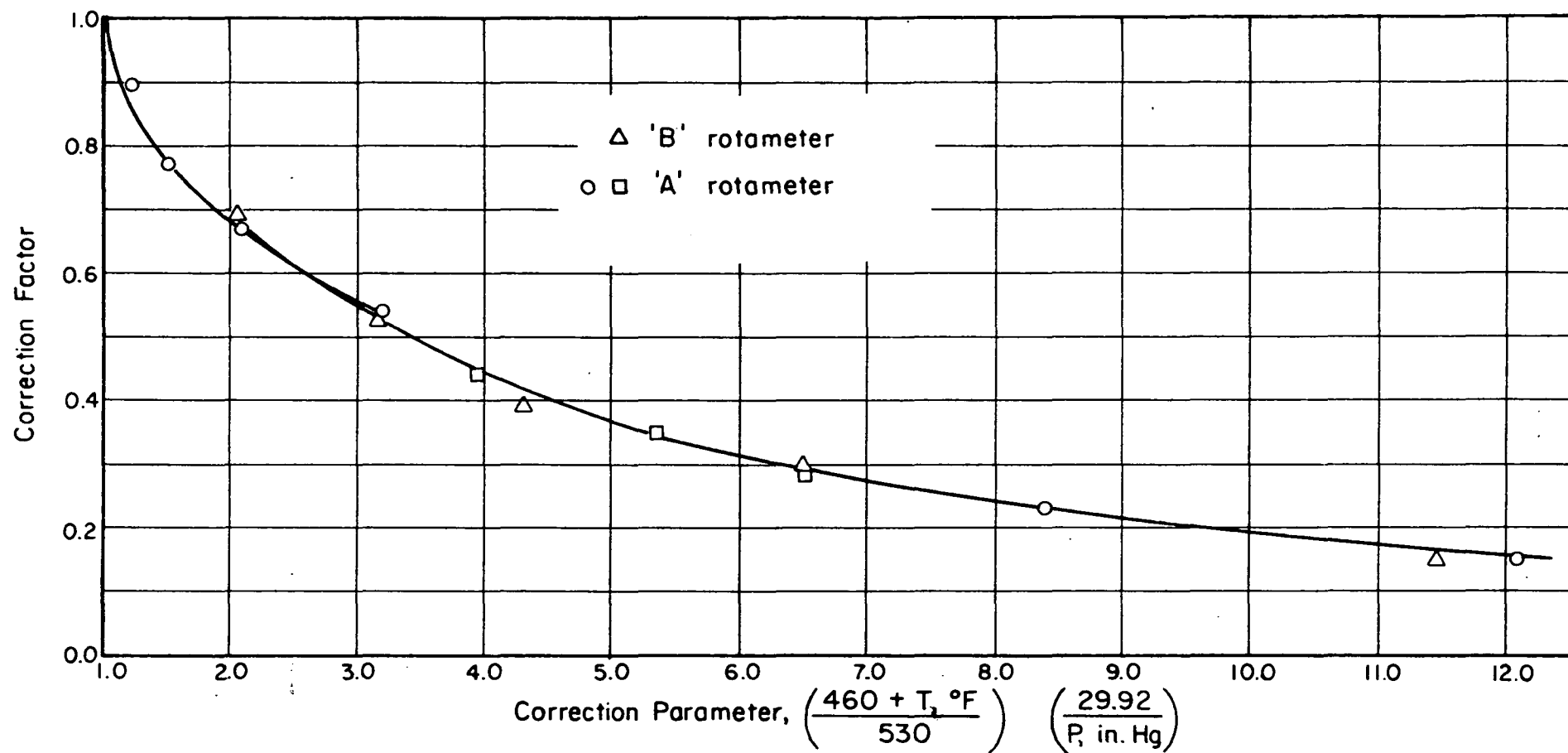


FIGURE B-16. TEMPERATURE AND PRESSURE CORRECTIONS FOR SAMPLING ROTAMETERS

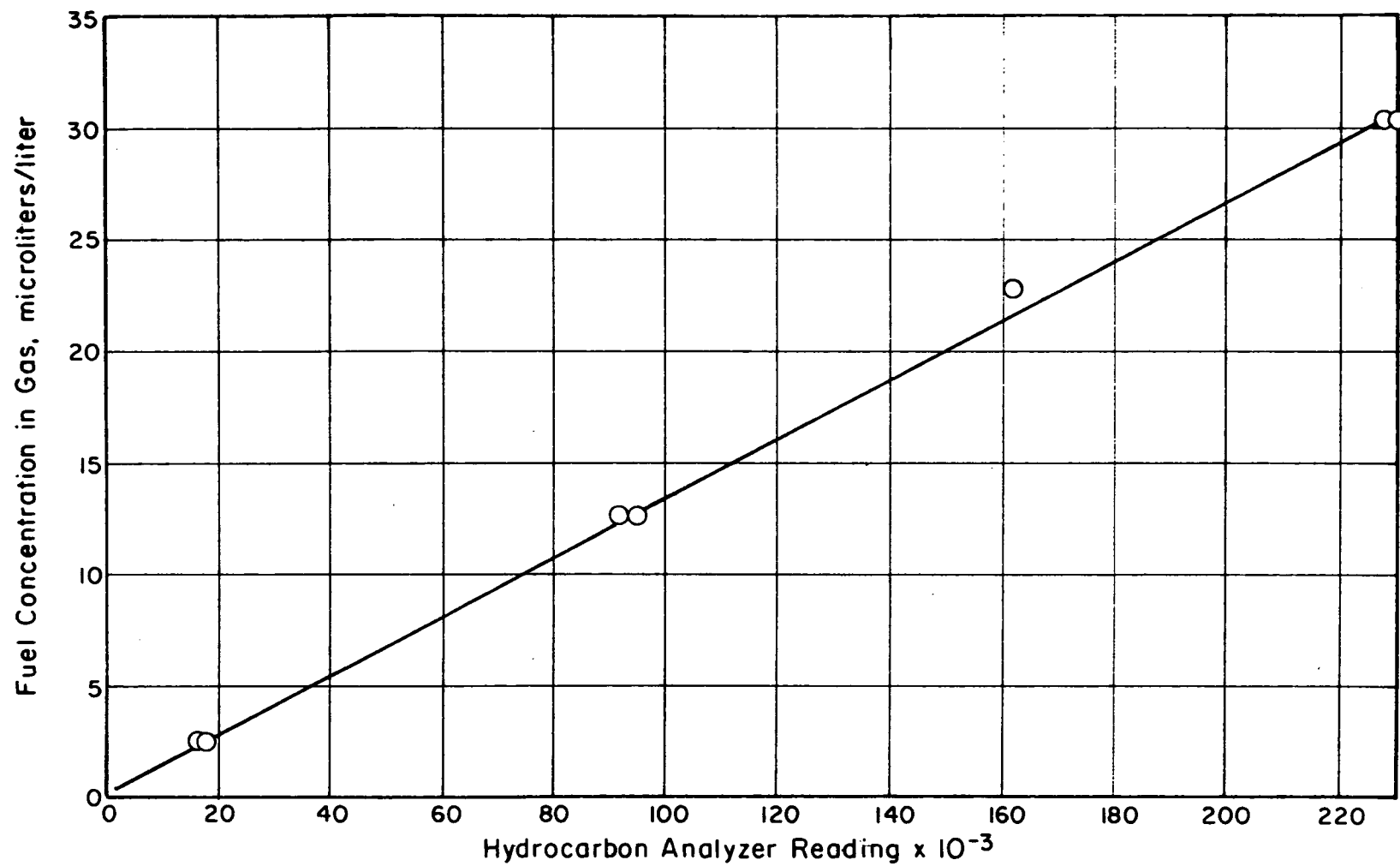


FIGURE B-17. HYDROCARBON ANALYZER CALIBRATION